TESIS DE LA UNIVERSIDAD DE ZARAGOZA

2019

78

Cristina del Amo Mateos

Microfluidic-based analysis of 3D cell migration under different biophysical and chemical gradients

Departamento

Instituto de Investigación en Ingeniería [I3A]

Director/es

GARCÍA AZNAR, JOSÉ MANUEL

ISSN 2254-7606

Prensas de la Universidad Universidad Zaragoza

ISSN 2254-7606

Universidad Zaragoza
1542

Tesis Doctoral

MICROFLUIDIC-BASED ANALYSIS OF 3D CELL MIGRATION UNDER DIFFERENT BIOPHYSICAL AND CHEMICAL GRADIENTS

Autor

Cristina del Amo Mateos

Director/es

GARCÍA AZNAR, JOSÉ MANUEL

UNIVERSIDAD DE ZARAGOZA

Instituto de Investigación en Ingeniería [I3A]

2018

Microfluidic-based analysis of 3D cell migration under different biophysical and chemical gradients

Dissertation presented by

Cristina Del Amo Mateos

for the degree of Doctor of Philosophy in Biomedical Engineering

Faculty advisor

José Manuel García Aznar

Multiscale in Mechanical and Biological Engineering (M2BE)

Aragon Institute of Engineering Research (I3A)

University of Zaragoza, 2018

A mis padres y hermana

Content

Agradecimientos / Acknowledgements

Con la defensa de esta tesis termina un capítulo más de mi vida, donde además del balance de conocimiento científico aprendido, del esfuerzo y dedicación invertida, ha sido fundamental el apoyo de muchas personas, desde lo profesional a lo personal. El sentimiento de enfrentarse a un libro con cientos de páginas en blanco, de adentrarse en un camino sin andar, eso fueron los comienzos de estos años. Sin duda, escribir hoy estas páginas no hubiera sido posible sin mi director de tesis, Dr. José Manuel García Aznar. Manu, mil gracias por todo, por la oportunidad que me brindaste para emprender este trabajo, por enfrentarme ante este y otros retos (gracias por insistirme tanto en hacer la estancia, una de las mejores experiencias de mi vida), por confiar en mí y en que sería capaz de conseguir alcanzarlos, pero sin duda, ¡gracias por estar siempre al pie del cañón!

Agradecer también a la Universidad de Zaragoza, al I3A, al Departamento de Ingeniería Mecánica; al European Research Council (proyecto ERC-2012-StG 306571), al Ministerio de Educación y Ciencia (FPU 91/2013 y EST15/00695), por la financiación concedida que ha hecho posible la realización de esta tesis doctoral.

Mi agradecimiento al grupo M2BE, con todos vosotros he conseguido superar y alcanzar la meta, mil gracias por el apoyo brindado. Mª José y Mª Ángeles, gracias por vuestro apoyo y amistad. Tirso, por tu siempre disponibilidad, y sin duda, por tus buenos consejos. Mis “quintos” de tesis, Jorge, Ismael y Mar, por esas charlas comunitarias sobre lo maravilloso de los últimos momentos de tesis. Carlos, por tus buenos consejos, tus infinitos scripts de Matlab y toda la ayuda aportada a lo largo de este trabajo. ¡Muchas gracias a todos!

Mi mayor gratitud hacia todos mis compañeros del laboratorio por el apoyo brindado durante todos estos años, especialmente Nieves, y Mar, quienes más han sufrido mis momentos de gloria y de frustración. Vanesa, Esther, Sandra, Yago, sin vosotros esto no hubiera sido lo mismo. Compañer@s, habéis hecho que estos últimos meses hayan sido los mejores de esta larga andadura. No me olvido del título otorgado, “Doctora en Tertulias”, siempre lo llevaré conmigo.

Durante estos cinco años unos se han ido y otros han llegado, Gracia, Oihana, Clara, gracias chicas por vuestros ánimos y recomendaciones. Alejandro, porque sin tí el capítulo 4 no hubiese sido lo mismo. Tampoco los ratos en el cuarto de cultivos hubieran sido tan amenos sin los compañeros del grupo vecino, Chema, María, Guillermo, Sandra, Theodora, Clara, Rebeca, Sara, Alodia, José Luis. Especial mención al equipo “bubble”, ¡los montadores de sistemas en flujo! A Carlos, Aitor, Pilar, Ana, Alberto, Juan, David, Andrea por todos los buenos momentos compartidos.

Este trabajo no hubiera sido posible sin la colaboración de muchos: Jesús Asín, por tu entrega y ayuda con los análisis estadísticos; Jorge Santolaria, por las impresiones del soporte; Ismael, por la paciencia invertida en el mecanizado; Marcelo, por tu ayuda con Comsol, gracias.

A Javier Mata, Raquel Moreno, Patricio y al departamento de Bioquímica y Biología Molecular de esta Universidad, gracias por darme la oportunidad de aprender a enseñar con vosotros.

I would like to thank Melody Swartz for the opportunity that she gave me to carry out my research stay in her lab, her unconditional support and kindness. Thanks also to her entire research group at the Institute of Molecular Engineering at The University of Chicago as well as to the other lab colleagues, Peyman, Kartiki, Katha, Chitavi, Sylvie, Maria Stella, Maria, Prisci, Scott, Elyse… Thanks for the wonderful moments I shared with you! Lea and Lambert, thank you for welcoming me into your home, helping me in everything and considering me one more of your Swartzians' family. Roulan, for your support with paper system and for our Boston adventures, I got to eat with chopsticks!

Thanks also Manu for giving me the opportunity to participate in international conferences, because besides all the scientific knowledge acquired, I have brought good friends; Christiana, Feihu, Davide, Estefania, I hope to see you soon!

Quisiera también dar las gracias a todas las personas con quién durante estos años he compartido mi vida:

A los pilares más importantes de mi vida, mi familia, sin vuestro incondicional y cariñoso apoyo nunca hubiera llegado hasta aquí y vivido lo que vivido. Especialmente a mis padres, Trini y Antonio, y hermana, Natalia, gracias por enseñarme a no rendirme nunca, por vuestro apoyo incondicional, por confiar en mí más que yo misma, sin vosotros esto no hubiera sido posible. A mi abuelo, tíos, tías y prim@s, por creer en mí y en que lo conseguiría. A mis abuelas y abuelo, porque donde quiera que estéis, sé que siempre habéis estado a mi lado.

A Roberto, mi compañero de vida, gracias por todos estos años a mi lado, por seguirme y acompañarme en mi camino.

A mis amig@s, Romina, María, Vero, Ana, Nuria, Marina, Marta… a pesar de la distancia siempre ahí, ¡que hubiera sido de mi sin vuestros *whatsapps*! Elena, porque la vida da muchas vueltas y nos ha juntado cuando más nos hemos necesitado. A Julia, pendiente de mis andanzas y mis logros. A Martin, por estar ahí siempre.

A todos los que ocupan un lugar especial en mi vida y que no he podido ver tanto como me hubiera gustado durante la elaboración de este trabajo, a aquellas personas que han estado presentes en mi camino y, aunque ya no están, han puesto su granito de arena para que hoy sea quién y cómo soy. En definitiva, a todos aquellos que de alguna forma me han acompañado durante todos estos años y, aunque no aparezcan aquí citados, han hecho posible que este trabajo hoy vea la luz.

Abstract

Several mechanochemical factors are involved in cell migration, fundamental to establish and maintain the proper organization of multicellular organisms. The alteration of migratory patterns of cells could be related to the development of several pathologies. Focusing this work on tissue regeneration, more specifically wound healing, bone regeneration and blood vessel formation, the main aim of this work is to advance in the understanding of how chemical or physical factors present in the cell niche can regulate the cell movement (fibroblasts, osteoblasts and endothelial cells respectively). In an effort to understand what mechanisms are involved, it has been seen that both the extracellular matrix surrounding tissue cells and the biomolecules present in the cellular microenvironment can affect the behavior of cells. In turn, interstitial fluid flow, defined as the convective transport of liquids through the extracellular matrix of tissue, is also capable of altering the morphology and cellular movement. Similarly, biomolecules, such as growth factors or drugs, modify the migration pattern. The main mechanisms studied throughout this thesis have been chemotaxis, durotaxis and rheotaxis. The biological processes for which these analyses have been performed were angiogenesis, wound healing and bone regeneration respectively.

For the in vitro study of these variables, and making use of novel microfabrication techniques such as microfluidics, new platforms for 3D cell culture have been developed. The microfluidic chips used allow replication of the ex vivo tissue microenvironment through the use of hydrogels and the generation of concentration gradients and controlled fluid flows. It should be noted that the versatility of this technology has allowed us to simultaneously study several microenvironmental factors, such as chemical gradients and matrix stiffness applied to fibroblast culture to understand its behavior in the wound area. In addition, these types of systems allow the visualization and/or monitoring of the cellular response in real time, being able to quantify the cellular migration. For the application of fluid flow, a novel system was designed to avoid the rupture of the hydrogels, allowing to obtain a stable interstitial flow inside the chip chamber.

Throughout this thesis, it has been seen that there are several factors involved in 3D cell migration. Not only variables such as the chemical gradient (studied in endothelial cells and fibroblasts) or the rigidity of the extracellular matrix (analyzed in fibroblasts and osteoblasts) affect cells. The architecture of the matrix, more specifically the disposition of the fibers that conform this matrix, has been identified as playing an important role in cell migration, also altering the morphology of cells, in this case osteoblasts.

Resumen

Numerosos factores mecanoquímicos están involucrados en la migración celular, fundamental para establecer y mantener la correcta organización de los organismos multicelulares. La alteración de los patrones migratorios de las células podría estar relacionada con el desarrollo de varias patologías. Enfocando este trabajo hacía la regeneración de tejidos, más concretamente en la cicatrización de heridas, regeneración ósea y formación de vasos sanguíneos, se ha pretendido avanzar en el conocimiento de cómo factores químicos o físicos, presentes en el nicho celular, podrían regular el movimiento celular (fibroblastos, osteoblastos y células endoteliales respectivamente). En el afán por entender qué mecanismos están involucrados, se ha visto que tanto la matriz extracelular que rodea a las células de los tejidos, como las biomoléculas presentes en el microambiente celular pueden afectar al comportamiento de las células. A su vez, el flujo de fluido intersticial, definido como el transporte convectivo de líquidos a través de la matriz extracelular del tejido, es también capaz de alterar la morfología y el movimiento celular. De forma similar, las biomoléculas, como los factores de crecimiento o los fármacos, modifican el patrón de migración. Los principales mecanismos estudiados a lo largo de esta tesis han sido la quimiotaxis, la durotaxis y la reotaxis. Los procesos biológicos para los que se ha realizado estos análisis han sido angiogénesis, cicatrización de heridas y regeneración ósea respectivamente.

Para el estudio in vitro de estas variables, y haciendo uso de novedosas técnicas de microfabricación como la microfluídica, se han desarrollado nuevas plataformas para el cultivo celular 3D. Los chips microfluídicos utilizados permiten replicar el microambiente tisular ex vivo mediante el uso de hidrogeles y la generación de gradientes de concentración y flujos de fluido controlados. Cabe destacar que la versatilidad de esta tecnología nos ha permitido el estudio simultáneo de varios factores microambientales, por ejemplo, los gradientes químicos y de rigidez de la matriz aplicados al cultivo de fibroblastos para entender su comportamiento en la zona de la herida. Además, este tipo de sistemas permiten la visualización y/o monitorización de la respuesta celular en tiempo real, pudiéndose cuantificar la migración celular. Para la aplicación del flujo de fluido se diseñó un novedoso sistema que evitaba la rotura de los hidrogeles, permitiendo obtener un flujo intersticial estable en el interior de la cámara del chip.

A lo largo de esta tesis, se ha visto que son diversos los factores involucrados en la migración celular 3D. No sólo variables como el gradiente químico (estudiado en células endoteliales y en fibroblastos) o la rigidez de la matriz extracelular (analizado en fibroblastos y osteoblastos) afectan a las células. La arquitectura de la matriz, y más concretamente la disposición de las fibras que conforman dicha matriz, se ha visto que desempeñan un papel relevante en la migración celular alterando también la morfología de las células, en este caso de los osteoblastos.

List of Figures

List of Tables

List of abbreviations

2D: two-dimensions

3D: three-dimensions

AML: acute myeloid leukemia

ANG2: Angiopoietin 2

BMP(s): bone morphogenetic protein(s)

BMP2: bone morphogenetic protein 2

BSA: Bovine serum albumin

CAD: computer aided drawing

cAMP: cyclic adenosine monophosphate

CF: coagulation factors

CI: chemotactic index

CNS: central nervous system

CO_2: carbon dioxide

Coll: collagen

DAPI: 4′,6-Diamidine-2′-phenylindole dihydrochloride

DLL4 Delta-like ligand 4

DMEM: Dulbecco's Modified Eagle's medium

EC(s): endothelial cell(s)

ECM: extracellular matrix

EGF(s): endothelial growth factor(s)

EGM2: endothelial cell growth media 2

ELISA: enzyme-linked immunosorbent assays

EPC: endothelial progenitor cell

FACS: fluorescent activated cell sorting

FCS: fetal calf serum

FF: interstitial fluid flow

FGF: fibroblast growth factor

FITC-dextran: fluorescein isothiocyanate-dextran

Fn: fibronectin

GAM: generalized additive model

GF(s): growth factor(s)

GFP: Green fluorescent protein

Gly: glycosaminoglycans

Grdl: Gridlock

HEK: human embryonic kidney

HOB: human osteoblast cells

HSC(s): hematopoietic stem cell(s)

HUVEC: human umbilical vein endothelial cells

HVIN1: human vinculin 1

IACS: Aragon Health Sciences Institute

IL: interleukins

IPA: isopropyl alcohol

kDa: kiloDalton

MDGF(s): macrophage-derived growth factor(s)

Mϕ: macrophage

MSC: mesenchymal stem cells

NHDF: normal human dermal fibroblasts

NODs: nearest obstacle distances

PAI-1: plaminogen activator inhibitor-1

PBS: phosphate buffered saline

PDGF: human platelet derived growth factor-BB

PDL: poly-D-lysine

PDMS: polydimethylsiloxane

PFA: paraformaldehyde

PGE2: prostaglandin E2

PMN(s): polymorphonuclear(s)

Pro: proteoglycans

PTFE: polytetrafluoroethylene

PVDF: polyvinylidene fluoride

ROI(s): region(s) of interest

RT: room temperature

Scl: stem cell leukemia

SEM: scanning electron microscope

Shh: Sonic hedgehog

SMC(s): smooth muscle cell(s)

TG2: transglutaminase 2

TGFβ1: human transforming growth factor- beta 1

TRITC: Tetramethylrhodamine

Tsp: thrombospondin

uPA: urokinase plasminogen activator

uPAR: urokinase plasminogen activator receptor

VEGF: vascular endothelial growth factor

Vn: vitronectin

vWF : von-Willebrand factor

Chapter 1

Introduction

1.1 Background

Cell migration is crucial in every biological processes, being strongly dependent on the surrounding microenvironment. Migration of cells is fundamental in both physiological and pathological processes, like embryonic development, wound healing, cancer metastasis, angiogenesis, and other regenerative events such as bone repair. Throughout this chapter, a state-of-the-art review of the methodologies used for 3D cell culture is presented. In addition, the main aim of this thesis has been focused on understanding the mechanisms involved in the 3D cell migration in three different biological processes: angiogenesis, wound healing and bone fracture healing, which will also be briefly explained thereafter.

1.1.1 Microfabrication in biological sciences

For more than a century, the conventional cell cultures were performed on traditional Petri dishes, growing cells in a plastic surface in two dimensions. Considering the differences between cell behavior in 2D vs 3D (i.e. see the differences on cell morphology depending on the culture in Figure 1.1), in terms of cell differentiation and tissue organization, microchip industry with microfluidics approaches presented a new way to culture cells in 3D replicating better the interactions of factors and tissue complexity inherent to *in vivo* conditions [1–3]. Microfabrication technologies such as photolithography, replica molding, and microcontact printing [1,4] have emerged as powerful tools for tissue engineering and cell biology.

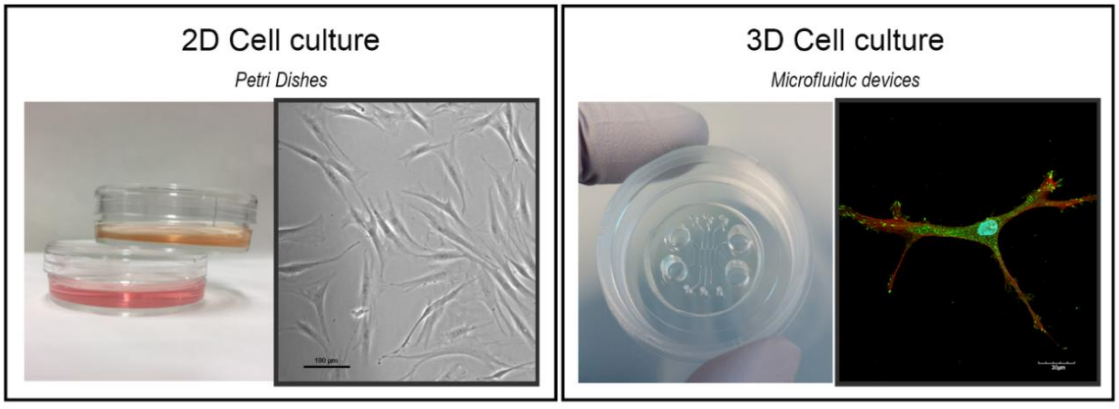

Figure 1. 1 Comparison of 2D vs 3D cell culture
In the left side human fibroblasts seeded in a Petri dish are shown. 3D human osteoblast embedded in collagen hydrogel into microfluidic device are in the right side of the figure.

Microfabrication is a process used to manufacture physical objects with dimensions in the range of micrometers to millimeters [5]. Another fundamental pillar of the microsystem technology is the microfluidics, the science of manipulating small amounts of fluids in microfabricated channels (from 10^{-9} to 10^{-18} liters). Devices manufactured for cell culture involve certain requirements not

necessary in other microsystems designed for physicochemical applications. The selected material for the fabrication of the chips, the geometry and dimensions of the cell culture area as well as the methodology for pumping and controlling fluid flow are some of the most important aspects to consider in these microplatforms [6].

Soft photolithography is the most popular technique usually employed to fabricate microdevices and is commonly accompanied by replica molding techniques. From the CAD, computer aided design of the desired geometry, an elastomeric stamp is fabricated from patterned silicon wafers to print or mold materials. The usual procedure for obtaining them will be summarized hereafter. First, it is necessary to clarify that the most common material used for this purpose is SU-8, a photosensitive epoxy resin.

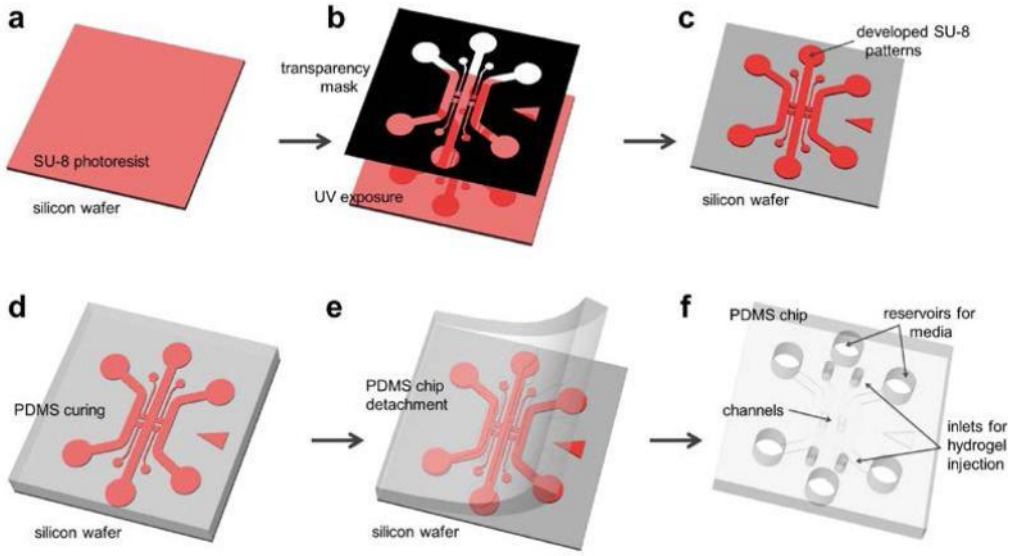

Figure 1. 2 Schematic of the photolithography (a-c) and soft lithography (d-f) procedure.
(a) SU-8 is spin-coated and pre-baked on a bare wafer. (b) Use a transparency photomask (black), UV light is exposed on the SU-8. (c) Exposed SU-8 is then post-exposure baked and developed to define channel patterns. (d) PDMS (polydimethylsiloxane) mixed solution is poured on the wafer and cured. (e) Cured PDMS is then peeled from the wafer. (f) Device is trimmed, punched and autoclaved ready for assembly. Figure and caption taken from [7]

After the wash and dehydration of the silicon wafer, the SU8 was added (1ml per inch), spined and placed in a hot plate increasing the temperature until it reaches 95°C, being then the photoresist prebaked for 30min. Afterwards, UV light exposition was necessary to fix the photomask geometry onto the wafer. Before the application of the developer in order to remove the regions non-exposed to the light, the wafer was baked again at 95°C for 30 min as in the previous step. The developer was neutralized in IPA (isopropyl alcohol), removing the non-desired parts and then, rinsed it with deionized water. Finally, the wafer was dried by nitrogen gas pressurization being ready for the following replica molding steps. Figure 1.2 summarizes this fabrication process.

Polydimethylsiloxane (PDMS) is the most popular silicon-based elastomeric material used in soft lithography and replica molding techniques. It presents low autofluorescence, optical

transparency at wavelengths as short as ~300 nm light and allows for visible light microscopy, being useful for the analysis and the optical monitoring of cell morphology and motility [8]. It is also non-cytotoxic and gas permeable, allowing for cell respiration, one of the properties that makes it desirable for *in vitro* experimentation [9]. In addition, its fabrication versatility as well as its capacity to easily bind to different materials has facilitated the microdevice adaptation for each experiment. The full description of each specific device will be presented in each corresponding chapter.

1.1.1.1 Microfluidic devices

3D cell culture models such as the future organ-on-chip devices have many potential applications in many areas, for instance, pharmaceutical industry for drug testing, chemical and cosmetics industries as alternative method of clinical outcomes, for identification of environmental toxins, or just for understanding the human body by integration of several organs mimetic interacting between them.

In recent years, the aim of finding a new form of *in vitro* cell culture closer to the *in vivo* conditions in which our tissue cells are found, has promoted the development of microfluidic techniques. The origin of this discipline dates back to a few decades ago being more orientated towards chemical cues or medical devices [10]. Microscale cell culture platforms have been created for generating dynamic fluid flows, nutrients and other chemical cues as supplies for cells, as well as spatio-temporal gradients, in a controlled manner inside these chambers. Efforts to achieve a new way of culture cells within extracellular matrix (ECM) allowing the replication of cell conditions inside the tissues, have promoted the creation of structures for 3D cell cultures. Microfluidic assays have also facilitated the study of mechanobiological aspects such as cell response depending on the alterations of the surrounding microenvironment, named this field as mechanotransduction [11].

In addition to the precise control of the cellular, physical and biochemical microenvironment using these platforms, there are other advantages such as single-cell manipulation and analysis, reduction of reaction volume of nano- or picoliters (thereby reducing costs and low reactant waist), execution of parallel experiments or the integration of multiple biological processes in a single system among others [12,13]. Figure 1.3 summarizes the main advantages and challenges of microfluidic experiments comparing to macroscopic cell cultures [14].

Van Duinen et al. have reported that the main application of the microfluidic 3D cell culture has trended towards cancer studies (including therapy discovery and selection) and vascular modelling [15]. There are many proposals in the literature to reproduce and characterize cell microenvironments [16–23], specially related with tumor niche. For example, the Kamm's group in MIT has developed several approaches to investigate intravasation and extravasation of tumor cells, coculturing different cell types in their microfluidic models as well as testing drug effects or the diffusion of molecules under these conditions [24–26]. Likewise, neurovascular [27], cardiac

[28] or renal [29] models of collective or single-cell migration, are some of the approaches analyzed with microfluidic systems recently presented in the literature.

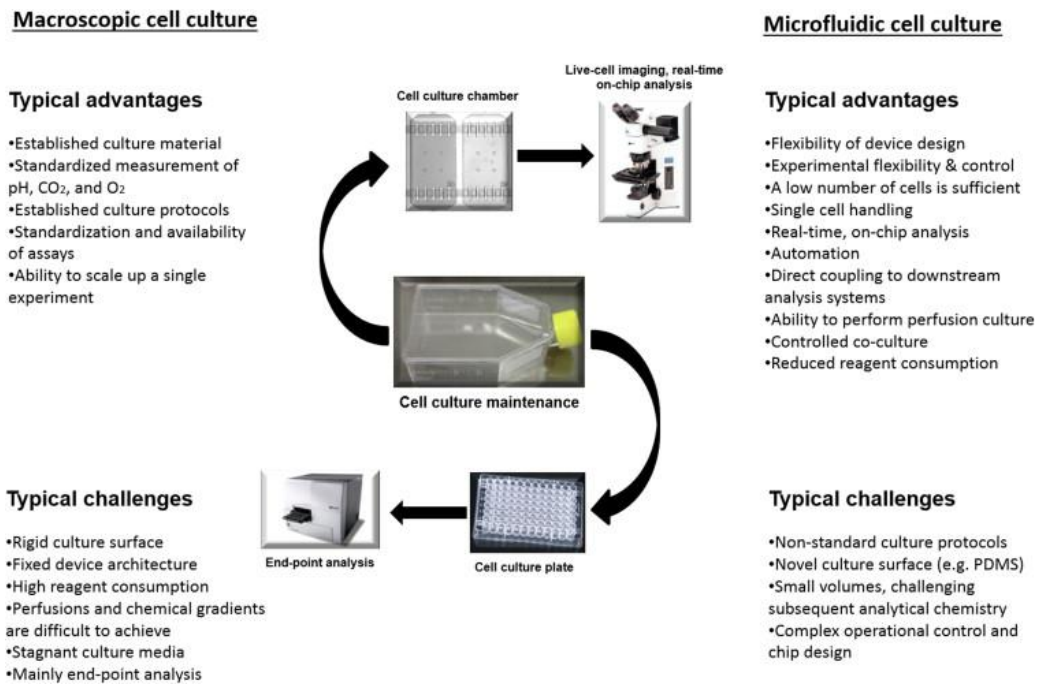

Figure 1. 3 Overview of advantages and challenges of both macroscopic and microfluidic cell culture
Figure and caption taken from [14]

The great flexibility to manufacture new designs and adapt them to the desired experiments, as well as the multiple fields of application, have promoted an increase in the use of these techniques making it an excellent proposal for cell research.

1.1.2 Cell guidance mechanisms

Through the complex environment of tissues, cell migration is affected by multiple external cues such as signaling molecules or biophysical features. New approaches and tools have enabled to understand the complex regulatory pathways highly involved in polarized cell migration.

Microfluidics has been an excellent tool for *in vitro* cellular analysis by offering a precise control of the cellular, physical and biochemical microenvironment. Channel distribution of microfluidic platforms has allowed the generation of precise mechanochemical gradients inside the chip during long periods of time in a more exact manner than in macroscale in vitro systems [12].

Depending on the stimulus and the gradient applied, the pattern of cell migration varies and can be differentiated into chemotaxis (regulated by chemical factors), mechanotaxis or tensotaxis, durotaxis (both driven by mechanical factors) among others, without disregarding the pressure gradient effects (Figure 1.4).

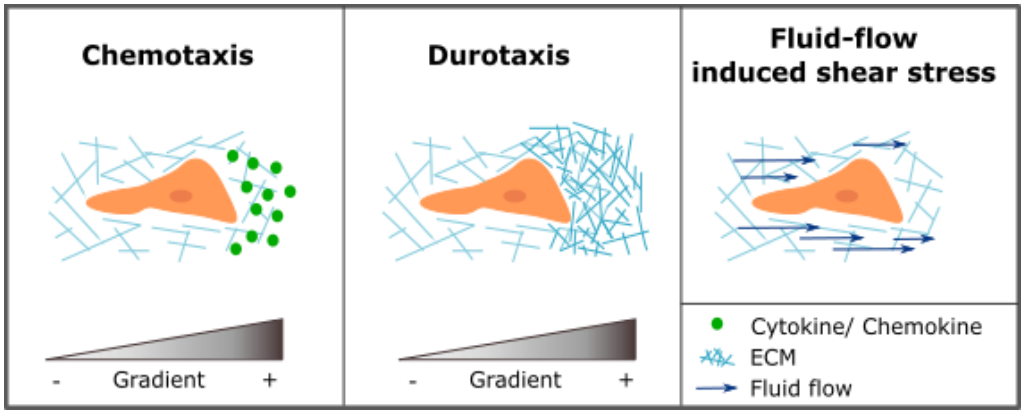

Figure 1. 4 Cell guidance mechanisms.
Some common types of cell movement induced by chemical (chemotaxis) or mechanical gradients (durotaxis: cell migration directed by stiffness gradients) and the effect of shear stress induced by fluid flow

1.1.2.1 Chemical gradients: chemotaxis

Chemotaxis, defined such as the ability of cells to sense a chemical gradient and respond by directional migration towards or away from the source, is essential for cell development and wound healing, also playing an important role in cancer, inflammatory process or autoimmune diseases [30,31]. Cells are able to sense the extracellular signals by membrane receptors adapting their response to the chemoattractant gradient. Cell polarization and the consequent protrusion formation towards chemotactic stimulus is thought to be regulated by changes in actin polymerization and membrane tension [32,33].

To analyze mechanobiological cues, microfluidic devices have proved to be robust tools to generate chemical gradients and to quantify cell migration by tracking software. Based on a simple platform structure with three channels, hydrogel would be located in the central chamber of this device presenting a porous structure conformed by collagen fibers (see Figure 1.5). This architecture allows the passive diffusivity of molecules at the same time that it opposes high resistance to liquid flow, enabling the gradient generation. Adjacent channels (inlet and outlet) supply nutrients to the cells embedded in hydrogel located in the central zone by laminar interstitial fluid flow.

Due to the high biological and physiological relevance of chemotaxis, understanding its mechanisms has been a long-term focus of cell migration research. Over the last years, many different tests have been proposed for cell migration especially to analyze cell response in presence of chemotactic factors (widely described in chapter 3). With the microfluidic techniques development, more efficient and quantitative evaluations of cell migration in spatiotemporally complex chemoattractant fields that better mimic in vivo situations have been achieved [34]. Furthermore, they give the ability to maintain and control chemical gradient as well as the real-time quantification of cell migration at single-cell level, which has led to an increase of its use for chemotaxis studies.

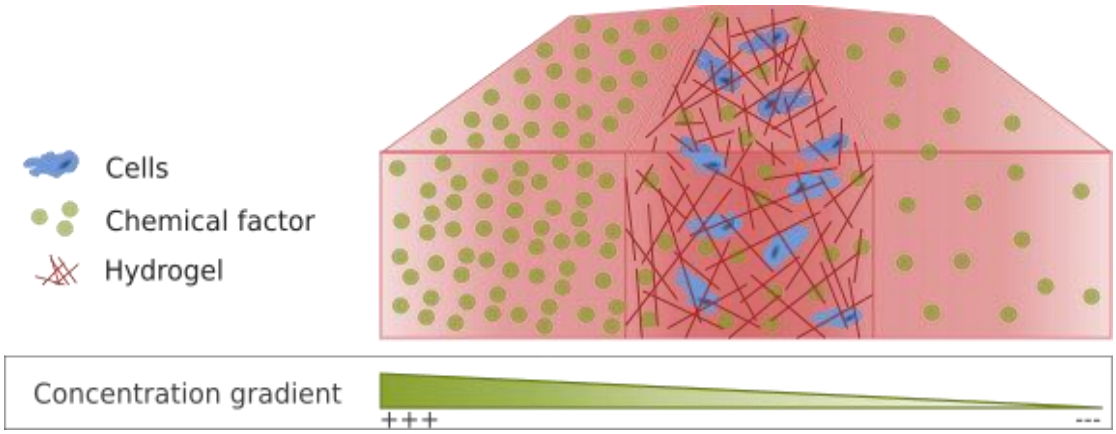

Figure 1. 5 Basic distribution of microfluidic devices for three-dimensional cell culture (cross-sectional view) Cells embedded in the hydrogel to mimic the extracellular matrix (red lines). Chemical gradient represented with green spots with higher concentration in the addition channel and less in the opposite channel.

1.1.2.2 Mechanical gradients: mechanotaxis

Focusing on the role of matrix stiffness and cell forces on cell migration, both stimuli are widely involved. In fact, they are very relevant in many biological processes, for example, bone regeneration or wound healing.

We have to keep in mind that cells are able to sense physical forces transducing it into biochemical signals via force-induced conformational changes which also alters ion channels or signaling cascades [32]. Therefore, if we distinguish the origin of the mechanical stimuli (substrate or cells) two different taxis phenomena may occurs: durotaxis and tensotaxis.

i Durotaxis

Extracellular matrix, a non-cellular structural component of tissues, contains many fibrous proteins and polysaccharides, surrounding cells and playing an important role on their migration [35]. Following the physical properties of the substrate that cells can sense, they select the directionality of their movement, being this migration modality known as durotaxis [36].

Previous studies have remarked the tendency of tumor cells to migrate towards a stiffer area, strongly associated with fibrotic zones of tumors or wounds in fibrosis [37]. The stiffness of the matrix regulates the directionality of movement. Cells detect the substrate stiffness by exerting forces on it and subsequently, altering the actin flows and modifying their cytoskeleton in order to detect the matrix deformations [32,38]. The way in which cells feel the differences in rigidity is not entirely clear. It seems that through mechanosensors, cells transduce mechanical gradients in intracellular signals [32]. However, the role of focal adhesions seems also crucial in cellular

response that varies in function of the cell type. For instance, Bollman et al. reported the different response of glial cells to the matrix stiffness in different ways, by increasing its area or the complexity of its morphology [39].

ii Tensotaxis

In addition to the cellular movement directed by substrate stiffness gradients, cellular migration may respond to signals resulting from stress gradients. Tensotaxis studies cell migration and proliferation in pre-strained regions on a substrate [35,40,41]. Previously published studies shown a modification in the alignment of fibroblasts cultured in prestrained collagen gels, following the cells the direction of the maximum principal strain of their environments [40]. Theoretical and experimental models of tensotaxis aim to know the effect that cellular forces applied in the extracellular microenvironment cause on cellular movement, as well as the effects of cell proliferation and cell death, cell interactions or the elastic properties of the substrate [35]. This model of mechanotaxis has a significant relevance in the understanding of the mechanisms involved in the collective cell migration, presents in many biological processes such as tissue regeneration, cancer and immune response to infection.

1.1.2.3 Fluid flow sensing

Cells such as endothelial cells are constantly subjected to shear stress caused by blood flow in vessels altering its migration [42]. In fact, several studies have shown the mechanical influence of fluid flow, inducing shear stress to the endothelial cells (ECs) and significantly affecting branching, capillarisation [43], sprout promotion [44,45] or vessel formation [46,47].

Signaling cascades, transmembrane receptors, such as integrins, as well as focal adhesions are essential mechanisms for directional migration [42]. Polacheck et al. analyzed the mechanotransduction mechanisms involved in tumor microenvironment, characterized by high interstitial fluid pressure and consequently by interstitial fluid flow [48]. Elevated fluid pressures also alter chemical transports. Thus, this fluid can regulate the cell behavior through diffusion of molecules such as cytokines and other growth factors (GFs) in chemotactic assays, or by itself.

The combination of scale and physics of microfluidic devices results in a laminar flow of liquids and gases within the system leading to diffusion of molecules [49]. There are many methodologies for applying fluid flow to cell-containing hydrogels in microfluidic devices (see Figure 1.6). This active pumping regulated by syringe pumps typically consists of a piston to push liquids out of a syringe with a defined volume, offering precise flow control and being simple to operate.

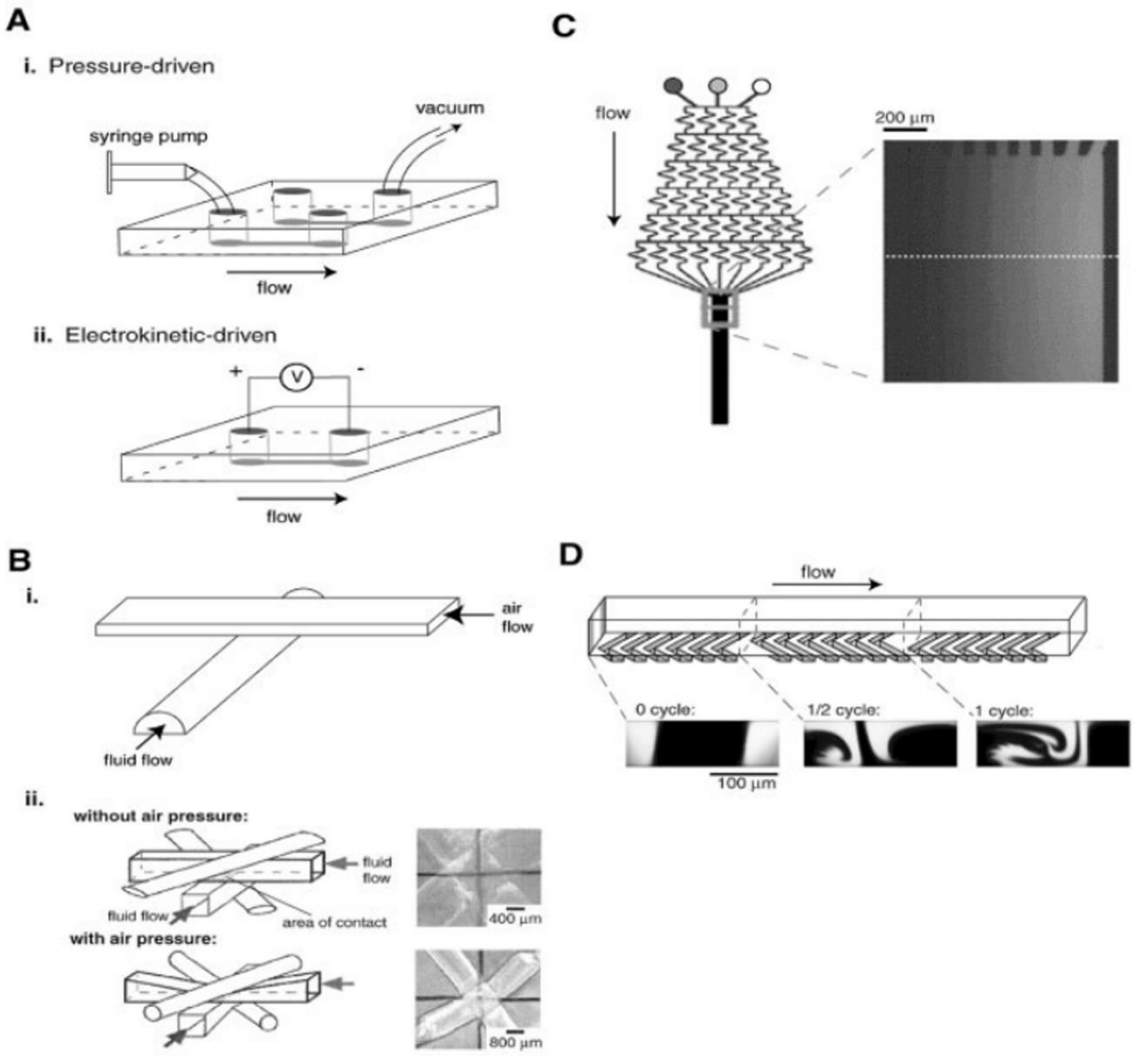

Figure 1. 6 Toolbox for PDMS-based microfluidic bioassays.
(A) Methods for driving fluid flow. (i) Pressure-driven flow using a vacuum at the outlet or a syringe pump at the inlet. (ii) Electrokinetic flow using a voltage applied across the microchannel. (B) Switches and valves for control of fluid movement. (i) Pneumatically actuated monolithic valve. When pressure is applied above, flow in the bottom rounded channel stops [18]. (ii) Channel crossing in which the fluid flow can be switched. When air pressure is applied above and below the crossing, the fluid turns 907 instead of flowing straight. Figure adapted from [20]. (C) Gradient generator using laminar flow. A solution or surface-bound molecular gradient is generated perpendicular to the direction of fluid flow in the microchannel. Figure adapted from [31]. (D) Chaotic mixer. Neighboring streams of fluids are passively mixed. Homogeneity is observed after 16 cycles of the staggered herringbone structure. Figure adapted from [32]. Figure and caption taken from [50]

Fluid flow relates to many physiological and pathological events such as cancer progression, vasodilation, angiogenesis in homeostasis. As Figure 1.7 shows, combining fluid flow with other mechanochemical stimulus provides another strategy to replicate the cell microenvironment. For example, mixing flow and strain by using deformable membranes helps modeling epithelium found in organs such as lungs, blood and lymphatic vessels (Figure 1.8-C) [51].

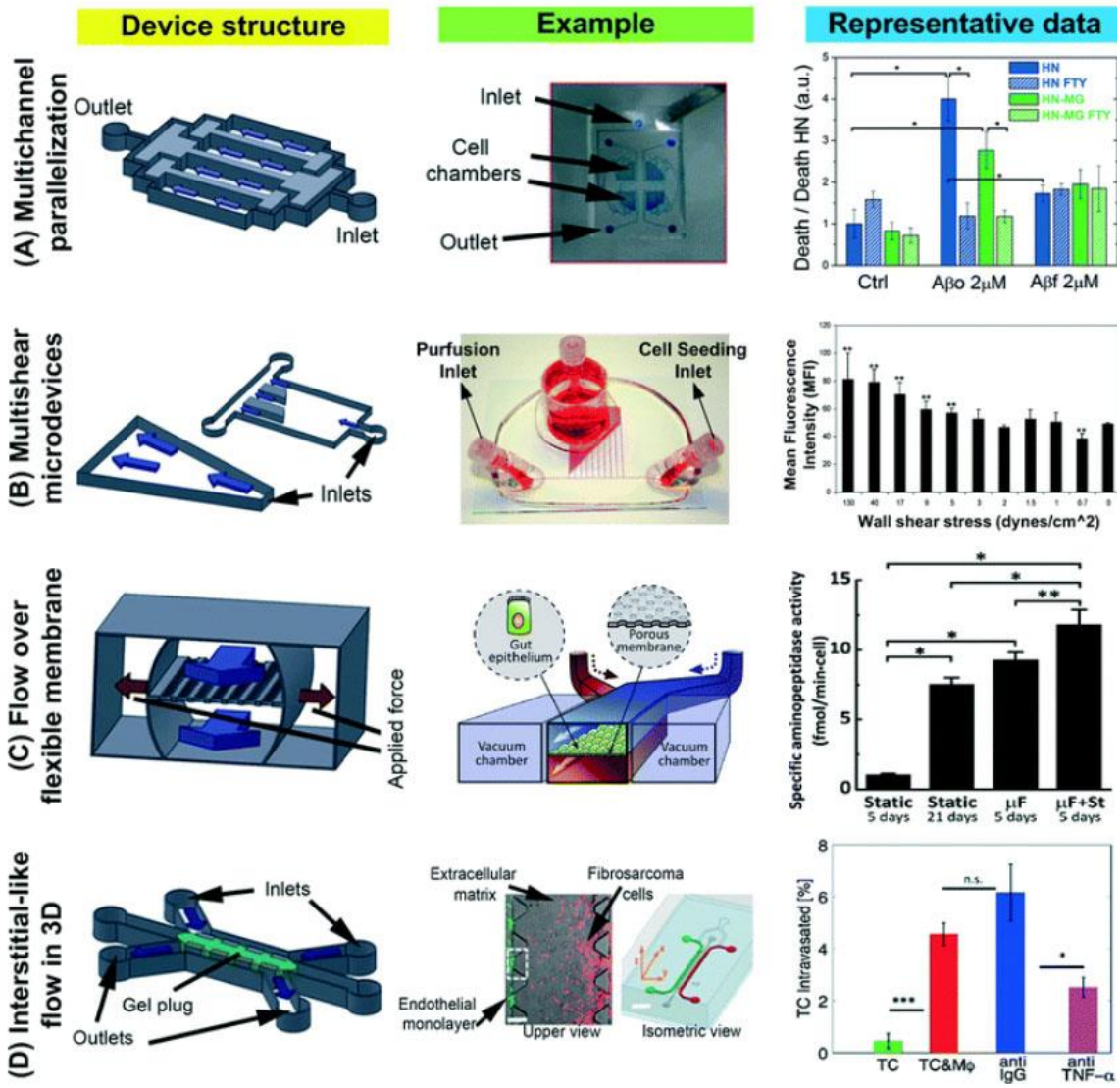

Figure 1. 7 Different typical microfluidic flow system configurations.
Blue arrows indicate flow direction in "Device Structure" column. (A) Multichannel configuration used for high-throughput drug screening on different populations of primary central nervous system (CNS) cells under physiological fluidic shear conditions (adapted from ref. 61). (B) Shear stress modulation based on difference in channel hydrodynamic resistance used to investigate secretion level of von-Willebrand factor (vWF) by human umbilical vein endothelial cells (HUVEC) (reproduced from ref. 74). (C) Combined flow and strain applied to cell-seeded porous membrane to mimic the human intestine (reproduced from ref. 91). On the basis of this concept, many organ-on-a-chip devices have been developed to study the physiological function of different organs such as blood vessels, lung, liver and kidney. (D) 3D microfluidic systems designed to control microenvironmental factors (e.g., cell-cell interaction, 3D ECM-like microenvironment) and perform live cell imaging while exploring the relationship between tumor cell intravasation and endothelial permeability in the context of cytokine induced endothelial cell activation and paracrine signaling loops (reprinted with permission from ref. 92). Figure and caption taken from [51].

Summarizing, to manipulate fluid flow-induced stresses by modulation of the geometrical configuration of cell culture microenvironment several approaches have emerged over the last years. From single flow channels to sophisticated platforms for multi-parameter parallel screening, such as multi-shear stress, have been developed [2,51–53].

Biological tissues, as a porous and elastic solid (poroelastic) saturated with liquid, are deformed by interstitial flow which in turn alters the interstitial fluid pressure and the resulting flow

field [54]. In addition to the matrix alterations via fluid flow, interfaces of 3D hydrogels can be created to simulate the microenvironmental conditions suffered by cells. For instance, fibroblast migration and phenotype could be influenced by the different stiffness of granulation tissue during wound healing [55]. As mentioned above, cell migration is mainly governed by the microenvironmental properties such as substrates and extracellular signaling molecules, acting as motogenic stimuli or directional guidance cues [56].

1.1.3 Biological processes

The technology previously described has allowed us to study how mechanochemical factors affect to important process in the human body such as wound healing or bone regeneration. When an injury occurs, angiogenesis, as essential phase for the reestablishment of the tissue, provides nutrients and oxygen to the affected area by formation of new blood vessels. This section describes the biological processes mentioned above, focusing on the main mechanisms that act on each of them.

1.1.3.1 Blood vessel formation: from vasculogenesis to angiogenesis

The first reports about the circulatory system formation date from Leonardo da Vinci speculations who suggested its developed like a tree from a seed (heart) by sprouting roots (the liver capillary meshwork) and a trunk with major branches (the aorta and arteries) [57]. Early in the embryo, vascular plexus forms from mesoderm by differentiation of angioblast into endothelial cells, resulting in the generation of primitive blood vessels [58,59]. This process, where ECs differentiate and proliferate *in situ* within a previous avascular tissue in order to form a primitive tubular network, has been defined such as vasculogenesis [57,60]. With the involvement of several molecular mechanisms and the contribution of hematopoietic stem cells (HSCs), the primary vascular network is established in the embryo including some of the major vessels such as the aorta and major veins and the connections between them [58]. When this initial network is modified, the process is named as angiogenic remodeling or angiogenesis (the formation of blood vessels from preexisting ones). These new capillaries can be formed by sprouting or by splitting form their vessel of origin to give rise to the mature vasculature. The process has been summarized in Figure 1.8. Initially in the yolk sac and later during the organogenesis, through sprouting angiogenesis, the vascular bed is developed [57]. During this process at embryo stages, proteolytic degradation of extracellular matrix followed by chemotactic migration and proliferation of ECs promote the lumen formation as well as the functional maturation of the endothelium [57].

Proangiogenic GFs play a relevant role on the sprout formation, being remarkable the effect of vascular endothelial growth factor (VEGF) which stimulates physiological and pathological angiogenesis. It should be mentioned the importance of hypoxia, an important stimulus for blood

vessels expansion [58,61]. For instance, before tissues grow, cells are oxygenated by simple diffusion of oxygen, however, with its thickening, transcription factors are activated causing the vessel formation. The effect of some of GFs involved in vascular growing will be deeply explained in chapter 2.

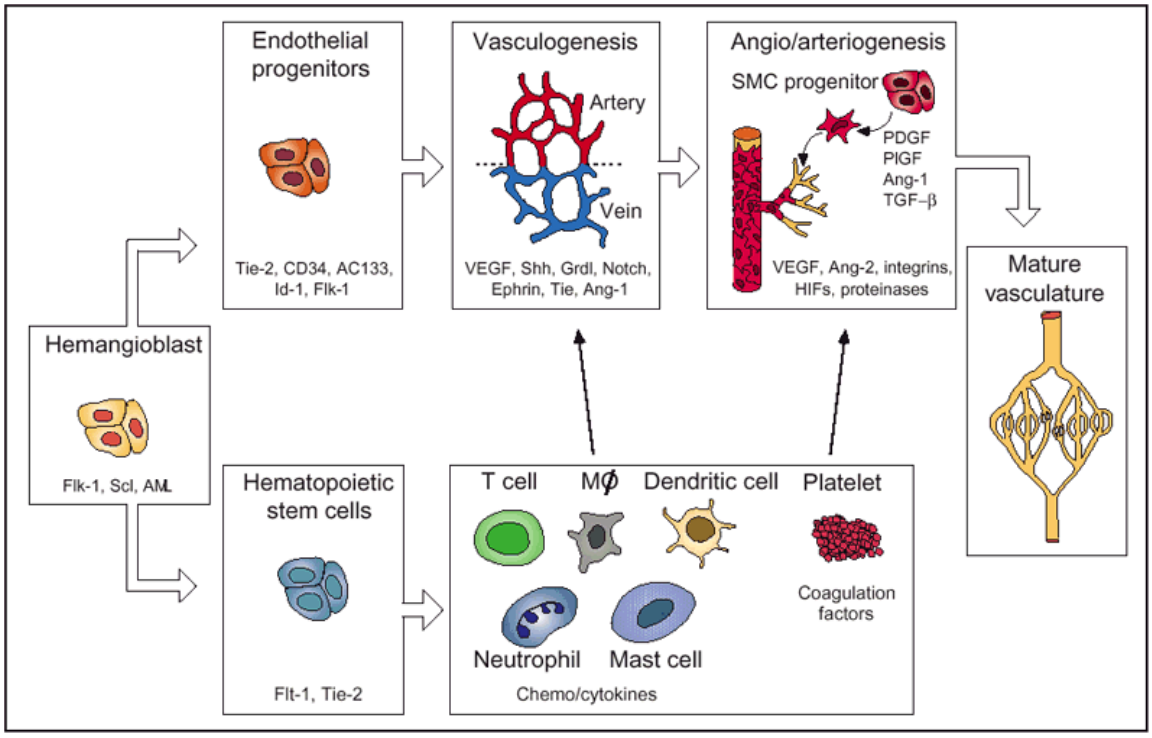

Figure 1. 8 Formation of a vascular network.
Endothelial progenitors differentiate to arterial and venous ECs, which assemble in a primitive capillary plexus. Vessels then sprout and become stabilized by smooth muscle cells (SMCs), differentiating from their progenitors. HSCs contribute to angiogenesis directly and indirectly, by differentiating to leukocytes or platelets. Only a partial list of molecules has been indicated in this figure. Shh, Sonic hedgehog; Grdl, Gridlock; Mφ, macrophage; AML, acute myeloid leukemia; Scl, stem cell leukemia. Edited from Eming et al,2007. Figure and caption taken from [58]

i Cell migration in angiogenesis

Endothelial cell adhesion and migration is primarily mediated through integrin binding to ECM transducing mechanochemical signals between the intracellular and extracellular environment [62]. There are some essential cells for the initiation and promotion of sprouting: tip, stalk and phalanx cells [63]. Figure 1.9 shows the main cues of sprouting formation based on physiological vascular effects of the angiopoietin-Tie system. From a monolayer of ECs, tip cell begins to migrate randomly, as far as the direction of 3D movement is concerned, but with an automatic polarity, usually defined by the extracellular factor, and maintaining the connection with adjacent cells, named stalk cells [63,64]. Tip cell is activated by vascular-endothelial growth factor inducing the migration of these ECs towards VEGF signals and increasing the stalk cell proliferation [65]. There are molecular mechanisms of signalization such as Notch in order to avoid the differentiation of

stalk cells into tip cells. Delta-like ligand (DLL4) is expressed on tip cells migrating to Notch receptors on stalk cells to prevent the transformation into tip cells [65]. The role of stalk cells is to proliferate and extend the sprout towards the VEGF gradient.

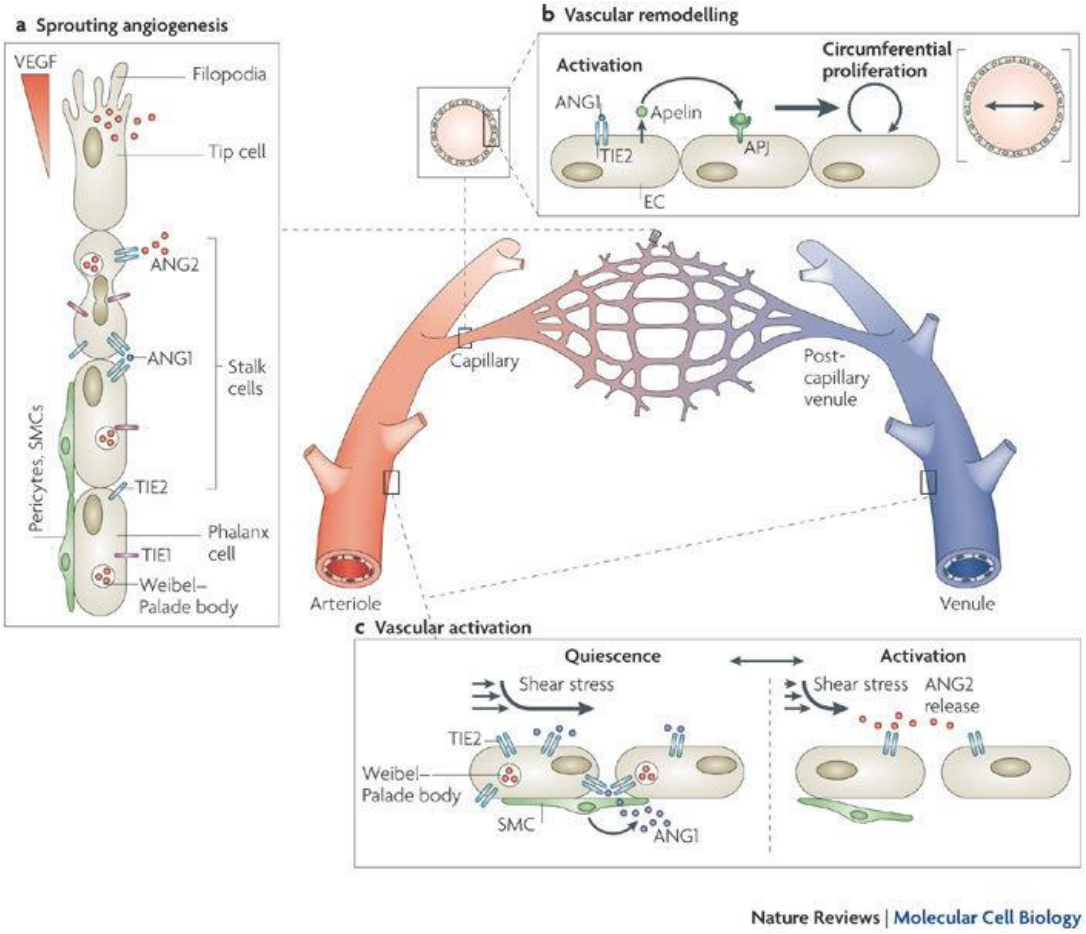

Figure 1. 9 Physiological vascular effects of the Angiopoietin–Tie system.

a | Sprouting angiogenesis is initiated in response to vascular endothelial growth factor gradients by invading endothelial cells (ECs), known as tip cells, that have numerous filopodia. These are followed by a zone of proliferating and differentiating ECs, known as stalk cells, that either lack or are only loosely covered by pericytes and smooth muscle cells. Below these stalk cells, phalanx cells are in intimate contact with pericytes and SMCs, which keep them in a protected, quiescent state. Tie receptors are expressed by stalk cells and phalanx cells. Angiopoietin 2 (ANG2; also known as ANGPT2) is abundantly expressed by angiogenic ECs89, but the precise positional expression pattern of ANG2 is not well defined. Stalk cells and phalanx cells might store ANG2 in Weibel–Palade bodies. Paracrine-acting ANG1 (also known as ANGPT1) might cluster TIE2 (also known as TEK) receptors of contacting ECs in trans124,125. b | The overexpression of ANG1 induces vascular remodelling that leads to the formation of vessels with a wider diameter. TIE2-mediated EC activation controls the expression of endothelial apelin, which in turn acts in an autocrine manner on EC-expressed G-protein-coupled APJ receptors, the downstream signalling of which contributes to the control of vessel diameter152. c | The quiescent EC phenotype is maintained by constitutive ANG1–TIE2 signalling. ANG1 clusters TIE2 junctionally at inter-endothelial cell junctions in trans to transduce survival signals. Differences in arterio-venous shear stress also control Ang–Tie signalling. During the transition from the quiescent to the activated phenotype, ECs liberate their endogenously stored pools of ANG2, and this antagonizes ANG1–TIE2 signalling to facilitate EC responsiveness to exogenous cytokines. As such, the absence or presence of stored ANG2 contributes to the control of the adaptive plasticity of the vascular endothelium. Image and caption adapted from [66]

ii Angiogenesis in wound healing and bone repair

The need of supply nutrients and oxygen to the tissues is fundamental for the proper development of the organism, from embryo to adult and in physiological and pathological conditions. Considering that the physiologic blood vessel formation has been previously described, henceforth, this thesis will be focused on the study of mechanisms for the reestablishment of tissue vascularization when damage is produced, especially in wound healing and bone fracture repair. Nevertheless, when an injured has appeared, there are several tissue-specific molecules released in the affected area also interacting in other processes such as the formation of new vessels. The relation between the most important angiogenic factor, VEGF, with the processes described above as well as the role of specific tissue factors on angiogenesis, will be explained below.

• Implication of angiogenesis in wound healing

Wound regeneration without angiogenesis would be inconceivable, being the formation of new blood vessels an indispensable component to restore the normal status of skin. As a dynamic process, wound healing involves complex interactions of ECM molecules, surrounding cells, leukocytes and soluble mediators which common goal is to achieve tissue integrity and homeostasis [67]. From hemostasis to tissue remodeling through inflammation and tissue formation, all of these phases present specific contributions on blood vessel growth and remodeling, summarized in Figure 1.10 [67]. The new vasculature acts as a source of nutrients and oxygen, also removing the waste products for the developing of granulation tissue [68]. Its name derives from the granular visual appearance being this new stroma, also known as neostroma, appeared during the early phase of cutaneous wound repair[69].

As this Figure 1.10 shows, there are many molecules released in the wound site exerting different actions on sprout development. For instance, VEGF -released in the injury site by ECs, fibroblasts, smooth muscle cells, platelets, neutrophils and macrophages [70]- is the most important and well-studied proangiogenic factor defined as essential for proper wound healing [71,72]. It presents direct and indirect effects in wound angiogenesis, increasing the vascular permeability while promotes the migration and proliferation of ECs. Figure 1.11 shows the main regulator effects of this molecule on angiogenesis.

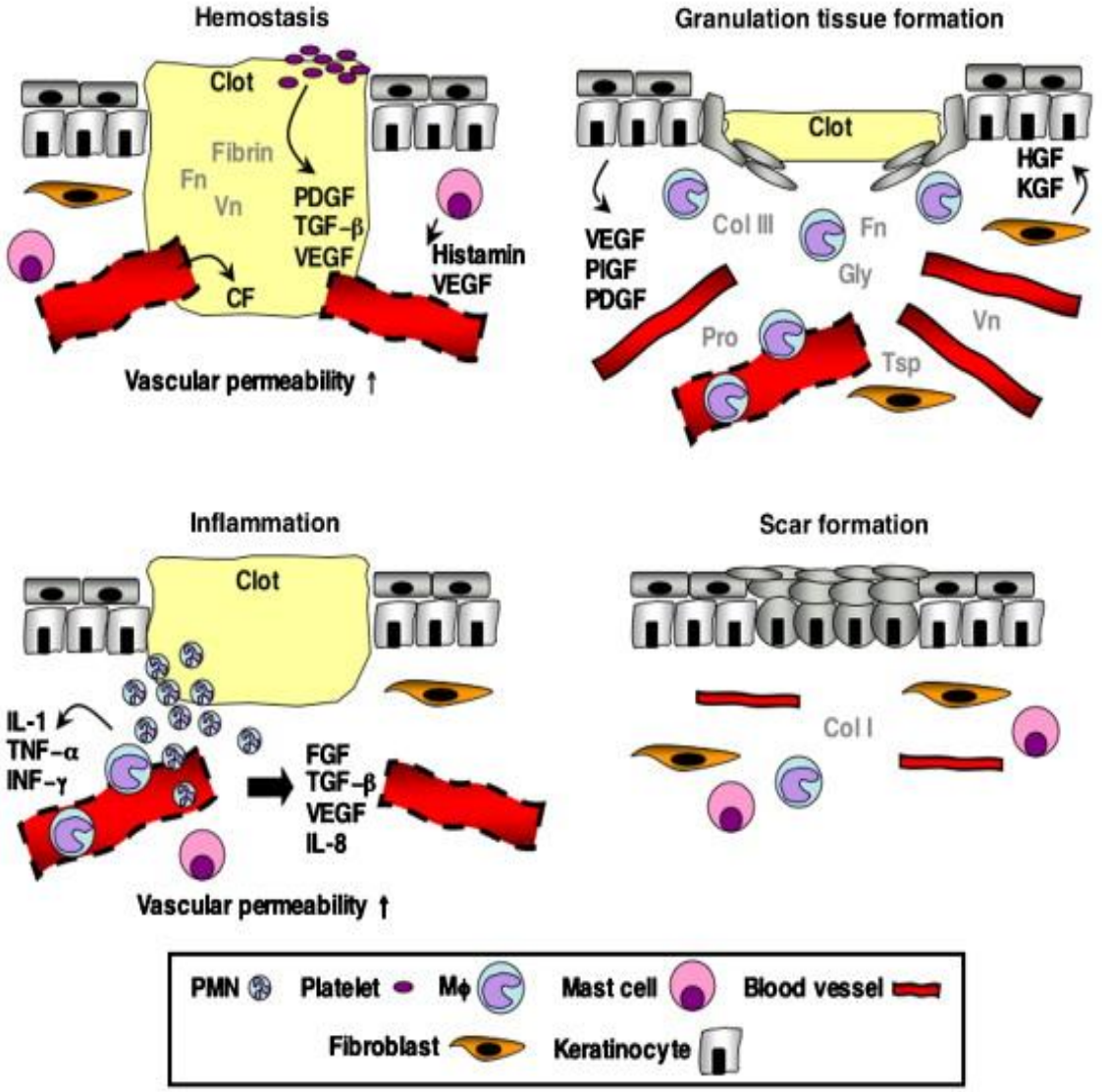

Figure 1. 10 Model of different phases of wound repair and their impact on angiogenesis.

Hemostasis is caused by leak of blood constituents and vasoactive factors into the wound site. Increased vascular permeability contributes to leaking of blood constituents into the wound environment. The hemostatic plug consists of platelets and ECM molecules (Fn, fibronectin; Vn, vitronectin), which facilitate invasion and migration of endothelial cells. Influx of PMNs (Polymorphonuclear leukocytes, neutrophils) and Mϕ characterize the inflammatory phase of repair; different subsets of leukocytes release angiogenic growth factors and pro-inflammatory cytokines, which control the recruitment of inflammatory and endothelial cells into the wound site. During granulation tissue formation activated Mϕ, endothelial cells and fibroblasts form a functional unit essential for efficient blood vessel growth. Fibroblasts deposit a complex provisional wound matrix consisting of glycosaminoglycans (Gly), proteoglycans (Pro), collagen III (Col III), thrombospondin (Tsp), Fn, and Vn, which promote endothelial tube formation and vessel growth. Transformation of granulation tissue into scar tissue is characterized by regression of capillaries and differentiation of newly formed blood vessels into mature vascular structures. This process is associated with a decrease in inflammation, presence of myofibroblasts and substitution of the provisional wound matrix into a collagenous matrix (CF, coagulation factors). Figure and caption taken from [67]

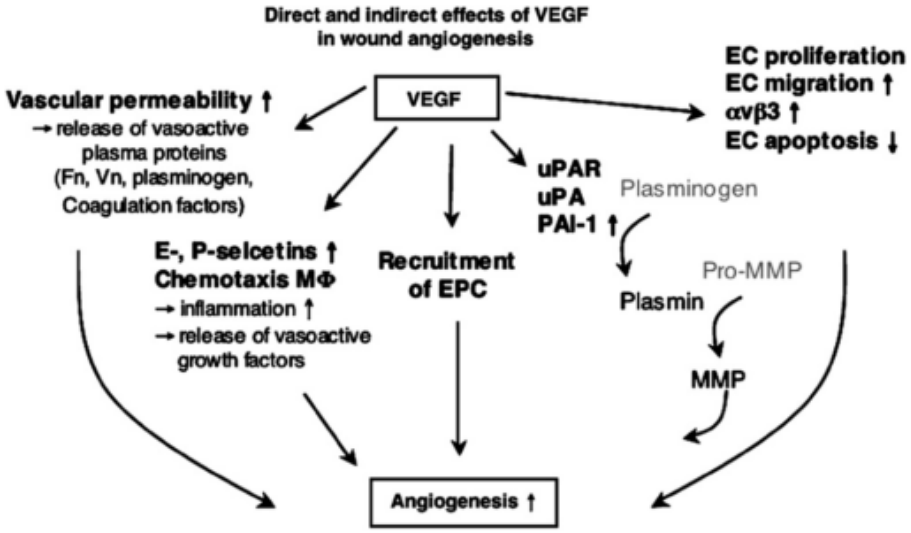

Figure 1. 11 Direct and indirect effects of VEGF on wound angiogenesis.

VEGF family members orchestrate complex interactions between extravasated plasma proteins and endothelial cell proteins during wound angiogenesis. (EPC, endothelial progenitor cell; uPAR: urokinase plasminogen activator receptor; uPA: urokinase plasminogen activator; PAI-1, plaminogen activator inhibitor-1; EC, endothelial cell). Figure and caption taken from [67]

Many different growth factors and inflammatory cytokines are released by platelets, such as platelet-derived growth factors (PDGF), transforming growth factors-beta (TGB-β), fibroblast growth factor (FGF) among others [73]. PDGF and TGF-β secretions seem to have indirect effects on wound repair through the promotion of vessel growth [74]. Involving in production of ECM components as well as in cell proliferation and migration, PDGF and TGF-β plays a remarkable role on wound angiogenesis [75]. In Chapter 2, the effect of these proteins on sprout formation and promotion will be deeply studied.

- Key role of angiogenesis in fracture healing

Following bone injury, the tear of cortical bone, periosteum and surrounding soft tissues also affects to numerous blood vessels, becoming in a hypoxic site. Disruption of blood vessels leads to activation of the coagulation cascade and the hematoma formation which finally will be turned into new bone [76]. Furthermore, the lack of nutrients and oxygen in tissues around the gap fracture encourages the appearance of necrosis in the area, inducing an inflammatory response [77]. Inflammatory cells, leukocytes and macrophages migrate to the region as well as fibroblasts, mesenchymal stem cells and endothelial cells [78,79] invade the area releasing GFs and cytokines [76,78]. Along the last decades, some works have proven the importance of bone vascularity for the tissue reestablishment, suggesting the existence of a vascular stimulating factor which operates

at bone injury [76]. Henceforth, this section will be focused on GFs role, the corresponding phases of bone fracture healing will be explained in detail in point 1.1.3.3.

Among the important regulators released during the healing process, VEGF production seems to be the coupling mechanism between angiogenesis and osteogenesis [78,80,81]. In the same way that VEGF induces endothelial cell proliferation or migration, it regulates the recruitment, survival and activity of osteoclasts and osteoblasts [78,81–83]. In addition to its essential role for normal angiogenesis, callus architecture and mineralization, VEGF is also involved in cartilage maturation and resorption, initiating the endochondral ossification by recruiting and/or differentiation of osteoblasts [78,81,84].

During the course of healing, several GFs are secreted such as fibroblast growth factors, platelet-derived growth factors, transforming growth factors-betas, vascular endothelial growth factor or bone morphogenetic proteins (BMP) [85]. For instance, Deckers et al. indicated that the stimulation of angiogenesis is induced by VEGF-A, molecule produced by osteoblast in response to BMPs [86]. This premise has been reaffirmed by others authors such as Eckardt H. et al. who suggested an intimate interplay between angiogenesis triggered by VEGF and BMPs in the formation of bone, also inducing direct activation of osteoblasts [87].

Considering the effect that VEGF exerts on osteoblasts and other surrounding cells, the aim of this work is focused on the effect that BMPs could have on ECs migration, mainly in the initiation of early sprouting.

1.1.3.2 Wound healing

In this section, the process of regeneration of a wound, its phases and the most relevant mechanisms involved will be discussed in depth.

Epidermis and dermis are the main layers which comprise the skin, the largest organ in the body. As the outer layer, epidermis acts as a barrier against water loss and infections whereas dermis contains blood vessels that supply oxygen and nutrients to the tissue, also removing the metabolic waste products [88]. Basement membrane separates the underlying dermis to the epidermis (see the skin structure in Figure 1.12).

When an injury occurs, the healing pathway is usually divided in four interconnected and overlapping stages: hemostasis, inflammation, proliferation and remodeling, involving a complex series of reactions and interactions between cells, extracellular matrix and molecular mediators [88–90]. Table 1.1, summarizes the main phases and their corresponding cellular and biophysiological events during wound healing [91].

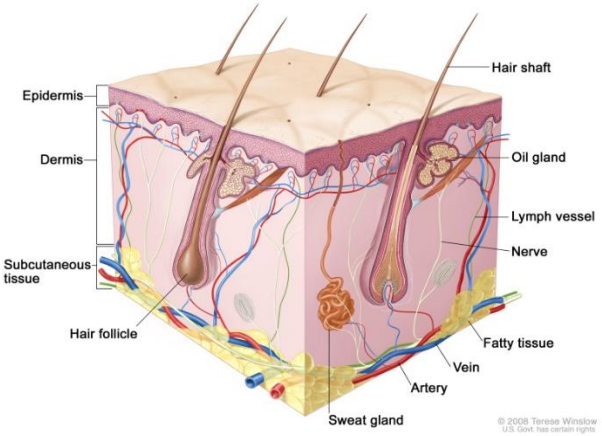

Figure 1. 12 Anatomy of the skin, showing the epidermis, dermis, and subcutaneous tissue.
Figure taken from National Cancer Institute ((http://www.cancer.gov))

PHASE	CELLULAR AND BIO-PHYSIOLOGICAL EVENTS
HEMOSTASIS	Vascular constriction Platelet aggregation, degranulation, and fibrin formation (thrombus)
INFLAMMATION	Neutrophil infiltration Monocyte infiltration and differentiation to macrophage Lymphocyte infiltration
PROLIFERATION	Re-epithelialization Angiogenesis Collagen synthesis ECM formation
REMODELING	Collagen remodeling Vascular maturation and regression

Table 1. 1 Normal wound-healing process. ECM, extracellular matrix.
Adapted from Guo and Di Pietro, 2010. Taken from [91]

Dermal tissue disruption involves the rupture of many capillaries or blood vessels. In the first stage of healing, called hemostasis, the body reacts to prevent blood loss through vascular constriction and clot formation. The intrinsic coagulation pathway begins with the recruitment of platelets and activation of fibrinogen to form a fibrin mesh by endothelial activated vasoconstriction followed by the coagulation cascade, in which numerous factors are involved. This provisional matrix made by collagen, thrombin and fibronectin allows cell migration and traps platelets with the consequent secretion of growth factors and pro-inflammatory cytokines [92]. In the same way, this causes a chemo-attractive effect to recruit more platelets, neutrophils and fibroblasts [89].

Once the blood loss has been interrupted, the inflammatory response begins (Figure 1.13-B), characterized by an influx of immune cells such as neutrophils, lymphocytes and monocytes,

which will then differentiate into macrophages. During this stage, macrophages are attracted by chemoattractants released by platelets at the wound site such as TGF-β, PDGF, interleukina 1 (IL-1). Before the proliferation phase, macrophages at the damaged area phagocyte bacteria, debris or apoptotic cells, leaving the area ready for epithelization [89].

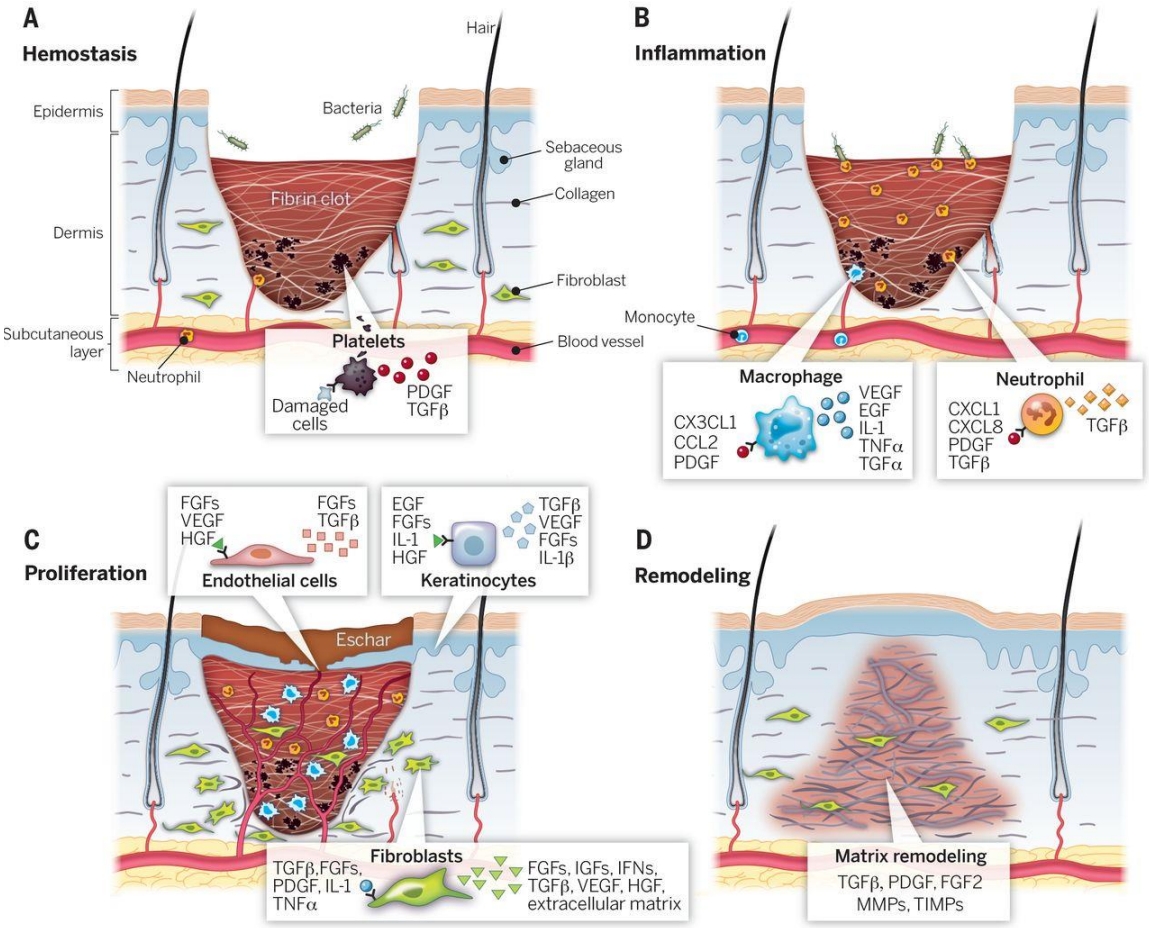

Figure 1. 13 . Stages of wound healing.
Wound healing is classically divided into four stages: (A) hemostasis, (B) inflammation, (C) proliferation, and (D) remodeling. Each stage is characterized by key molecular and cellular events and is coordinated by a host of secreted factors that are recognized and released by the cells of the wounding response. A representative subset of major factors are depicted. PDGF, platelet-derived growth factor;TGF, transforming growth factor; FGFs, fibroblast growth factors; IL-1, interleukin-1; TNF, tumor necrosis factor; KGF, keratinocyte growth factor; IGF, insulin-like growth factor; IFN, interferon; VEGF, vascular endothelial growth factor; HGF, hepatocyte growth factor; MMP, matrix metalloproteinase; TIMP, tissue inhibitor of metalloproteinase. Figure and caption taken from [93]

Fibroblasts also migrate from the surrounding undamaged ECM to the affected area for synthesis, deposition and remodeling of ECM during the proliferation phase [94]. Matrix proteins, such as collagen or fibronectin, act as substrate for cell movement and support for tissue integrity restoration [95]. Therefore, fibroblasts, the main cell type during the proliferation phase, are crucial for tissue restoration through collagen production- the main component of ECM and scaffold for vascular network expansion. Together with macrophages, they release growth factors that promote

the stimulation of other cell types such as keratinocytes and endothelial cells [89]. Both cell types form part of the granulation tissue that replaces the provisional ECM few days after injury [96].

Thus, macrophage-derived growth factors (MDGFs), endothelial growth factors (EGFs), VEGFs and TGF-β are some of the growth factors released at the wound site during this phase promoting the recruitment of more macrophages and fibroblasts. The release of growth factors by keratinocytes, among other cell types, stimulates the release of proteases into the endothelial cells (ECs) of surrounding tissue [89]. Through proteolytic degradation of the basal membrane and ECs stimulation promoted by GFs such as VEGF or TGF-β, these cells begin to reorganize and form capillary sprouts. The angiogenic process, strongly regulated by growth factors, cytokines and inhibitors, enhances tissue recovery by providing oxygen to the wound bed with the formation of new blood vessels. The phases so far mentioned comprise the first weeks after the damage has occurred. However, the remodeling phase comprises several months (see the timeline in Figure 1.14). Initially, fibroblasts replace the fibrin mesh formed during the hemostatic phase with collagen matrix, which will be subsequently remodeled and reorganized. In this phase, fibroblasts, induced by mechano-chemical signals, differentiate into myofibroblasts aligning along the new ECM and causing wound contraction.

Over the last few years, several studies have been focused on understanding the interactions between GFs and ECM in the wound regeneration process playing both a fundamental role in the tissue restoration. *In vivo* and *in vitro* models have been proposed to investigate some of the mechanisms involved, in order to delineate the complex interactions between cells- matrix-molecules in the wound site. These new perspectives are necessary for the achievement of more effective therapies in physio-pathological processes

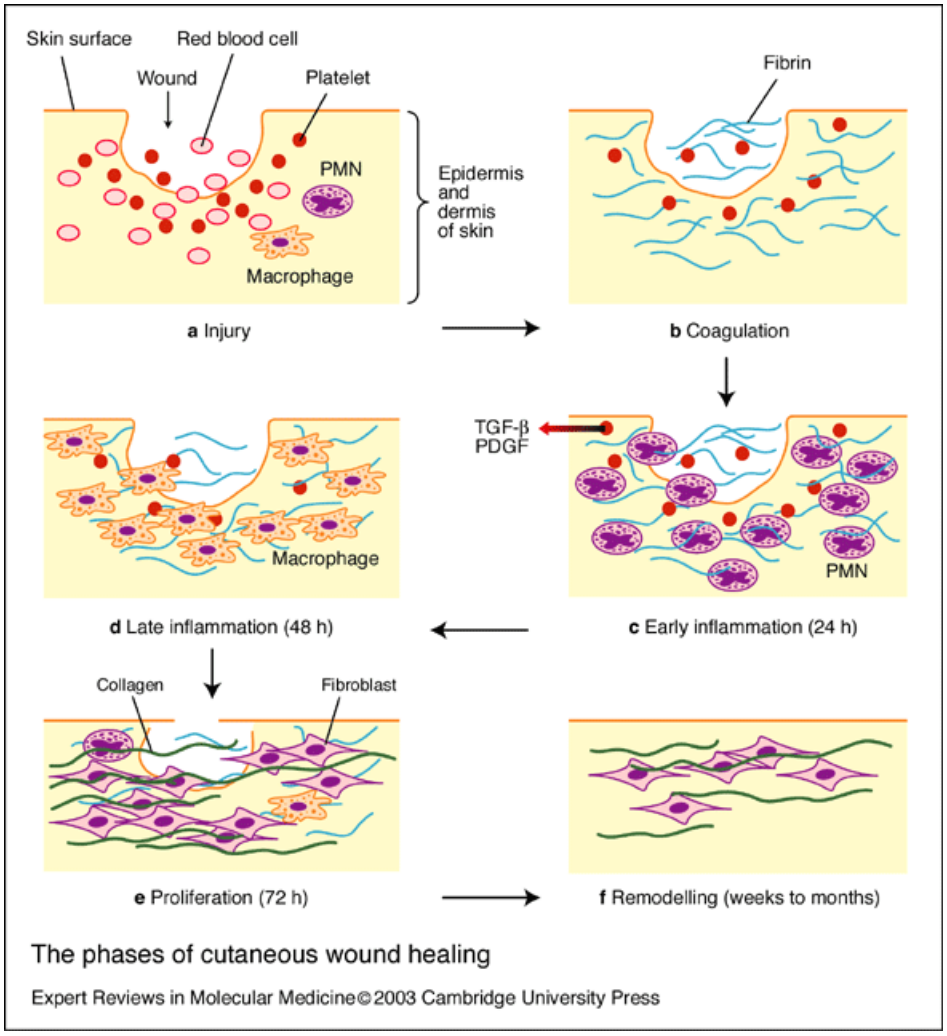

Figure 1. 14 Wound healing phases and their time progression.
Figure taken from Expert Reviews in Molecular Medicine © 2003 Cambridge University Press.

1.1.3.3 Bone regeneration

Bone is a highly specialized tissue in the human body exerting important functions on locomotion, support and protection of soft tissues; calcium, phosphate and growth factors storage and harboring of bone marrow [97,98]. The physiological structure of bone is represented in Figure 1.15-A.

Bone is a self-supporting tissue, regenerating itself in response to an injury –bone fracture healing- and in maintaining bone strength and mineral homeostasis -bone remodeling. Figure 1.15 summarized both processes which will be briefly explained below.

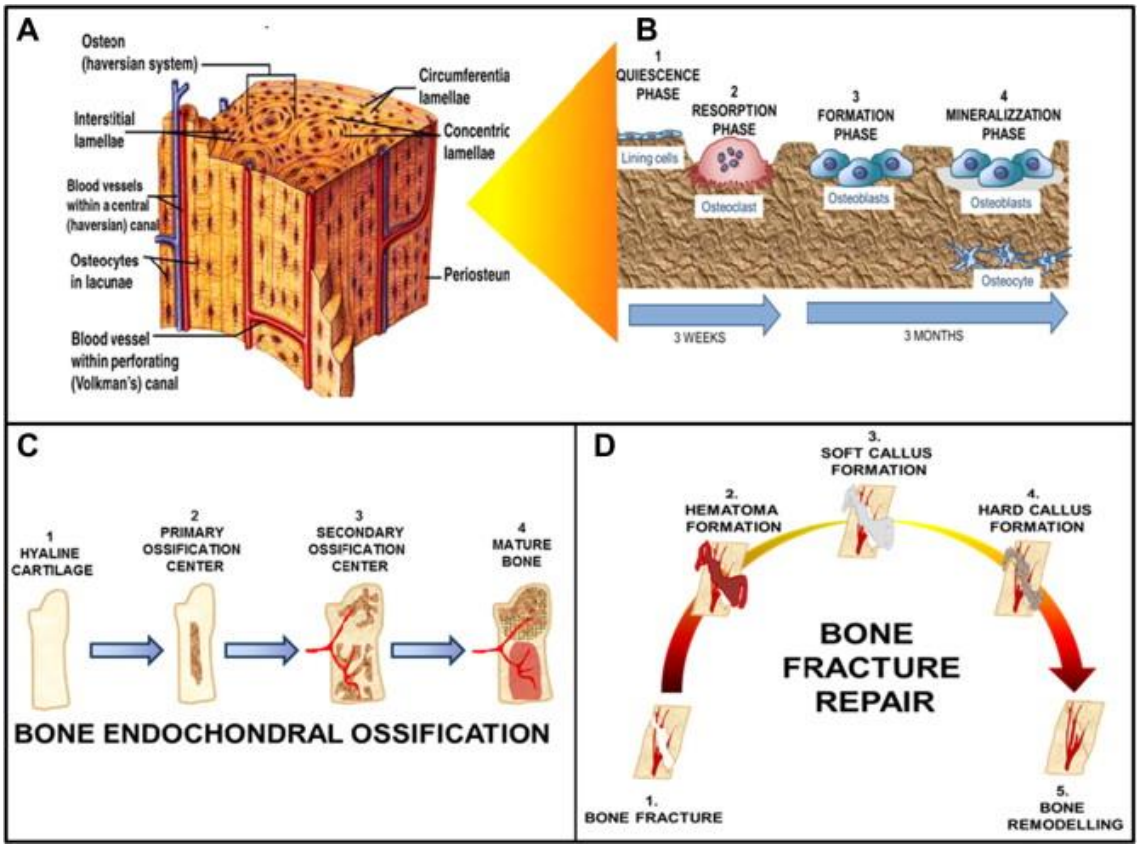

Figure 1. 15 Summary of bone regenerative processes.
(A) Anatomical illustration of bone vasculature adapted from [http://www.anatomiahumana.ucv.cl/kine1/top2.html]. (B) Adult bone undergoes constant remodeling to maintain their structural integrity. This process consists of an osteoclast - mediated bone reabsorption and osteoblast-mediated new bone formation and mineralization phase. (C) Endochondral model of bone formation during embryo development. At first the hyaline cartilage substitutes as the new bone structure. The central hypertrophic chondrocytes start degenerating and the matrix surrounding them begins to calcify the future diaphyseal area forming the primary ossification center. Complete degeneration of the central area and calcification of the matrix results in formation of the secondary ossification center. Vascular penetration into the secondary structure initiates osteogenesis by supplementing the area with osteoprogenitor cells, chondroclasts, and hematopoietic cells, resulting in the formation of the mature bone. (D) Schematic representation of events mediated during bone fracture repair. Figure and caption taken from [99]

i Bone remodeling

Physiologically, remodeling process allows the repair of old and damaged bone adjusting the bone architecture to changes in external loading. This connective tissue is formed by four types of cells: osteoblasts, bone lining cells, osteocytes and osteoclasts, with crucial functions for tissue regeneration, interacting with other cell types such as macrophages. The physiological process of bone formation consists of several stages (represented in Figure 1.16) which will be briefly described below.

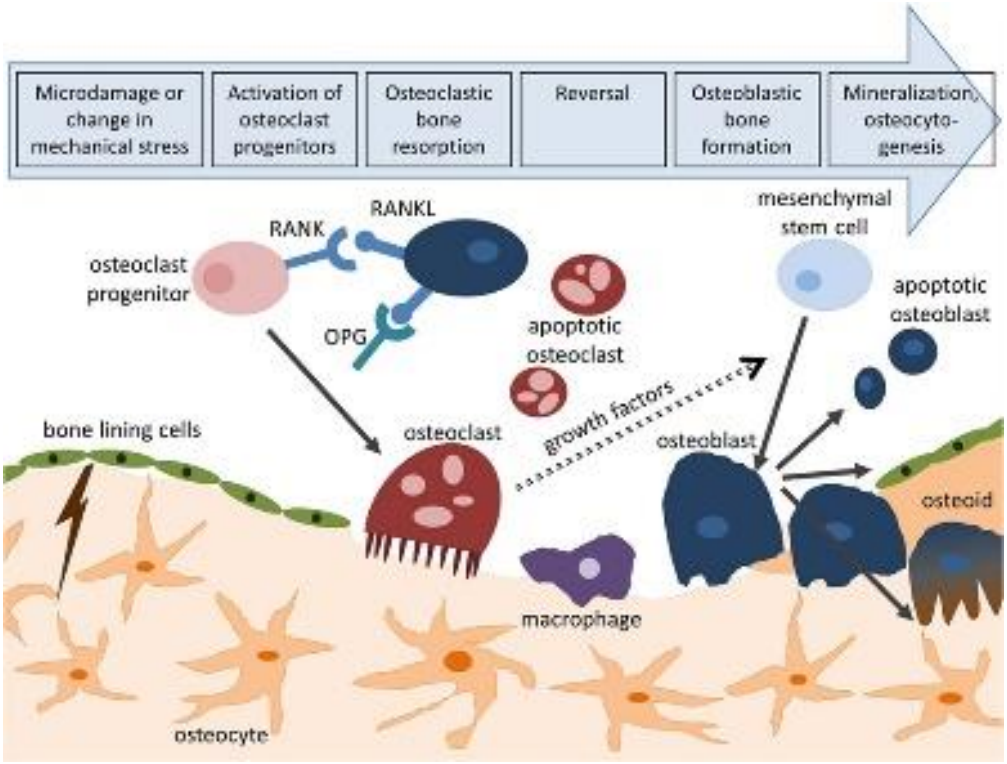

Figure 1. 16 Bone remodeling cycle.
Bone remodeling is initiated by microcracks or changes in mechanical loading and consists of four consecutive steps: activation, resorption, reversal, and formation. Activation of osteoclasts is controlled through the RANK/RANKL/OPG pathway. Following bone deposition, osteoblasts can differentiate to osteocytes (osteocytogenesis), turn to bone-lining cells, or enter apoptosis. Figure and caption taken from [97]

The bone remodeling cycle comprises three phases starting with the bone resorption by osteoclasts, the period from resorption to new bone formation and finally, the bone formation by osteoblasts [98].

Focusing on osteoblasts, they are exposed to the mechanochemical signals of the microenvironment being able to alter their responses accordingly and depositing new matrix which becomes mineralized [100,101]. Comprising 4-6% of cells located along the bone surface, osteoblasts present a cuboidal shape and morphological characteristics such as an abundant rough endoplasmic reticulum and prominent Golgi apparatus accompanied by several secretory vesicles [98]. The deposition of organic matrix (mainly type I collagen) by osteoblast, is the first step to synthesize bone matrix followed by its mineralization in the vesicular and fibrillar phases [98]. Osteoblast migration towards the damage area to complete the remodeling process is essential for the reestablishment of the tissue [102].

Bone homeostasis as well as the bone mass balance is maintained by the relation between osteoclastic bone resorption and osteoblastic bone formation, with the consequent calcium release and deposition regulated by mechanochemical signals, maintaining bone mass at steady-state levels [101,103]. The bone regenerative process begins with the differentiation and maturation of osteoblast precursors into osteoblasts capable of secreting collagen which will be mineralized to generate new bone [104]. Defined as a dynamic and complex structure that adapts to the changes

in its functional environment, bone presents a mechanism by which its cells sense the deposition or resorption of bone tissue and it has not been determined completely [105]. Mechanical loading is crucial in bone formation stimulating the osteoblastic differentiation and proliferation [106,107] and it has been widely accepted through different theories (experimental and theoretically) about in the lacunar-canalicular system of bones by many authors [105,108–111].

ii Bone fracture healing

Following bone fracture, similar stages of embryonic skeletal development occur in the damage area, finalizing with the reestablishment of the tissue physiology [112,113]. Depending on its size and the amount of mechanical stability, the process can be differentiated such as primary or secondary healing [114]. In the first case, the gap size presents an extreme stability and a negligible affected area, while secondary healing implies moderate sizes and stability, occurring in the vast majority of bone injuries [112,115]. In addition, primary bone healing is characterized by the lack of callous formation and the consequent activity of osteoclasts and osteoblasts to reestablish tissue functionality. In contrast, the formation of soft callous is characteristic of secondary bone healing, where two modes of ossification are differentiated: intramembranous and endochondral. Intramembranous ossification is identified by the differentiation of mesenchymal stem cells into osteoblasts to directly create bone tissue in an anabolic process, while in the endochondral these cells will differentiate into chondrocytes that create cartilage tissue [114].

Secondary bone healing can be divided in four temporal phases: (1) inflammation, (2) callus differentiation or repairing, (3) ossification and (3) remodeling [115–117]. Immediately before the inflammation stage, fracture gap is filled with the blood lost from the breakage vessels. After the emergence of the inflammation and hematoma during the first stage (Figure 1.17), mesenchymal stem cells (MSC) will be differentiated into fibrous tissue, cartilage and, finally, bone in the damaged area, spurred by the release of biological factors such as transforming growth factor beta superfamily, bone morphogenetic proteins, interleukins (IL-6, IL17F, IL1β), among other proteins [99,118,119]. The formation of cartilaginous callus by skeletal and endothelial cells refills the gap between bone fragments, progressing to hard callus in the most common form of bone healing named endochondral ossification [114]. In the secondary fracture healing, the migration of osteoblasts is necessary, occurring both individually and collectively, to deposit new bone [120]. Via focal adhesions, osteoblasts recognize the substrates adhering to it and modifying their behavior depending on the matrix component architecture or the mechano-chemical stimuli applied [120]. Once the fracture gap has been ossified, the restoration of the bone architecture is recovered with the resorption of the external callus and the remodeling of disorganized woven bone by osteoclasts and osteoblasts.

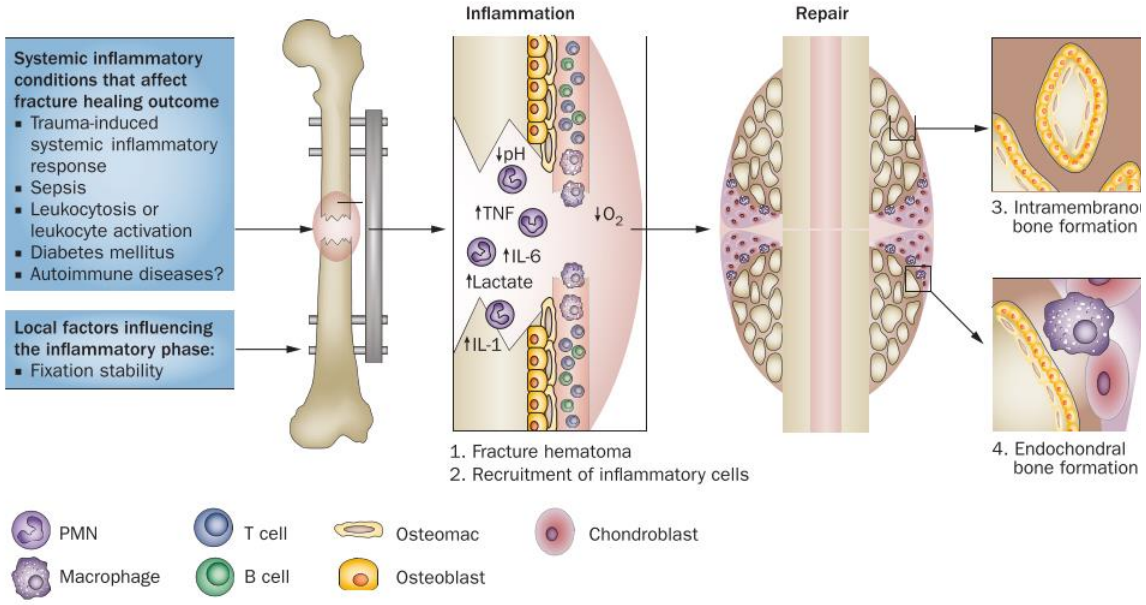

Figure 1. 17 Schematic representation of inflammation and repair during bone fracture healing.
Immediately after the initial trauma, the fracture hematoma is formed as a result of blood clotting. The fracture hematoma is characterized by hypoxia and low pH, and contains proinflammatory and anti-inflammatory cytokines together with inflammatory cells from the peripheral blood (1). During the initial inflammatory phase of bone healing, immune cells are rapidly recruited to the site of injury (2), neutrophils being the first cells to invade the callus, followed by macrophages and lymphocytes. During the repair phase, osteomacs are pivotal for osteoblast-driven mineralization in zones of intramembranous ossification (3), whereas inflammatory macrophages mainly contribute to endochondral bone formation (4). Several systemic (severe trauma, leukocytosis, diabetes mellitus and possibly autoimmune diseases) and local factors (fixation stability) affect inflammatory processes at the fracture site, and can result in impaired fracture healing. Abbreviations: PMN, polymorphnuclear neutrophils Figure and caption taken from [119].

Mechanical loading as well as other complex interactions among local and systemic regulatory factors such as growth factors or cytokines, are essential for proper bone function including the reestablishment of structural integrity in fracture healing [121,122]. To understand in detail the mechanisms involved in such process, experimental methodologies as well as computational simulations and modelling have been performed in order to design novel healing strategies for future treatments [115,117,123–125].

1.1.4 Methodology used in this work

This section has been specially designed to summarize the main techniques used in each chapter, highlighting the major handicaps found in each one.

The microfluidic technology used to perform the experiments in this thesis has allowed us creating and studying 3D cell culture microenvironments under different spatiotemporal chemical gradients, generating ECM interfaces and applying different mechanical stimulus.

The basal structure of these microfluidics chips, originally designed by Roger Kamm Laboratory [7] and implemented in our experiments as a collaboration between both research groups, consists of a central chamber where hydrogel is located and two adjacent channels for cell culture medium addition (see Figure 1.18).

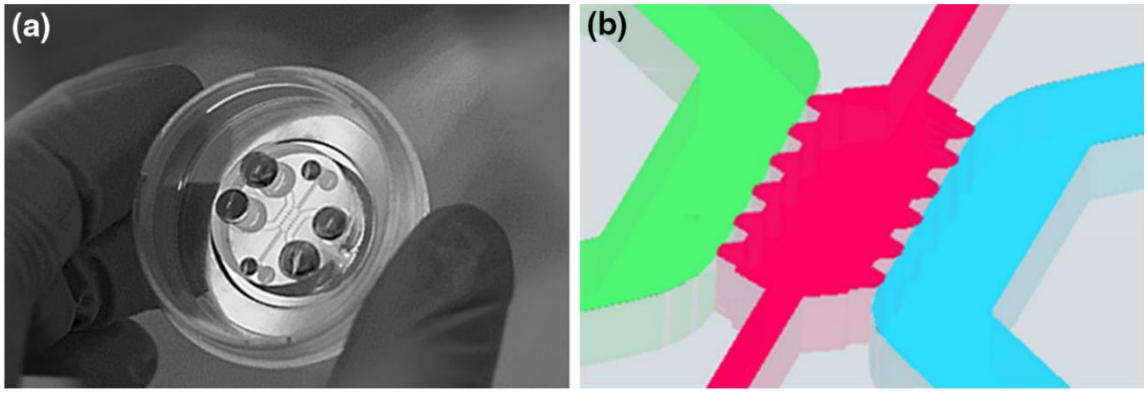

Figure 1. 18 Microfluidic platform
The microdevice fits within a 35 mm glass-bottom petri dish, as shown in picture (a). The detailed schematic (b) shows the geometry of the microfluidic device. The hydrogel is kept confined within the central channel (pink), whose dimensions are 2.5 × 1.3 mm. The auxiliary channels (pink) assist the hydrogel injection into the central cage. In direct contact to the gel, two main media channels (1 mm-width, green and blue) ensure hydration and diffusion through the hydrogel. The height of the channels is of 240 μm all over the geometry. Figure and caption taken from [126].

However, the versatility of this technology allows the user to manipulate this distribution in function of the experiments to develop. For instance, it can be adapted increasing the number of channels, the distance between them as well as the height in order to ensure a 3D cell distribution. One of the most important characteristic of chip geometry, which has been designed by Roger Kamm's Lab and maintained in every design, has been the hexagonal shape of the pillars. This particular distribution was proposed to confine the hydrogels through surface tension avoiding the hydrogel lost when it is hydrated.

The ***procedure for microfluidic device fabrication*** is explained below:

- SU8-wafer silanization by addition of 10 ul of perfluorinated trichlorosilane (UCT Specialties (T2492-KG)) during 2h in order to avoid the irreversible PDMS bonding to the wafer. Keep the wafer inside a desiccator during this protocol
- Addition of PDMS mixed by 10:1 base to curing agent ratio. For the first time, 90g of PDMS mixed was added while in following times the amount was reduced up to 30g in total (just for the drawn area).
- Degasification of the polymer before and after addition onto the silicon wafer
- Polymerization of PDMS into the oven at 80ºC overnight
- After the cool down and relax of the replica molded-layer of PDMS it can be extracted. The first layer after the treatment should be discarded due to its cytotoxicity
- For device individualization, different diameter punches were used. Depending on the device shape, round or rectangular punch has been utilized.
- Channel-inlet ports were also perforated with biopsy punches: 1.5 mm of diameter for gel-charge channel, 3 or 4 mm diameter for reservoirs.
- PDMS devices were autoclaved twice (first in humid cycle followed by dry cycle) in order to sterilize it. Then, they were incubated at 80ºC overnight for drying it.
- The irreversible bonding of chips was achieved through plasma treatment of cover-glass, for rectangular devices, or 35mm-glass bottom petri dishes, for round ones, followed by PDL (poly-D-lysine hydrobromide) solution addition to the channels in sterile conditions.
- Maintaining treated chips for at least 4 h into the incubator to enhance the hydrogel-PDMS surface attachment, they were thoroughly washed with cell culture grade water and dried again at 80 ºC for 48 hours approximately.
- Finally, the devices were cooled and ready to use.

1.2 Objectives

This thesis is aimed to investigate the role of mechanochemical factors on cell migration in tissue regeneration. Within the framework of the European Insilico-Cell Project (ERC), this work has tried to study the cell behavior by using microfluidic platforms that replicate more faithfully the *in vivo* conditions of cells in tissues. Angiogenesis, wound healing and bone fracture healing have been the three main lines of application, where the effect of chemical or mechanical factors has been studied in an individual or combined way in a single chip. Thus, this work aims to biomimetize the regenerative processes that commonly occur in the tissues of our body.

Based on the premises of previous studies about the most important factors involved in each of these processes, this work is organized in function of the stimulus gradient applied to the cell culture. Firstly, considering the importance of chemical gradients on angiogenesis, one chapter of this thesis is focused on unravelling how endothelial cell migration, specially sprouting promotion, could be affected by some GFs released in the damaged area in both processes. As a combination of the study of mechanochemical factors, specically matrix properties and chemotaxis, the other two lines of research were proposed. On one side, the effect of collagen gradients on fibroblast migration combined with chemotactic study, and on the other side, the osteoblast behavior when a flow rate is applied to the 3D culture in conjunction with changes in matrix stiffness and architecture.

Other relevant tasks have been developed in this work such as the development of new geometries designed specifically for the experiments, the numerical simulations to characterize fluid flow in the microfluidic devices, fluid-flow set-up as well as the introduction of new strategies of fabrication such as 3D printing technologies.

1.3 Thesis overview

This first chapter has offered a general framework along with a review of the state of the art of microfluidics and the main lines of research of this thesis: angiogenesis, wound healing and bone fracture regeneration. Based on the premises of previous studies about the most important factors involved in each of these processes, this work was organized in function of the stimulus gradient applied to the cell culture. Next, a brief description of each chapter is presented.

Considering the importance of chemical gradients on angiogenesis, Chapter 2 has been focused on knowing how endothelial cells migration, specially sprouting promotion, could be affected by some GFs released in the damaged area, creating a controlled chemical gradient.

On the other hand, the effect of the combination of 3D chemotaxis and durotaxis by collagen step gradients is analyzed. This Chapter 3 also includes the development of a new microfluidic device. This new design simplifies the usual mechanisms employed to quantify chemotaxis also bringing the option of hydrogel interface generation as well as the corresponding studies related to cell migration.

The effect of mechanical factors has been analyzed in Chapter 4. The combination of matrix architecture modification and fluid flow as well as its individual analysis will be the methodology proposed along this chapter to understand cell behavior simulating bone fracture healing.

In Chapter 5, the global conclusions of the previous chapter are summarized also combined with brief suggestions about possible future research lines. A special mention with the achievements obtained during the development of the thesis, such as scientific publications, contributions to congresses, or research stays have been included. A Spanish version of Chapter 5 has been included in Chapter 6.

A summary of all the contributions from this PhD Dissertation are presented in Chapter 7 (in both languages).

Finally, ELISA inmunoassays and its results are showed in the Appendix. To know the diffusion of our molecules through the hydrogel we have performed this inmunoassays. Several conditions have been tested for our microfluidic devices.

Chapter 2

Induction of angiogenic sprouts by means of growth factor gradients

Abstract *

Angiogenesis or neovascularization is the main dynamic process that culminates in sprout formation from existing vessels. As it has been described in the previous chapter, the blood vessels formation comprises a collective migration process of endothelial cells (ECs). After tissue injury, the vascularity is interrupted, triggering the regeneration process and the release of different growth factors (GFs). The main aim of this work is to quantify the effect of specific GFs during the initial stage of sprout formation, namely: vascular endothelial growth factor (VEGF), platelet derived growth factor-BB (namely as PDGF), human transforming growth factor- beta 1 (TGFβ) and bone morphogenetic protein 2 (BMP-2), all of them involved in regenerative processes. For this purpose, a novel algorithm implemented in MATLAB designed by the M2BE group has been used to quantify the advance of the endothelial cell (EC) monolayer over time and the sprout structure in 3D. Our results show that VEGF is the main regulatory GF on angiogenesis processes, producing longer sprouts with higher frequency. However, the chemoattractant effect of VEGF depends on its concentration and its spatiotemporal location, having a critical impact on the sprout time evolution. PDGF has a global negative effect on both the number and length of sprouts. TGFβ enhances sprout length at earlier times, although its effect gradually disappears over time. Finally, BMP-2 produces, overall, less number and shorter sprouts, but was the only GF with a positive evolution at longer times, producing fewer but longer sprouts.

Keywords: *Sprouting, Angiogenesis, Growth factors, Microfluidics, Collective Cell Migration*

This Chapter 2 corresponds to the article already published as:* ***C. Del Amo**, C. Borau, R. Gutiérrez, J. Asín, and J. M. García-Aznar,* ***"Quantification of angiogenic sprouting under different growth factors in a microfluidic platform****," J. Biomech., vol. 49, no. 8, pp. 1340–1346, May 2016.* [127]

2.1 Introduction

In Chapter 1, cell mechanisms involved in cell migration as well as the main regenerative process have been reported. The formation of blood vessels is a fundamental process, both in embryonic and adult stage, and it is involved in physiological and/or pathological processes. With high importance in metastatic processes, angiogenesis is also crucial in restoring normal tissue conditions when damage occurs. Regeneration processes take place in all living tissues after some injury or damage is produced. The reestablishment of the global vascular network and its connection with the damaged tissue is one of the first steps to restore the tissue functionality, involving several molecular mechanisms [72,128]. This current chapter has been focused on the study of sprout formation under GFs addition, characteristic of wound and bone regeneration.

Angiogenesis is the process of new blood vessel growth from preexisting ones [129–132] and it is mainly guided by VEGF (Vascular Endothelial Growth Factor) gradients, one of the most potent proangiogenic growth factors (GFs) [72,133,134], and other signals such as oxygen [135,136]. Chemotactic and polarizing effects of VEGF have been thoroughly analyzed in previous works [134] and its relevance inducing sprout formation have been confirmed by many research works [72,136–139].

Nevertheless, there are other GFs implicated in tissue vascularization such as Human Transforming Growth Factor- Beta (TGFβ), Human Platelet Derived Growth Factor-BB (PDGF-BB, henceforth referred in this Thesis as PDGF) and Bone Morphogenetic Proteins (BMPs) among others. For instance, PDGF is implicated in osteogenesis, acting as mitogen for osteoblast and increasing VEGF expression [131]. The secretion of PDGF in fracture healing contributes to marrow stromal cells recruitment, which may in turn increase the liberation of other angiogenic factors [140,141]. Additionally, PDGF stabilizes blood vessels by recruiting of pericytes, whereas VEGF promotes endothelial cell (EC) growth [142]. Regarding TGFβ, its proangiogenic effect depends on assay conditions. In vivo, TGFβ contributes to the stimulation of macrophages which release angiogenic factors, whereas in vitro, TGFβ inhibits the ECs growth and proliferation, thus decreasing the sprout formation [69]. The main factor involved in bone regeneration is BMP-2 (Human Bone Morphogenetic Protein 2), which affects EC proliferation and migration [143] and promotes the chemotaxis and differentiation towards the osteogenic pathway [144]. Table 2.1 shows a summary of the main impact of the GFs on tissue regeneration.

As section 1.1.1 has described, microfluidic systems have emerged as potential tools to recreate aspects of cell migration or tissue organization. These devices have gained great popularity due to the easy reproduction, control and monitoring of a wide variety of microenvironmental factors. In this work, this technology has been used to reproduce fundamental aspects of angiogenesis, such as those presented by Jeon et al. and Zervantonakis et al. to simulate wound healing or tumor growth [25,145]. Other works using similar microdevices have been focused on regeneration processes such as the generation of 3D capillary beds in vitro [146], anti-angiogenesis drug screening [147] or on cellular dynamics to analyze cell migration in sprouting processes [46].

Growth Factor (GF)	Characteristics	Effects	References
Vascular Endotelial Growth Factor (VEGF)	Some isoforms: VEGF-A, VEGF-B, VEGF-C, VEGF-D and PlGF(placental growth factor) *VEGF-A: homodimer with a molecular weight of 40kDa and 165 amino acid residues/ subunit.*	Cell Proliferation, migration, differentiation Increasing of vascular permeability, formation of new blood vessels	[69,139,148]
Human Platelet Derived Growth Factor-BB (*PDGF-BB*)	Protein of 24.3 kDa, a disulfide-linked homodimer of two chains of 218 amino acids	Cell proliferation, angiogenesis and fibrosis Recruitment and proliferation of pericytes during angiogenesis	[149,150]
Human Transforming Growth Factor-Beta 1 (*TGFβ1*)	Protein of 25kDa synthesized by human platelets, has a central role in cell growth regulation, differentiation and function.	Cell proliferation, migration and capillary tube formation	[143,150]
Human Bone Morphogenetic Protein (*BMP2*)	Protein with 26kDa belonging to TGFβ superfamily	Bone formation Growth, differentiation, chemotaxis and apoptosis.	[144,151,152]

Table 2. 1 Summary of the impact of different GFs on cell and tissue behavior.

By complementing the advantages of microfluidics, the high versatility of PDMS to design different cell culture platforms and protocols has allowed the analysis of molecular signalling involved in angiogenesis in previous studies [153]. However, to the best of our knowledge, none of them have analyzed under similar conditions the temporal effect of several GFs on angiogenesis. The main aims of this work have been:

1. To quantify the capacity of four different GFs involved in angiogenic processes (namely VEGF, PDGF, TGF, and BMP-2) by using a collagen type I scaffold as a replicate of the ECM microenvironment

2. To evaluate the angiogenic effect on the ECs monolayer by measuring the frequency and the length of the formed sprouts during 24 hours.

2.2 Materials and methods

2.2.1 Microfluidic device

In order to study the evolution of EC monolayer, the geometry and fabrication of microdevices used in this experiment was based on the methods implemented by Farahat et al. [138]. These devices present a central chamber filled with hydrogel, and two lateral channels for cell seeding (EC channel) and the supply of different growth factors (GF channel) (see Figure 2.1 for geometric details).

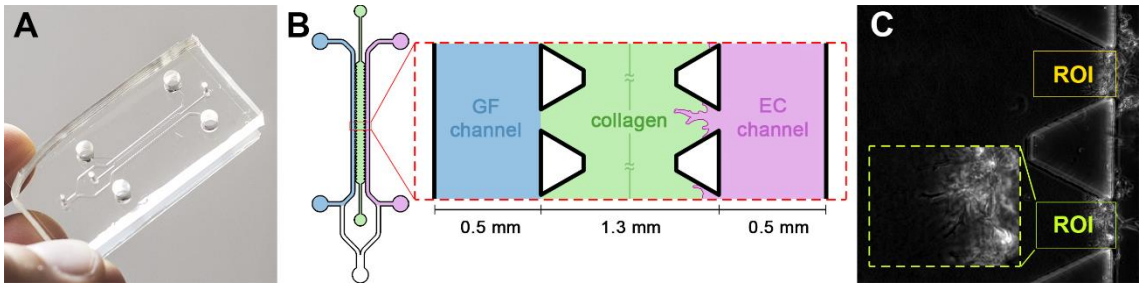

Figure 2. 1 Microfluidic device for sprout analysis.
A) Self-made microfluidic device prototype used in our assays. Geometry was obtained from the work of [138]. B) Top view and inset of the device geometry with a central chamber (green) and two lateral channels (blue: growth factor (GF channel), pink: endothelial cell seeding (EC channel)). Channel and pillar heights (and therefore gel thickness) are 120 microns. C) Example image from the experiments: cells forming sprouts between two micropillars of the device. Yellow and green windows are the actual regions of interest (ROIs) submitted to analysis

2.2.2 Collagen hydrogel scaffold in a microfluidic assay

Collagen is the most abundant fibrous protein in the extracellular matrix, existing at least 16 different types, but being the most predominant types I, II and III [154]. Although other fundamental proteins such as fibrin or laminin constitute ECM, collagen (presents on muscle, bone, skin or blood vessels) has been the hydrogel selected for the experiments performed along this Thesis. The collagen hydrogel was prepared from type I collagen gel solution (Corning Collagen I, Rat Tail. 3mg/ml) at 2.5 mg/ml following the methodology proposed by Farahat et al. and Zervantonakis et al. [25,138], with phosphate buffered saline (PBS; Lonza), NAOH and EGM2 (Endothelial Cell Growth Media, Lonza). It was softly pipetted into the devices and polymerized for 40min in a humid chamber, at 37º C and 5% CO_2. After that, the matrix was hydrated and incubated overnight at the same conditions. The mechanical properties of 2.5 mg/ml collagen gels have been characterized in literature [155–157], presenting a storage modulus G' ~ 18 Pa. In regards to the transport properties of these gels, and according to the measurements of Farahat et al.[138] , GF concentration decreases almost linearly from the source channel and across the collagen, with a diffusion coefficient of $5 \cdot 10^{-11}$ m^2/s. Using the same protocol, Zervantonakis et al. found the diffusive permeability to range from $0.75 \pm 0.093 \cdot 10^{-7}$ m/s to $4.08 \pm 1.11 \cdot 10^{-7}$ m/s [25]. Furthermore, the characterization of molecules transport in the geometry used in this experiment can be found in the

work previously published by Farahat et al. (see Figure 2.2) [138]. Another example of quantification of chemical gradients in collagen by using microfluidic devices has been reported by Moreno-Arotzena et al [158].

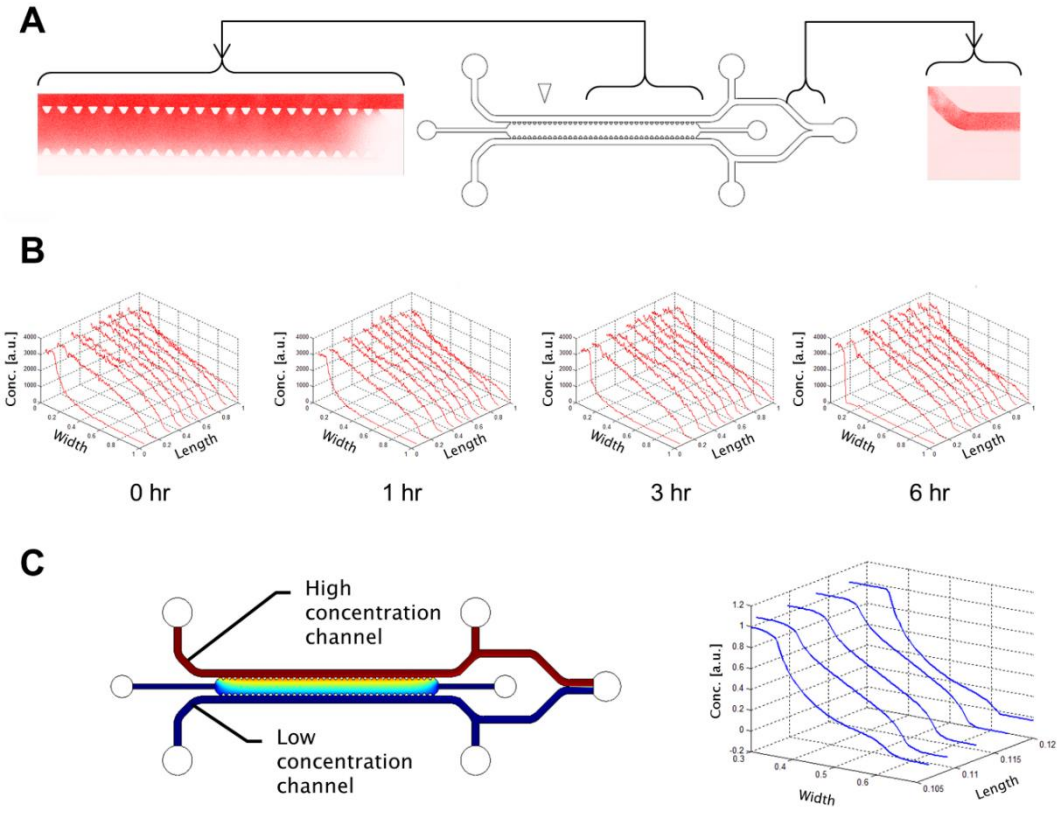

Figure 2. 2. Characterization of device transport characteristics in the absence of monolayers. Characterization was done via Texas Red conjugated 40 kDa Dextran in lieu of VEGF (which has a molecular weight of 38 kDa) A) Gradients are estimated via fluorescent intensity measurements along the entire gel region B) The generation gradients that are stable in time when device is under flow of 2 µL/min. Gradients are shown stable over a 6 hour time period. C) Numeric simulations reveal concentration profiles along the length of the channel, and confirm gradient profiles similar to those observed experimentally. Figure and caption taken from [138]

2.2.3 Cell culture and seeding

For the formation of the monolayer, Human Umbilical Vein Endothelial Cells (HUVEC, C2519A, Lonza) in passages 3-8 and 70-90% confluence were seeded in the microfluidic devices with a concentration of $1.5 \cdot 10^6$ cell/ml. Endothelial cell growth basal media (EGM-2, Lonza) was used as cell culture medium.

Firstly, EGM2 was used to equilibrate the microdevices, which had been treated in the previous 24 hours, and incubated them for 2 hours. Secondly, 20 µl of ECs suspension were filled by a previously dried lateral channel (Figure 2.3A). The seeded devices were placed in a humid box for 40 min and oriented vertically to promote the deposition of cells on the collagen hydrogel (Figure 2.3B). After cell incubation, the EC channel was washed to remove the surplus cells, hence leaving a monolayer (Figure 2.3C). Finally, the growth factors were added at the GF channel. Conditions used in each assay are shown in Table 2.2.

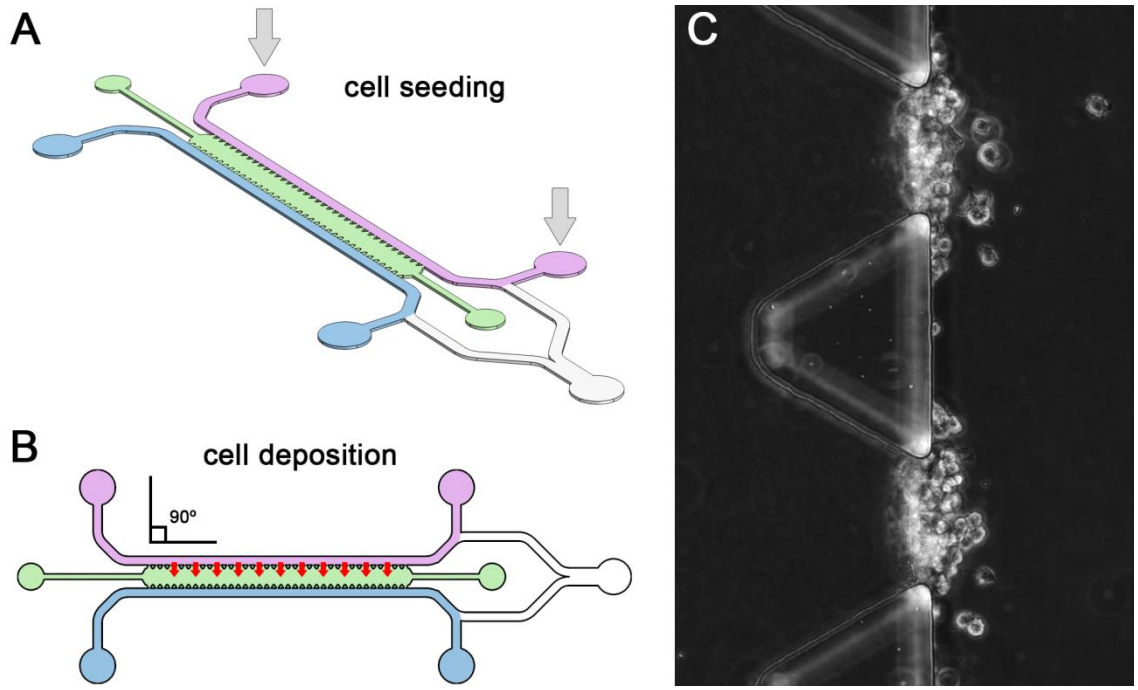

Figure 2. 3 Endothelial cell seeding procedure for monolayer formation.
A) 3D representation of the microdevice. Endothelial cells are seeded through the input channels pointed by the gray arrows. B) After cell seeding, the microdevice is tilted 90º (oriented vertically) to promote cell deposition to the collagen. C) Once the monolayer is formed, surplus cells are washed so that only cells stuck to the collagen remain. These are the initial conditions for every assay before image acquisition.

Condition	GF channel	EC channel	References
0-0	EGM-2*	EGM-2	--
0-vegf	EGM-2	40ng/ml [VEGF]	[147]
vegf-0	40ng/ml	EGM-2	--
vegf-vegf	50ng/ml [VEGF]	40ng/ml [VEGF]	[159]
tgfb-vegf	10ng/ml [TGFβ]	40ng/ml [VEGF]	[160]
pdgf-vegf	10ng/ml [PDGF]	40ng/ml [VEGF]	[160]
bmp-vegf	2ng/ml [BMP-2]	40ng/ml [VEGF]	[161]

Table 2. 2 Different GFs conditions found in the literature that have been applied in microfluidics-based experiments of angiogenesis
Concentration of GFs at each channel. *EGM-2: Endothelial cell growth media

2.2.4 Design of experiment

The experiment was designed to obtain enough samples for each condition so that the statistical analysis was able to distinguish specific effects of the different GFs. Application of VEGF only in the EC channel was chosen as the reference/control condition (0-vegf). Each additional condition (vegf-vegf, tgfb-vegf, pdgf-vegf, bmp-vegf) was replicated 4 times, always accompanied by a control experiment (0-vegf). Finally, to isolate the effects of VEGF and complete the study, 2 replicates of the null condition (0-0) and 2 of the control-inverted condition (vegf-0) were performed (See Table 2.3).

Condition	#replicates	#ROIs	#sprouts	%length>30	Length (µm)		
					Mean	*sd*	*Skweness*
0-0	2	22	22947	2.7	9.01	8.66	3.65
0-vegf	16	66	90814	13.9	16.48	18.72	2.67
vegf-0	2	16	23260	28.7	25.79	25.76	2.02
vegf-vegf	4	25	26255	13.4	16.77	18.56	3.28
tgfb-vegf	4	28	28907	6.7	11.74	13.23	3.02
pdgf-vegf	4	24	22229	12.7	15.47	18.62	2.78
bmp-vegf	4	14	18788	8.9	12.76	14.81	2.96

Table 2. 3 . Main descriptive indicators: number of replicates per condition, number of processed ROIs, total number of measured sprouts, percentage of sprouts longer than 30 µm, mean length, standard deviation and skewness of the distribution.
Note the different number of ROIs per condition due to the variability in the number of finally selected regions caused by the disposal of invalid samples.

2.2.5 Sprout tracking and quantification

Cell tracking was initiated in the monolayer two hours after ECs seeding and GFs incorporation and maintained for 24 hours with 37ºC, 95% humidity and 5% of CO_2 conditions. Phase contrast images were captured every 20 min.

The geometry of the microdevice used in this experiment has 36 micropillars alongside the EC channel, and therefore there are 37 regions of interest (ROIs) to quantify cell sprouting (Figure 2.1C). Among all of them, up to 16 ROIs per replicate were selected, although only those regions of higher image quality were kept for processing. Each of these ROIs represents 10 z-stacks (one slice every 20 µm) overtime (about 70 frames). In sum, up to 195 ROIs have been processed, or in other words more than $1.35 \cdot 10^5$ images, and measured more than $2.3 \cdot 10^5$ sprouts (See Table 2.3). A hand-coded script with a graphical interface using MATLAB has been used for the image analysis. This script (like the other MATLAB algorithms used for data processing in this Thesis) has been developed by PhD Carlos Borau in the context of the European Project INSILICO-CELL. It automatically cleans the noise from the input images and segments background from cell mass by using different filters (Figure 2.4A).

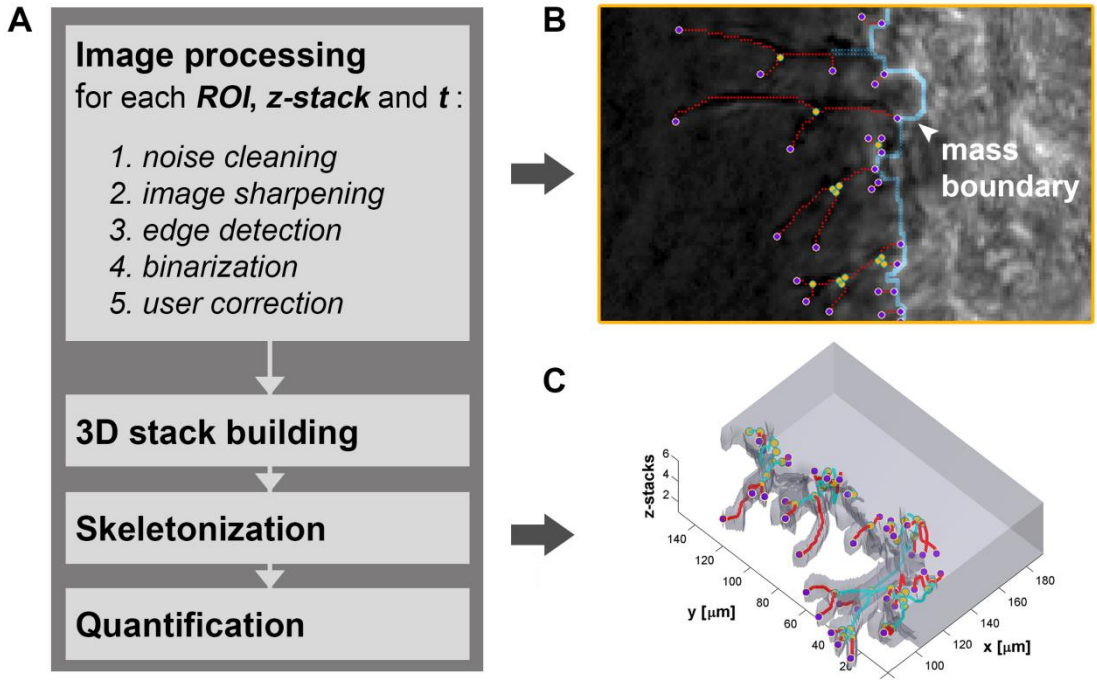

Figure 2. 4 Scheme of image processing for sprout quantification
A) Workflow scheme of the developed image-processing code. B) Image shown to the user for manual correction. When necessary, the user is allowed to draw masks to add/remove specific regions so that the script can re-process the image. Purple/yellow circles represent end/branch points of the computed 2D sprouts. Red dots represent pixels corresponding to sprouts. Light blue line highlights the cell mass boundary (leading edge), used as reference to measure the sprout lengths. C) 3D reconstruction of the z-stacks at a specific time step. Semi-transparent gray represents the cell mass, whereas cell sprouts are plotted as red/cyan segments. These segments are colored in red when they join a branch-point with an end-point, and in cyan when they join two branch-points. This coloring method provides visual information regarding the sprout network complexity, although both type of segments are considered equivalent for the numerical quantification.

Besides, it permits the user to define masks to correct or discard any frame or part of it if necessary (e.g. highly blurred captures). Figure 2.4-B shows an example of an image seen by the user while checking the frames. Once this process is finished, the z-stacks of each temporal frame are joined in a 3D volume which skeleton is computed [162] (see Figure 2.4-C). Finally, all the necessary data are automatically collected for the statistical analysis.

2.2.6 Statistical analysis

In collaboration with the researcher PhD Jesús Asín from the Statistical Department, this section has been performed. Statistical hypothesis tests were implemented in order to analyze the significance of differences between sprouting length distributions under different conditions. An elevated sample size of sprouts was obtained for all conditions, ranging from 18788 to 90814 (See Table 2.3). The skewed right distribution shown in Figure 2.5 shows a non-normal distribution that is associated with high variability. Then, non-parametric tests based on ranks were the best option to compare this model of distribution. Firstly, Kruskall-Wallis (KW) tests were used to check the null hypothesis establishing that the length distribution is unchanged regarding the conditions. Secondly, when the null was rejected at 0.01 significance level, a multiple comparison test

(simultaneous confidence level of 95%) was applied to distinguish conditions that were significantly different (see in Figures 2.6, 2.7, 2.8).

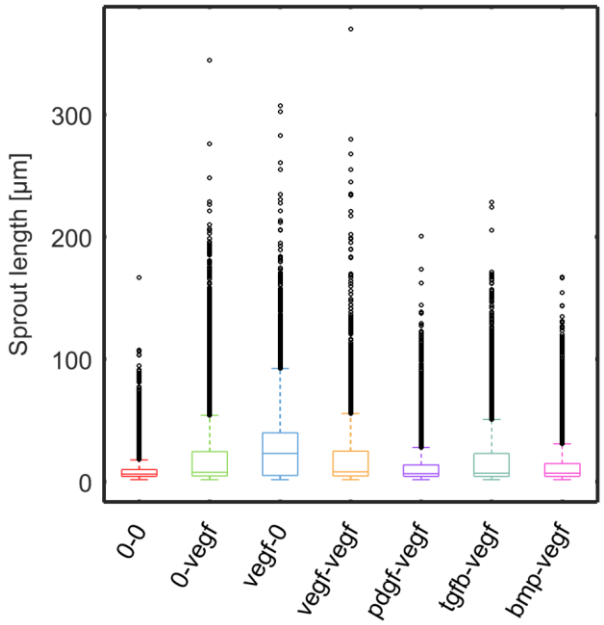

Figure 2. 5 Length distribution of all sprouts for each condition.
All the cases show an asymmetric distribution with high values (up to 300 µm). Condition (vegf-0) presents the greatest dispersion whereas condition (0-0) has the most concentrated data.

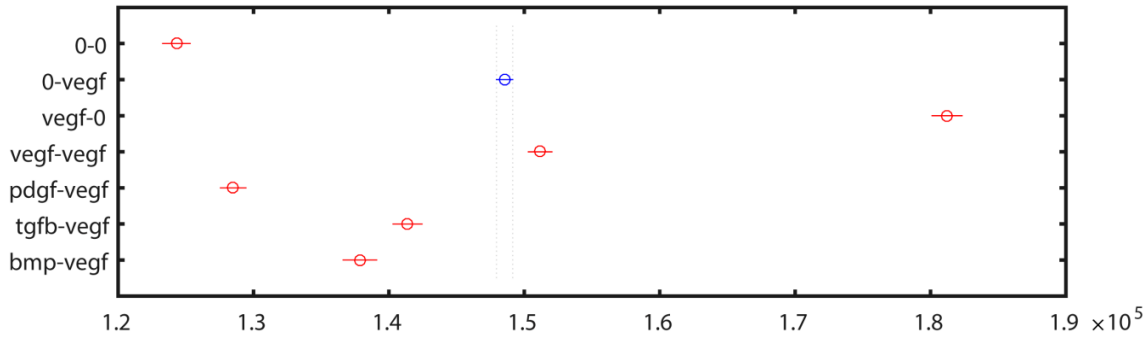

Figure 2. 6 Sprout length distribution
A median test (Kruskal-Wallis) confirmed that all the groups (conditions) had mean ranks significantly different among each other ($p < 0.01$). Control condition (0-vegf) is highlighted in blue.

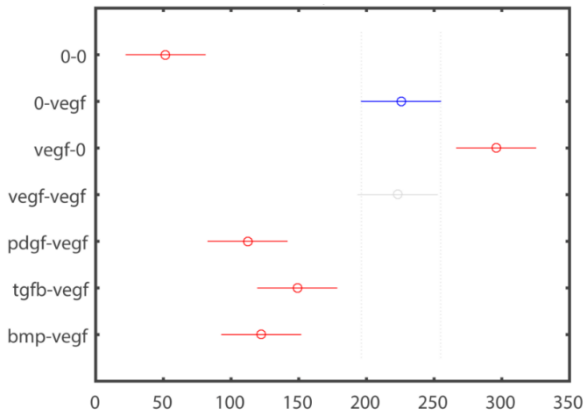

Figure 2. 7 Number of long sprouts.
A median test (Kruskal-Wallis) confirmed that all the conditions, except condition 4 (vegf-vegf) had mean ranks significantly different to the control case (0-vegf) ($p < 0.01$). Control condition (0-vegf) is highlighted in blue.

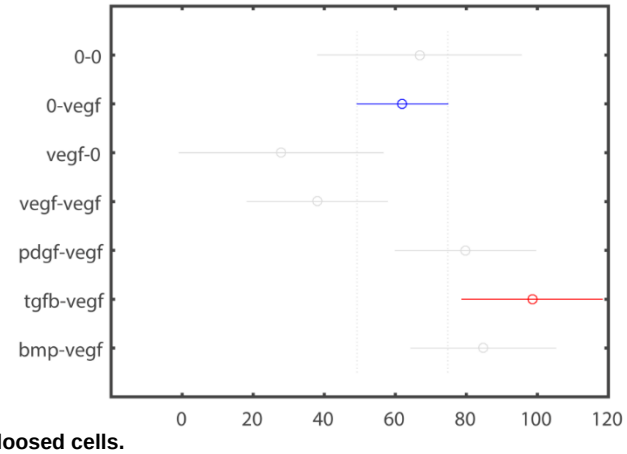

Figure 2. 8 Number of loosed cells.
A median test (Kruskal-Wallis) confirmed that only condition 6 (tgfb-vegf) had a mean rank significantly different to the control case (0-vegf) ($p < 0.01$). Control condition (0-vegf) is highlighted in blue.

2.3 Results

2.3.1 Measurements of VEGF-induced sprouting

Four different conditions were used in order to test the effect of VEGF on the EC monolayer: i) null concentration in both channels *(0-0)* ii) VEGF only in the ECs channel *(0-vegf)*, iii) VEGF only in the GFs channel *(vegf-0)* and iv) VEGF in both channels *(vegf-vegf)*.

On the other hand, two groups of results were created to perform the analysis: i) all sprouts and ii) only long sprouts. A sprout was considered long when its 3D length was higher than 30 µm. We choose this threshold since HUVEC cell size usually range between 20-40 µm [163]. Additionally, we measured our cells confirming that their medium size was in the same range.

Regarding the length data of all sprouts, it is remarkable the highly skewed distribution for all conditions (Figure 2.5, Table 2.3), with condition *(vegf-0)* having the greatest dispersion. In spite

of their similarities, a median test (Kruskal-Wallis) confirmed that all the groups had mean ranks significantly different among each other ($p < 0.01$) (Figure 2.6).

The frequency of sprout formation was tracked over time every 20 minutes. Compared to condition *(0-vegf),* condition *(0-0)* produced a similar amount of sprouts (Figure 2.9A), however, very few of them were long (Figure 2.9B). Condition *(vegf-0)* presented the greatest number of sprouts during the first half of the experiment (Figure 2.9A), although its effect was reduced over time. However, the number of long sprouts was higher during the whole period (Figure 2.9 B), which is reflected in the significantly higher number of total sprouts per ROI (Figure 2.9C). The opposite effect was observed in condition *(vegf-vegf)* where the growth of sprouts was minimal at the beginning, but increased with time until the number of long sprouts was the highest among all conditions (Figure 2.9B). On average, the total number of long sprouts was similar (no significant differences) compared to condition *(0-vegf)* (Figure 2.9C).

Overall, sprout length distribution was highly concentrated at low values, so that the frequency of long sprout formation was rather low. In any case, the mean sprout length over time was higher for condition (*vegf-0*), lower for condition (*0-0*), and similar for condition (*vegf-vegf*) compared to the condition (*0-vegf*) (Figure 2.9D).

2.3.2 Chemotactic effect of non-specific angiogenic factors

In this work, it has been analyzed whether specific GFs of wound healing (PDGF and TGFβ) or bone regeneration (BMP2) could stimulate the vessel formation.

The negative effect of nonspecific angiogenic factors was neatly observed, especially in the frequency of sprout formation. The number of sprouts for conditions (*pdgf-vegf*), (*tgfb-vegf*) and (*bmp-vegf*) was significantly lower compared to condition (*0-vegf*) during most of the time (Figure 2.9A, C), being this difference more critical for long sprouts. In fact, in these conditions, long sprouts practically disappeared at the end of the experiment (Figure 2.9B).

Regarding sprout lengths, the trends were similar to those observed in the frequency data, with these conditions getting overall shorter sprouts compared to condition (*0-vegf*). However, condition (*bmp-vegf*) showed an interesting behavior during the last hours of the experiment. While the number of sprouts was greatly reduced compared to the initial times, the length of these sprouts was larger, even superior to those produced in the condition (*0-vegf*) (Figure 2.9D).

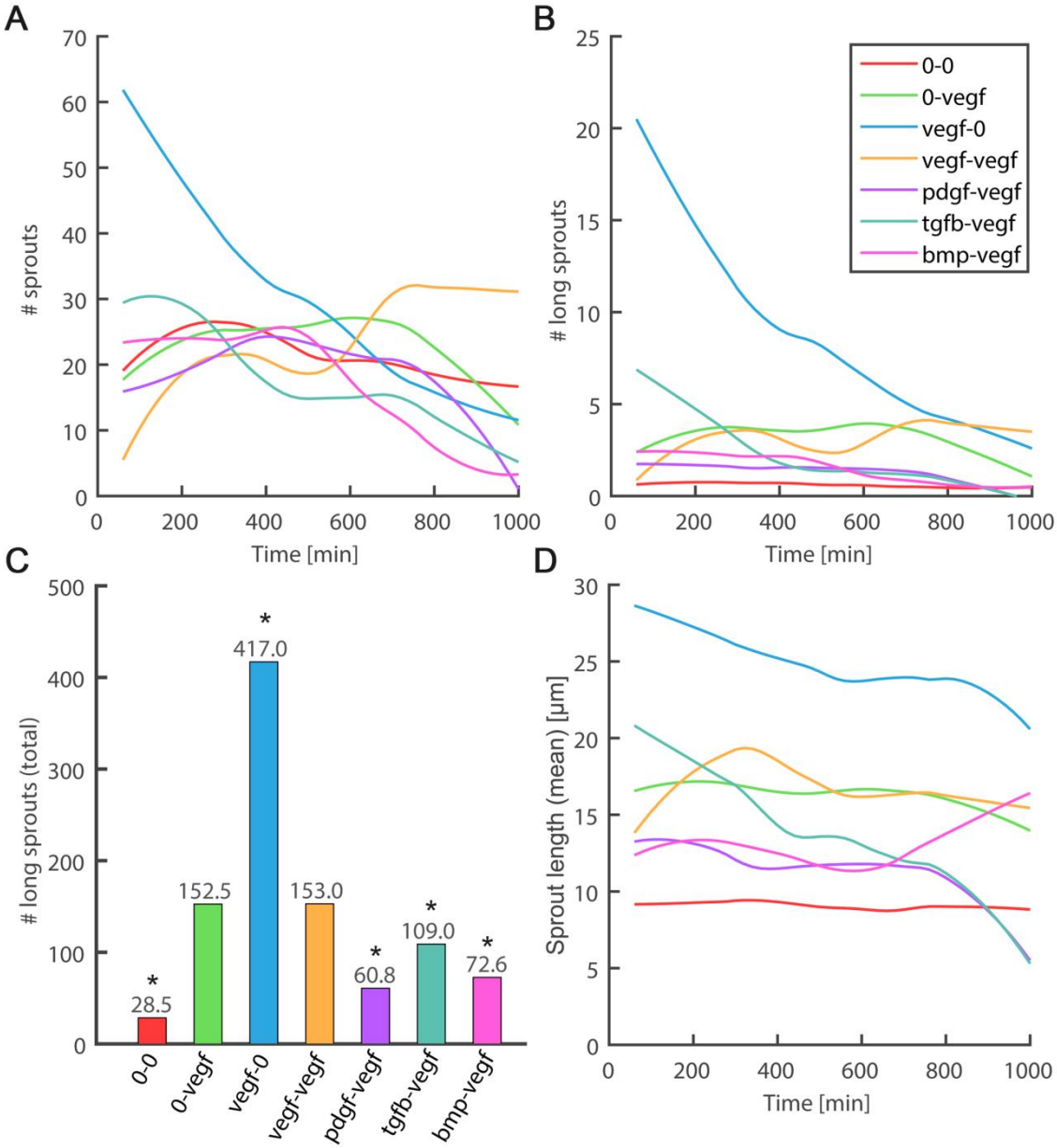

Figure 2. 9 Obtained results from sprouts quantification

Number of sprouts (A) and long sprouts > 30 µm (B) per ROI over time. C) Total number of long sprouts per ROI. * indicates ($p < 0.01$) in a Kruskal Wallis median test (Figure 2.7). D) Mean of the sprout length distribution over time. Panels A, B and D share legend and are plotted using a r-Loess smoothing filter. At earlier times, condition (vegf-0) produced the largest number of sprouts (A), a third of which were long (B). This effect gradually disappeared, yet the number of observed long sprouts was higher compared to the case (0-vegf) at the end of the experiments. Condition (vegf-vegf) reduced the number of sprouts (both short and long) at the beginning, although this effect was reversed as time advanced, producing the highest number of sprouts during the last steps. The other conditions, had negative effects on the number of sprouts produced, which almost disappeared in the last hours. Overall, condition (vegf-0) produced a significant higher number of long sprouts (C) which is reflected in a higher value of the mean sprout length over time (D). Condition (vegf-vegf) was similar to the condition (0-vegf) with no significant differences in the total number of sprouts. Mean values of sprout length were slightly higher at the end of the experiment. Conditions (pdgf-vegf), (tgfb-vegf) and (bmp-vegf) presented overall fewer and shorter sprouts compared to condition (0-vegf), critically decreasing the sprout length at later times except for condition (bmp-vegf) which, interestingly, produced longer sprouts during the last hours (D).

2.3.3 Quantification of failed sprouts

For the successful formation of sprouts, cells make many attempts, some of them succeed but others do not. Another aim of this work was focused on the quantification of the number of failed sprouts attempts in each ROI. For this purpose, it has been counted the number of cells loosed from the cell mass (the monolayer) trying to create a new sprout. Some of the tip cells left the monolayer and some returned to it after a while. However, at the moment they were unattached, we assessed them as a failed sprout. As shown in Figure 2.10, although the median value of loosed cells was different for all conditions compared to condition (*0-vegf*), only condition (*tgfb-vegf*) presented significant differences. Overall, conditions including VEGF as GF (*(0-vegf), (vegf-0) and (vegf-vegf)*) did not promote the migration of individual cells and therefore the connection between cells was maintained over time. In fact, looking together at the high number of loosed cells of conditions (*pdgf-vegf*), (*tgfb-vegf*) and (*bmp-vegf*) (Figure 2.10), and their low number of long sprouts produced (Figure 2.9), suggests a direct relationship between the propensity of cells to get unattached from the monolayer and the frequency of successful sprouts.

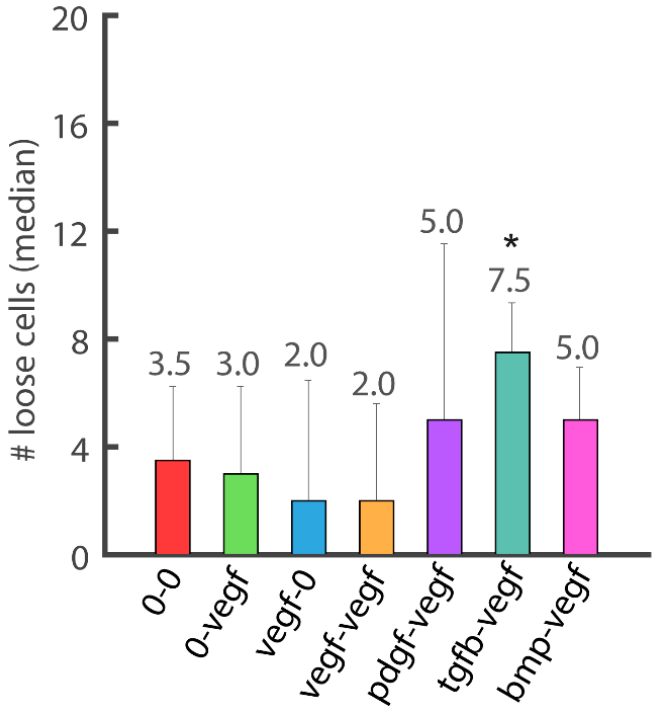

Figure 2. 10 Number of cells loosed from the main mass per ROI (median value).
Compared to the condition (0-vegf), the number of cells that failed to form a sprout was lower for conditions (vegf-0) and (vegf-vegf), and higher for the rest of them, although the difference was statistically significant only for condition (tgfb-vegf) ($p < 0.01$) (Figure 2.7).

2.4 Discussion

Considering the specific objectives referred in the Introduction section of this chapter, the paracrine effects of GFs commonly released by different cell types (epithelial cells, ECs or osteogenic cells) on the formation of novel angiogenic sprouts has been analyzed.

From our experiments, the first conclusion could be that the application of VEGF in the GF channel significantly enhanced the angiogenic response compared to non-specific factors. The generation of a chemoattractant gradient in the direction of sprout growth, (*condition (vegf-0)*), promoted sprouting and cell reorganization, producing longer sprouts with higher frequency. This effect was stronger at earlier times (Figure 2.9A, B, D). As time progressed and the concentration of VEGF decreased, the number of sprouts as well as their length also decreased, although the number of long sprouts and the mean sprout length kept at higher values compared to the condition *(0-vegf)* (Figure 2.9 B,D).

To test the effect of VEGF when present in both channels, a concentration gradient between the GF and the EC channel *(condition (vegf-vegf))* was created. The initial decrease in sprout formation (Figure 2.9A, B) suggests a saturation of VEGF receptors in ECs, not responding to the chemoattractant signal probably due to the distortion of DII4/Notch signaling activity [139,164]. In any case, sprout formation frequency was recovered, and the number of long sprouts was the highest among all the conditions during the last hours (Figure 2.9B). Mean sprout length was similar, and sometimes higher than the condition *(0-vegf)* (Figure 2.9C). The average number of loose cells was similar compared to the condition *(0-vegf)* (Figure 2.10), suggesting that the overexposure to VEGF may inhibit sprouting but still does not promote single cell migration.

The endothelium secretes several GFs such as PDGF and it may act in an autocrine or a paracrine way, amplifying the angiogenic response [165]. In previous studies, PDGF was determined to affect EC indirectly by inducing the release of VEGF [166]. Moreover, Banfi et al. concluded that the co-expression of VEGF and PDGF was able to induce efficacious angiogenesis [142]. However, our results showed the negative effect of condition *(pdgf-vegf*) on sprout development. This could be explained by the non-optimal balance of concentration between PDGF and VEGF and the inappropriate spatiotemporal gradient. In fact, in some kinds of tumors, the recruitment and proliferation of pericytes (special vascular cells) increase the PDGF expression but do not increase the vascular development [167].

TFGβ may promote tumor growth by enhancing angiogenesis [167]. Previous works have demonstrated that shallow gradients of TGFβ (0.5-2 ng/ml) show no discernable effect on sprout formation [168]. Our results revealed that the effect of higher concentrations of TGFβ (10 ng/ml) was neither relevant on angiogenic processes. In fact, there was a significant high number of loose cells (failed sprouts) suggesting that single cell migration is promoted, which could explain the low effectiveness of this GF to form long sprouts.

Previous reports have shown the modest effect of BMP2 on HUVEC migration and therefore on sprout formation [152]. In our results we confirmed this inhibiting effect, although we

observed a delayed effect leading to the formation of long sprouts at final phases. The number of loose cells was similar to *(pdgf-vegf)* assay, presenting the same behavior regarding sprout formation and elongation.

The software developed by M2BE Group and used to quantify sprouting from microscopy images, has provided us freedom and total adaptability for the required analysis. It is worth noting that despite the potential of our code, it presents some limitations, since its effectiveness relies on image quality. Blurriness, brightness, water drops due to condensation or other image artifacts require specific attention and adjustments. Additionally, the image-processing workflow is time-consuming. While the automatic processes present almost no computational cost (a few hours at most to build the 3D volume and measure the sprouts of a whole microdevice), the time required by the user to check specific frames and add the proper masks may reach weeks of work.

To summarize, our results show that VEGF is the main proangiogenic factor, able to stimulate the sprout formation especially when applied in the GF channel, opposite to the EC monolayer. This fact indicates that the induction of a VEGF gradient enhances the angiogenesis process. The chemoattractant effect of this growth factor could be employed for instance to accelerate regenerative processes, which could be crucial for tissue regenerative purposes. On the other hand, TFGβ was found to be the main factor inhibiting sprout formation and thus, it could be used to suppress the angiogenic process in tumor expansion. The effect of the rest of non-specific factors (PDGF and BMP2) were not relevant to enhance sprouting, although the effect of BMP at longer times should be further studied to better understand its behavior.

After presenting in this chapter a study of the effect of paracrine factors in a model of collective migration, the following chapters will be focused on the analysis of individual cell migration under different mechano-chemical factors.

Chapter 3

Combination of chemical and collagen hydrogel step gradients to quantify 3D fibroblast migration

Abstract *

Cell migration is an essential process involved in crucial stages of tissue formation, regeneration or immune function as well as in pathological processes including tumor development or metastasis. During the last years, the effect of gradients of soluble molecules on cell migration has been widely studied, and complex systems have been used to analyze cell behavior under simultaneous mechano-chemical stimuli. Most of these chemotactic assays have, however, focused on specific substrates in 2D. The aim of the present work is to develop a novel microfluidic-based chip that allows studying the long-term chemoattractant effect of growth factors (GFs) on 3D cell migration, also providing the possibility to analyze the influence of the interface generated between different adjacent hydrogels. Namely, 1.5, 2, 2.5 and 4 mg/ml concentrations of collagen type I were alternatively combined with concentrations of 5, 10 or 50 ng/ml of PDGF (human platelet derived growth factor-BB) and VEGF (vascular endothelial growth factor, as a negative control). To achieve this goal, a new microfluidic device has been designed which includes three adjacent chambers to introduce hydrogels that allow generating a collagen concentration step gradient. This versatile and simple platform was tested by using dermal human fibroblasts embedded in 3D collagen matrices. Images taken over a week were processed to quantify the number of cells in each zone. In terms of cell distribution, results shown that the presence of PDGF, especially in small concentrations, was strongly chemoattractant for dermal human fibroblasts across the gels regardless their collagen concentration and step gradient direction, whereas the effects of VEGF or collagen step gradient concentrations alone were negligible. **

Keywords: *chemotaxis, microfluidics chip, collagen-based gels, chemical gradient, statistical analysis, cell tracking*

This Chapter 3 corresponds to the article already published as:* ***C. Del Amo**, C. Borau, N. Movilla, J. Asín, and J. M. Garcia-Aznar, "****Quantifying 3D chemotaxis in microfluidic-based chips with step gradients of collagen hydrogel concentrations****," Integr. Biol., pp. 1–27, 2017*. [169]

3.1 Introduction

Many biological processes that occur during normal and pathological function require the migration of cells in response to chemical gradients [170]. The regulation of cell migration by gradients of soluble molecules, also known as chemotaxis, has been widely studied during the last years [171–176]. In the previous chapter, the effect of various growth factors (GFs) on sprouting formation in the early stages was discussed. In this Chapter 3, a new methodology for the quantification of chemotaxis will be presented, tested for the migration of individual cells, but with a wide potential to be applied to other cellular models.

Considering the important role that chemotaxis plays in cell physiology, the directed migration of cells is crucially involved in other biological processes such as wound repair or inflammatory immune responses [34]. However, its study presents some difficulties since cells interact with each other and the extracellular matrix in their natural microenvironment, affecting their morphology and phenotype [177] and varying depending on each cell type [178].

Different kinds of *in vitro* assays have been used to simplify the biological variables controlling the chemical gradient as well as cell movement and orientation [9,173]. For instance, common Transwell assays promote the random and fast movement of cells in response to a chemical stimulus (chemokinesis) and the differential growth and adhesion of cells under the influence of gradients of diffusible chemicals from a source [172]. Also, the Boyden Chamber is one of the earliest and simplest assays normally used to study chemotaxis, consisting of two chambers (upper and lower) separated by a porous membrane through which cells can migrate [9,179–184]. Other type of assays such as T-Transwell or colorimetric tests present membrane filters separating the top chamber, where cells were seeded at the first stages, from the bottom zone, where cells are collected for quantification [181]. The material of the membrane filter, which recreates the extracellular matrix (ECM), varies for each assay, from polycarbonate to matrigel or collagen [174,180,185–192], as well as the kind of analysis performed. The Zigmond Chamber (based on the Boyden Chamber) is an alternative method where a narrow space separates both characteristic chambers of chemotaxis assays and permits a direct-viewing of cells moving across the bridge between those chambers [9,182]. Owing to the need to achieve better optical characteristics and accuracy, the Dunn Chamber was developed, which consists of a glass microscope slide with two concentric annular wells [9,182]. Cell solution is added into the central chamber moving over the bridge between both wells and being visualized under the microscope [9]. Following this idea, further improvements were achieved with the Insall Chamber, including an easy handling and the possible use of oil immersion lenses [173].

Morphology, migration and other cell behaviors are also influenced by physical gradients. Indeed, the effect of substrate stiffness on directed cell migration has been widely explored due to its significant role during tissue development, immune response, metastasis or wound healing [37,193–197]. Many authors have studied cell migration under different mechanical conditions, characterizing the gels that often play the role of extracellular matrix. The stiffness of these gels is usually related to their collagen concentration and associated to changes in pore size. For instance,

Fraley et al. measured the elastic modulus (G' (Pa)) of several hydrogels and found that collagen concentrations of 1.5, 2 and 2.5mg/ml lead to much lower values (under 100Pa) compared to 4mg/ml collagen type I (500Pa approximately) [198].

Due to the importance that microfluidic technology has acquired during last years, multiple systems have been developed to study the mobility of cells under different controlled conditions such as fluid flow and chemoattractant molecules [9,187–189,199–206]. As alternative to two-dimensional chambers for the quantitative effect of chemical modulators, some 3D models have been designed to represent better the *in vivo* situation [207]. Different materials as well as organisms (cells or bacteria) have been part of thorough research in terms of chemoattraction by chemical particles using three dimensional microfluidic chips [208]. Reusable metal devices designed by Vasaturo et al. or Caserta et al. allowed the user generating chemoattractant gradients in 3D by diffusion through a porous membrane [207,209]. In addition, this technology has facilitated 3D assays to analyze realistic migratory behavior of cells by recreating the local microenvironment of tissues [210].

In this work, a novel and versatile microfluidic device was developed. It allows the quantification of 3D cell migration through the interface of continuous collagen-based gels with different concentrations. This chip also allows the simultaneous application of chemical gradients on 3D embedded cells. In sum, our tool could be used to investigate several unresolved queries involved in cell migration. In particular, it has been studied the cell behavior by combining different growth factors ((human platelet derived growth factor-BB, abbreviated as PDGF) and vascular endothelial growth factor (VEGF) in different concentrations) and collagen concentration step gradients in each zone or chamber, separated by an interface. The chemotactic effect of PDGF on fibroblast has been widely studied, being used as a positive control in this work to know the behavior of cells under different concentrations of this GF [126,211]. On the other hand, VEGF is released by fibroblasts as an inactive molecule [212], so, it has been used as a negative control.

Once again, highlight the high versatility of this microfluidic platforms to analyze cell migration within 3D matrices, as well as its simplicity. This makes it a useful multi-condition tool, capable of simulating and taking into account multiple variables at the same time, better biomimicking the actual tissue conditions.

3.2 Methods and materials

3.2.1 Design and fabrication of microchips

Following the methodology described in Section 1.1.4, and previously implemented by Shin et al. [213], the microfluidic chips were fabricated in PDMS (Polydimethylsiloxane, Sylgard 184, Dow Corning GmbH). A positive SU8 350±30 µm relief pattern of the designed geometry was obtained through soft lithography techniques. After silicon wafer polymerization, the devices were individualized from the PDMS molds and sterilized in wet and dry cycle of autoclaved. Surface

plasma treatment was used to bond the PDMS with the glass-bottom of 35 mm petri dishes (Ibidi) followed by the addition of the poly-D-lysine (PDL) to enhance the surface-matrix attachment.

Based on the main characteristics of the microfluidic devices designed by Farahat et al. [138], a new geometry was developed by using trapezoidal columns to support the hydrogel via surface tension (see Figure 3.1). The chip consists on a central chamber divided in three channels. The central cavity lodges the cells seeded while two symmetric and adjacent channels allow hydrogel filling. Two extra lateral channels allow the introduction of cell culture medium and growth factors in order to create the chemical gradient. Figure 3.1D illustrates the main chip dimensions. Figure 3.2 shows a picture of the microdevice next to a coin to compare the scale.

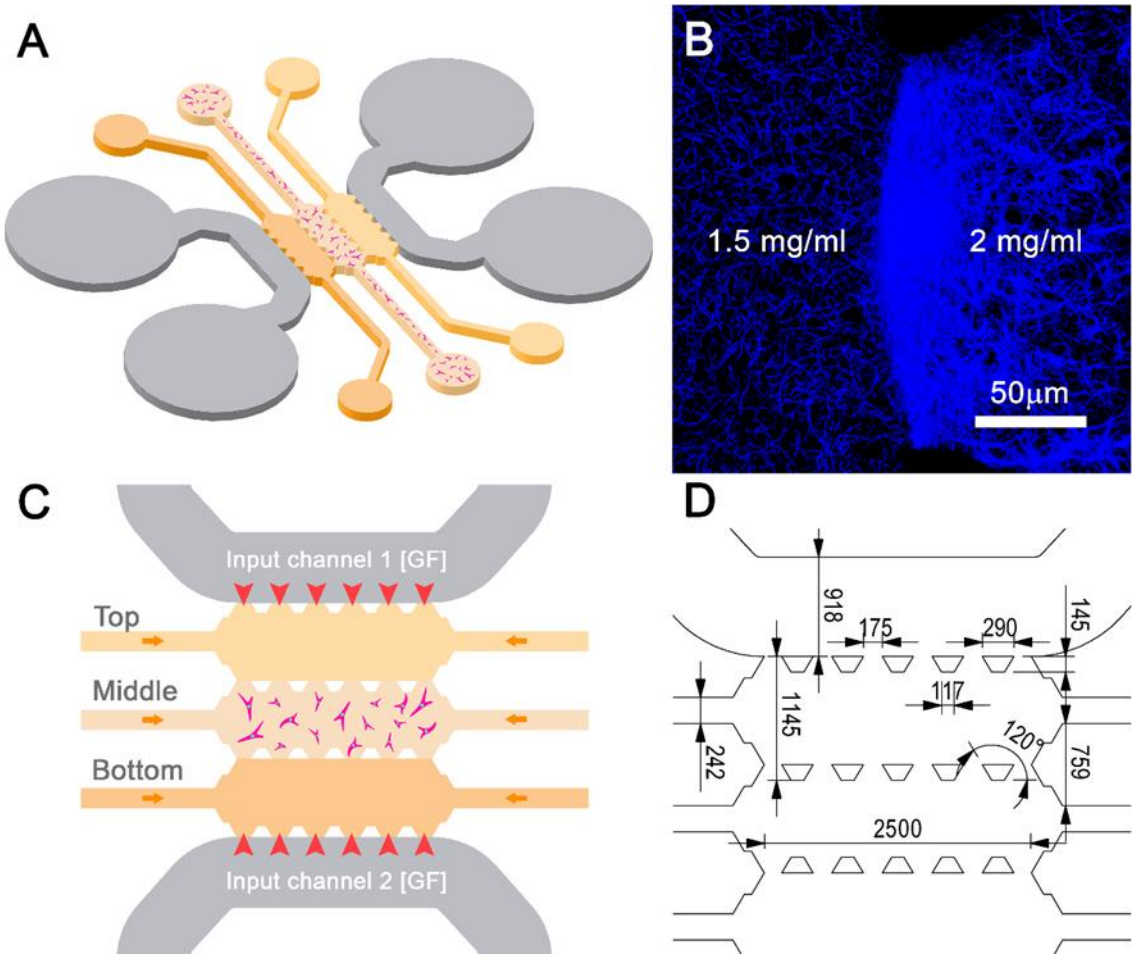

Figure 3. 1 Geometry of microfluidic devices.
A) 3D view. B) Interface generated between two gels of different collagen concentration (3D network of 1.5-2 mg/ml collagens obtained by confocal reflection between two micropillars). C) Distribution of hydrogels and addition channels. Cells, already embedded in the collagen hydrogel, are seeded in the middle channel. Top and bottom channels are filled with collagen only (loading direction represented by the orange horizontal arrows. Input channels are used to introduce GF and induce a chemical gradient (red vertical arrows). D) Geometrical dimensions in µm. The chip thickness is 350±30 µm.

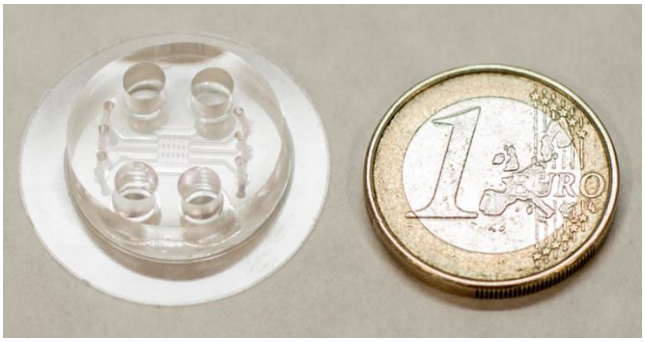

Figure 3. 2 Image of the microdevice next to a coin.

3.2.2 Cell line and lentivirus production

In order to facilitate the processing of the images obtained in these assays, it was decided to use fibroblasts transfected with green fluorescent protein (GFP). The presence of fluorescent green protein facilitates the automatic and visual identification of cells when images are processed by the user with the Matlab algorithms.

The following procedure has been developed by the Cell Culture Service at IACS (Aragon Health Sciences Institute) since the regulations prevent us from working with viruses in our facilities. NHDF cells were cultured in Fibroblast Cell Basal medium with growth supplements (Lonza) in a 37ºC humidified incubator with 5% CO_2. HEK 293T (human embryonic kidney) cells were cultured in DMEM containing 10% FCS (Lonza) and 100U/ml penicillin (Life Technologies) in a 37ºC humidified incubator with 5% CO_2 in order to generate the virus. 293T cells were seeded at $4 \cdot 10^6$ cells per 100mm dish and incubated at 37º under 5% CO_2, one day before transfection. These embryonic cells were co-transfected with 3 µg of pLOX-CWgfp (Addgene Plasmid #12241), 3µg of psPAX2 (Addgene Plasmid #12260) and 3 µg of pMD2G (Addgene Plasmid #12259) by using Fugene 6 reagent (Promega). At about 18 hours post-transfection, the media was replaced with fresh media, and 48-72 hours post-transfection, the supernatant containing the viruses was collected, filtered through a 0.45-µm pore size filter (Whatman), and added 1 µl of polybrene (10mg/ml) to 1ml of virus to enhance lentiviral transduction. The infective virus was stored at -80ºC.

On the other hand, NHDF cells were seeded in 6-well culture dishes at 100,000 cells per well and incubated 24h at 37ºC and 5% CO_2. Culture medium was removed, replaced with lentiviral particles, and incubated for 48h at 37°C and 5% CO_2. After removal of lentiviral particles, fresh medium was added and cultures were examined for GFP expression by using fluorescence microscopy. The expression of GFP could be visually detected 24 h after virus treatment. NHDF cells were subsequently analyzed using fluorescent activated cell sorting (FACS) method to physically isolate only NHDF-GFP clones.

3.2.3 Collagen-based gels and cell seed

As it has been mentioned in Chapter 2, type I collagen gel solution was used to prepare the collagen hydrogels of different concentrations, namely 1.5, 2 and 2.5 mg/ml from Corning Collagen I, Rat Tail 3.26 mg/ml, and 4mg/ml from Corning Collagen I, Rat Tail 11 mg/ml. Following the methodology proposed by Farahat et al. [138] and Zervantonakis et al. [214] to mix the phosphate buffered saline (PBS; Lonza), NAOH and FGM2 (Fibroblast Growth Media, Lonza), 13 µl of hydrogel containing cells, was softly pipetted into the central chamber and polymerized for 20 min in a humid chamber, at 37º and 5% CO_2. The same conditions of polymerization were applied during the addition of hydrogels without cells to the lateral chambers. After that, the matrix was hydrated and incubated overnight at incubator conditions.

Normal human dermal fibroblasts (NHDF)-GFP transfected with lentiviral particles and isolated by cell sorting by the Cell Culture Service in IACS were used in these assays. The cell passage after transfection was 9 and cells were used up to passage 16 using Fibroblast Growth Medium (FGM2, Lonza) and grown until 80% confluence being harvested sequentially by using trypsin/EDTA and the centrifugation of the suspension during 5 minutes to conclude with a final cell concentration of $0.4 \cdot 10^6 cells \cdot ml^{-1}$ in the collagen hydrogel.

3.2.4 Hydrogel interfaces and chemical gradient

The consecutive polymerization of each adjacent hydrogel was the methodology followed to generate interfaces. Since the central hydrogel was the first matrix added to the device, a meniscus-like shape appears by surface tension and is maintained while the others gels introduced by the lateral channels settle and establish the crosslinking between networks (see Figure 3.1B). Confocal reflection of hydrogels was performed according to the specified instructions described in the image acquisition section to visualize these interfaces. Despite the variability found in these interfaces in terms of thickness, mainly due to the manual process, no significant effects on cell motility were observed among different repetitions and different chips. Sections were analyzed with a Super Plan Fluor 40X objective using z-stack scanning and obtaining slice images of this region each 2µm to check the ability of cells to cross the interface (Figure 3.3).

The characterization of growth factors transport used as chemoattractant in our assays, diffusion experiments using 20-kDa fluorescent-labelled dextran (FITC (fluorescein isothiocyanate)-dextran, Sigma Aldrich, Germany) were performed. This particle has been used due to the similarities with PDGF in the molecular weight (25.4 kDa) as well as in other diffusivity constants [158]. The solution was injected simultaneously in both reservoirs of the same channel, diffusing homogeneously along the hydrogels. PBS was used to refill the opposite reservoirs in order to equilibrate the system.

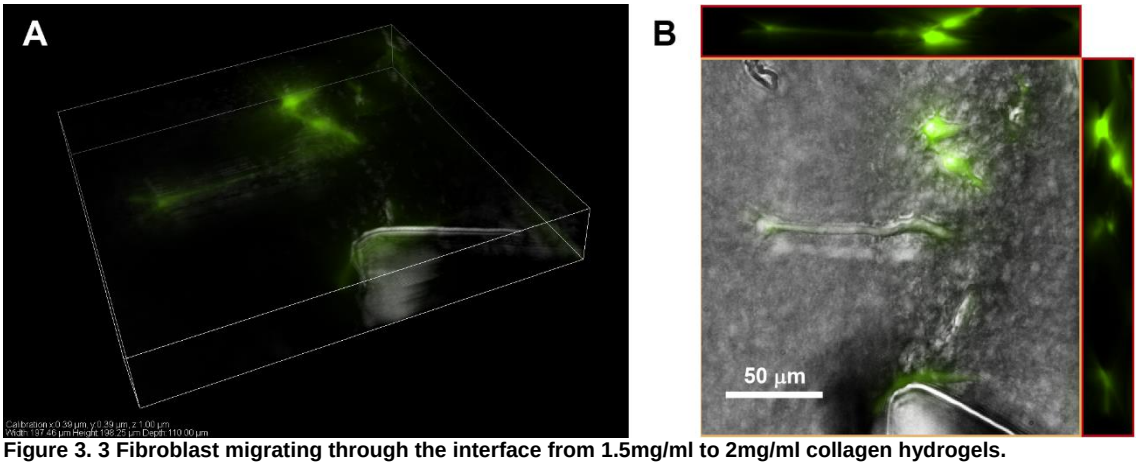

Figure 3. 3 Fibroblast migrating through the interface from 1.5mg/ml to 2mg/ml collagen hydrogels.
A) 3D reconstruction. B) Top view and orthogonal projections.

2X CPI Plan APO objective was used to visualize the diffusion phenomenon in a Nikon D-Eclipse C1 Confocal Microscope, acquiring fluorescent images every 500 msec for a total of 3 hours. Furthermore, the diffusion profile was obtained for the rectangular area between two trapezoidal posts starting in the entrance of channel 1 up to the end of channel 2, following the nomenclature given in Figure 3.1C.

3.2.5 Experimental setup

After the overnight incubation of seeded microdevices, the corresponding GFs following the conditions specified in Table 3.1 were added into the indicated input channel. Control devices were only rehydrated with cell growth media. To minimize evaporation effect on GF concentration, channels were refilled every two days with the appropriate culture medium. In this process, the medium was removed from one of the reservoirs of each channel equilibrating by pressure differences before the diffusion process starts and achieving the same height of liquid in both reservoirs of the same side of the device.

The goal of the first assay was to know the isolated effect of the GFs gradient on cell migration through the interface of hydrogels with the same collagen concentration. Assays 2 and 3 were, on the other hand, conceived to analyze the effect of the interfaces between matrices with different collagen concentrations. GF gradients were also added to elucidate whether their effects are influenced by the step gradients of collagen concentration.

Assay 1: uniform gel					
	Input 1	Top	Middle	Bottom	Input 2
Condition	**[GF](ng/ml)**	**[Collagen] (mg/ml)**			**[GF](ng/ml)**
Control	0	2	2	2	0
PDGF*	5	2	2	2	0
PDGF	50	2	2	2	0
VEGF**	10	2	2	2	0
Assay 2: single step gradient hydrogels					
	Input 1	Top	Middle	Bottom	Input 2
Condition	**[GF](ng/ml)**	**[Collagen] (mg/ml)**			**[GF](ng/ml)**
Control	0	1.5	2	2.5	0
PDGF	5	1.5	2	2.5	0
	0	1.5	2	2.5	5
VEGF	10	1.5	2	2.5	0
	0	1.5	2	2.5	10
Assay 3: Double step gradient hydrogels					
	Input 1	Top	Middle	Bottom	Input 2
Condition	**[GF](ng/ml)**	**[Collagen] (mg/ml)**			**[GF](ng/ml)**
Control	0	2	1.5	4	0
PDGF	5	2	1.5	4	0
	0	2	1.5	4	5

Table 3. 1 Experimental setup conditions.
GF concentrations of 0 ng/ml indicate that the channel was only hydrated with FGM2. Cells are seeded in the middle channel. *PDGF-BB (Human Platelet Derived Growth Factor-BB, abbreviated as PDGF (Gibco®) **VEGF (Vascular Endothelial Growth Factor, Gibco®).

3.2.6 Image acquisition, processing and data analysis

For both the visualization of the collagen network interface and the acquisition of complete images, a Nikon D-Eclipse C1 Confocal Microscope equipped with a Plan Apo VC 60XH objective and multichannel fluorescent imaging was used. Phase contrast and fluorescent (GFP) images were captured with a Plan Fluor 10X/ 0.30 OFN25 PH1 DLL Nikon Objective every 24 hours for 8 consecutive days. The experiment was reproduced three independent times. The focal plane was selected to be in the middle along the z-axis of the device, focusing cells completely embedded within the 3D network. The reference for the mosaics of the images was the central point of the device which was roughly given by the cross formed by the vertical line crossing the third pillar and the horizontal line dividing the central chamber. In any case, all images were automatically re-aligned through fixed reference points. Each image was then automatically analyzed with a custom-made MATLAB script to count the number of cells in each channel (see Figure 3.4). Figure 3.5 shows a tiled view for different days and different conditions. These data were further analyzed to extract statistical results by means of regression models with the appreciable support and assistance of PhD Jesús Asín (see Statistical Modeling section).

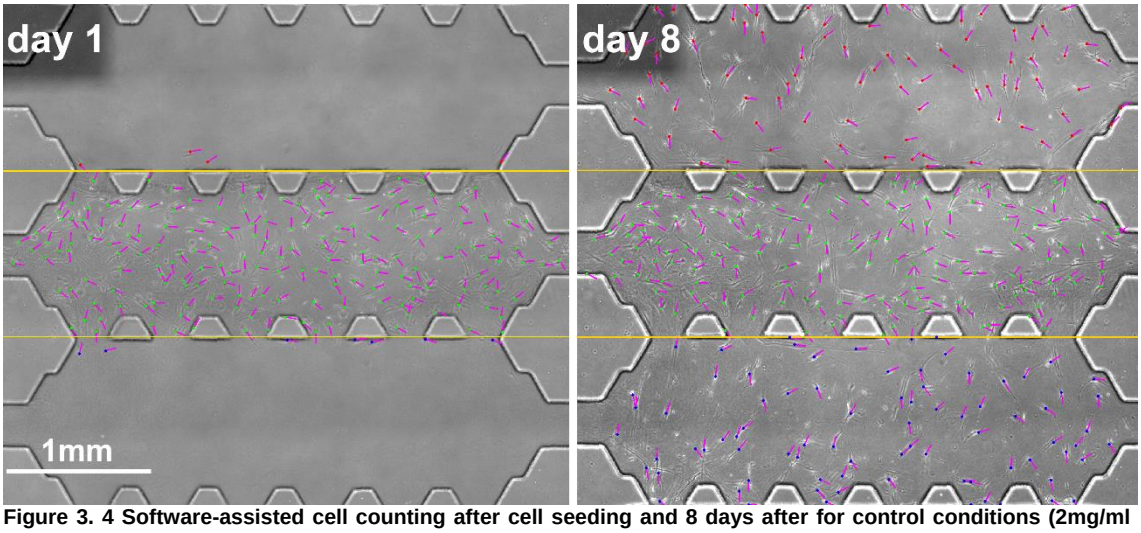

Figure 3. 4 Software-assisted cell counting after cell seeding and 8 days after for control conditions (2mg/ml collagen in each channel).
Yellow lines represent the zone limits (corresponding to collagen interfaces). Colored dots represent cell centroids (green: middle channel, red: top channel, blue: bottom channel). Purple straight lines represent cell orientation (data not explored in this work). Images were captured with a Nikon D-Eclipse Microscope with a Plan Fluor 10X Objective.

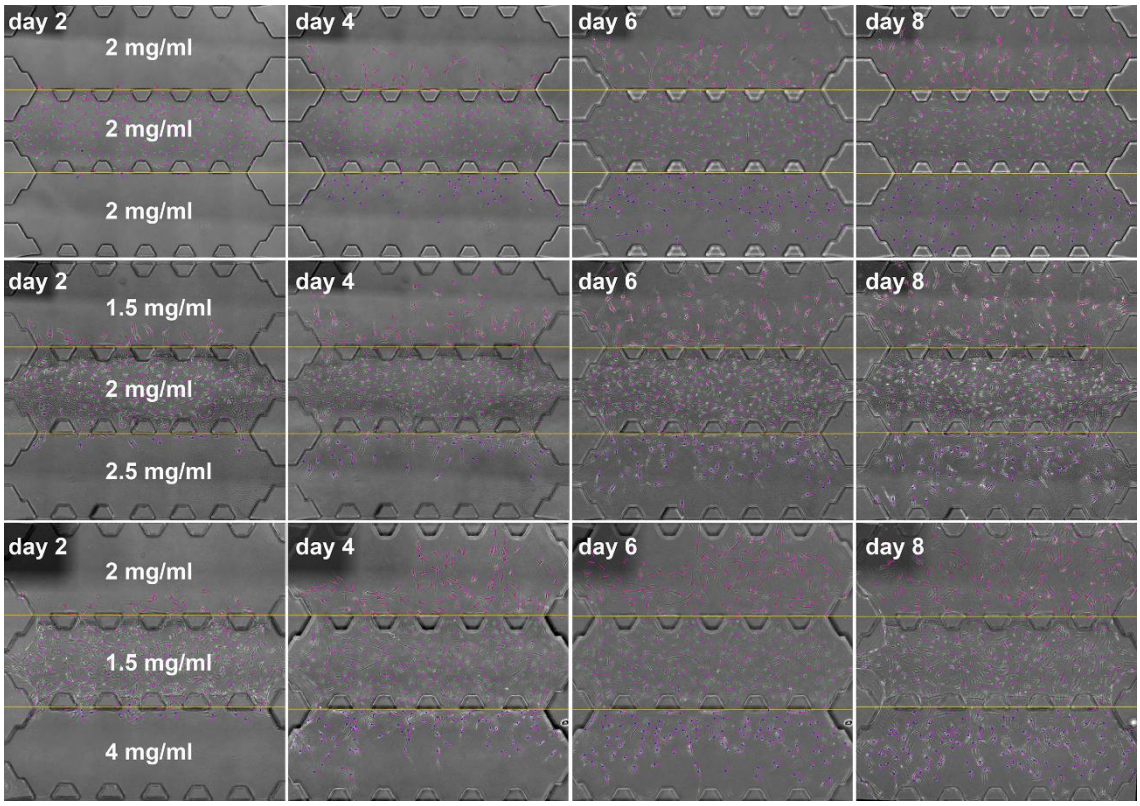

Figure 3. 5 Tiled view of cell distribution at day 2,4,6 and 8 for different collagen concentration distributions.

3.2.7 Statistical modeling

Statistical analysis of results was based on a multinomial logistic regression model. For a categorized response, *Y* takes values in a range of *m* categories (denoted as 1, 2, …, *m*) and has an associated vector of *k* covariates $(x_1,...,x_k)$. The probability that *Y* is in the category *i,* conditional to covariates, is expressed as:

$$P(Y=i\left|x_1,\ldots,\mathrm{x}_k\right.)=p_i\left(x_1,\ldots,\mathrm{x}_k\right)=\frac{\exp(\sum_{j=1}^{k}\beta_{(i)j}x_j)}{1+\sum_{l=1}^{m-1}\exp(\sum_{j=1}^{k}\beta_{(l)j}x_j)}\,i=1,2,...m-1 \tag{3.1}$$

$$P(Y=m\left|x_1,\ldots,\mathrm{x}_k\right.)=p_m\left(x_1,\ldots,\mathrm{x}_k\right)=\frac{1}{1+\sum_{l=1}^{m-1}\exp(\sum_{j=1}^{k}\beta_{(l)j}x_j)} \tag{3.2}$$

$$\frac{p_i\left(t, x_1, ..., \mathrm{x}_k\right)}{p_m\left(t, x_1, ..., \mathrm{x}_k\right)} = \exp(\sum_{j=1}^{k} \beta_{(i)j} x_j) \tag{3.3}$$

This last expression permits an easy interpretation of $\beta_{(i)j}$ coefficients, quantifying the change of the probability ratio relative to the reference category *m* associated to a change in covariate x_j .

This regression framework is used to model the probability that a cell is in top, middle and bottom channel. Note that, since cells are seeded in the middle channel, this zone is taken as reference. For instance, the probability of cells to be in top part is expressed as:

$$P(Y_t = 1 | x_i, \ldots, \mathrm{x}_k) = p_1\left(t, x_i, \ldots, \mathrm{x}_k\right) = \frac{\exp(g_1\left(t\right) + \sum_{j=1}^{k} \beta_{(1)j} x_j)}{1 + \exp(g_1\left(t\right) + \sum_{j=1}^{k} \beta_{(1)j} x_j) + \exp(g_3(t) + \sum_{j=1}^{k} \beta_{(3)j} x_j)} \tag{3.4}$$

Here, covariates are defined as: time, collagen concentration, and GF dose in each zone. The impact of each of those variables is based on the beta coefficients which determine the respective attractive $(\beta_{(i)j} > 0)$ or repellent $(\beta_{(i)j} < 0)$ effect on cell migration. Hence, the estimated probability associated to a zone in a specific time and a specific condition is interpreted as the proportion of cells that could be expected in this zone at this time.

A Generalized Additive Model (GAM) [215] is used during the exploratory phase in order to find the adequate shape of functions g_i and to search for some non-linear relationships between covariates.

R package VGAM, maximum likelihood estimation and Wald tests (corrected for overdispersion) were used for inference and contrasts for covariate effects on this regression framework [216,217].

3.2.8 Evaluation of the chemotactic index

To facilitate the interpretation of the results obtained in this work, an alternative chemotactic index *(CI)* has been proposed with a phenomenological perspective. There exist a wide variety of definitions for this index in the literature [209,218–220], however, in this work, *CI* is simply defined as the difference between the estimated proportion of cells in a zone with GF and the opposite zone (where there is not any GF). Hence, we propose this definition:

$$CI = P_i - P_j \tag{3.5}$$

where *i* represents the channel with GF and *j* the opposite one.

In this way, positive values indicate attraction whereas negative ones indicate repulsion. This *CI* therefore ranges from -1 (purely repulsive) to 1 (purely attractive), being 0 the neutral case where cells migrate equally to both zones.

3.3 Results and discussion

Since the initial number of cells seeded in the central chamber varies for each assay, we propose a study based on the proportion of cells in each zone. As the total sum holds (100%), we can build a statistical model that predicts the probability of cells being in a particular zone depending on the micro-environmental conditions, namely GFs and collagen concentration (see Statistical Modeling section). These conditions are summarized in Table 3.1. Cells were tracked for each assay every 24h over a week, including the initial state, so that time (*t*) in the model represents days and ranges from 1 to 8.

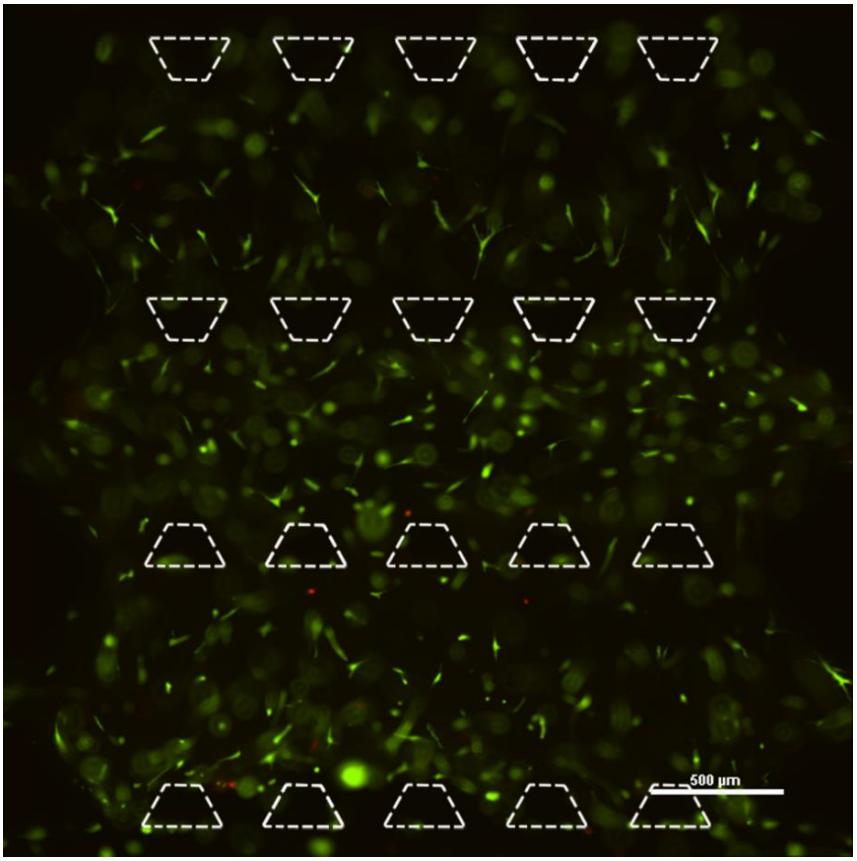

Figure 3. 6 Fluorescence image of NHDF-GFP cells stained with Live/Dead Cytotoxicity Assay Kit.
Viable cells at day 8 of culture are shown in green whereas dead cells are in red. Image was captured using a Nikon D-Eclipse C1 equipped with a CFI PL 10X AN 0,3 WD 16mm objective

Moreover, the viability of cells at the end of the experiment (day 8) was analyzed with a Live/ Dead Viability/ Cytotoxicity Assay Kit (Molecular Probes) demonstrating that most of cells were alive after this time of culture (Figure 3.6). In addition, the status of fibroblast has been visualized along the experiment presenting an elongated shape and their usual morphology in 3D (see Figure 3.7).

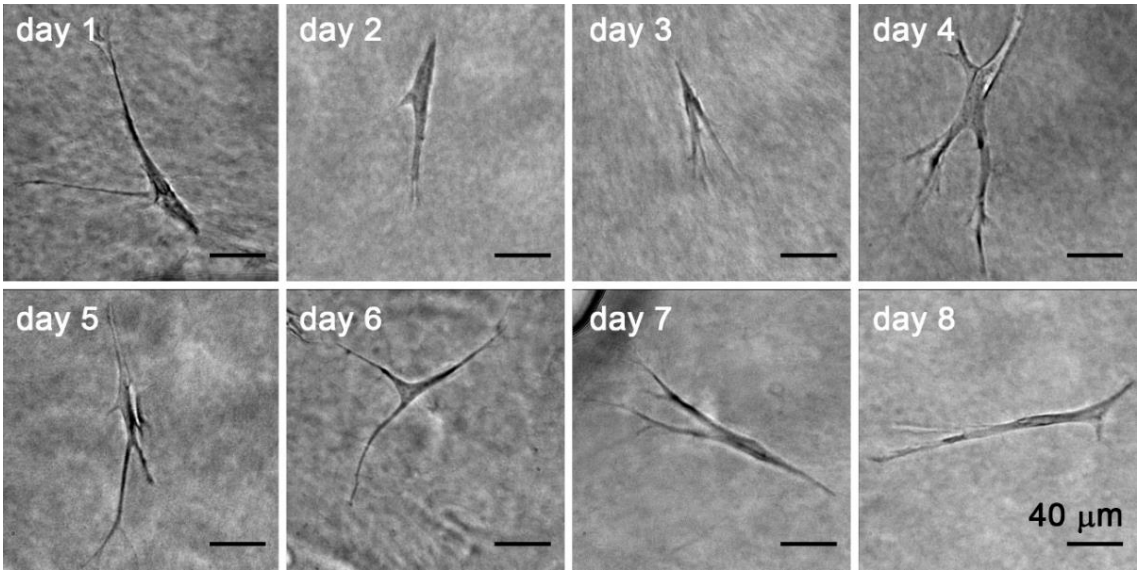

Figure 3. 7 Fibroblast morphology along the experiment in 3D collagen matrices.
Cells were imaged using phase-contrast microscopy with a 40X objective. Scale bar represents 40μm.

3.3.1 Influence of collagen concentration

Collagen concentrations of 1.5, 2, 2.5 and 4 mg/ml were used to form interfaces between the microdevice hydrogel channels in a different distribution for each assay (see Table 3.1). Comparing cell distribution evolution for the controls of each assay, allows isolating the effect of collagen concentration and step gradient direction. The final ratio of cells in each zone was practically identical (0.24) for all assays, regardless of collagen concentration and spatial position. The temporal evolution was very similar too, if slightly slower during the first days in the assay 1 (with completely uniform collagen distribution) (Figure 3.8).

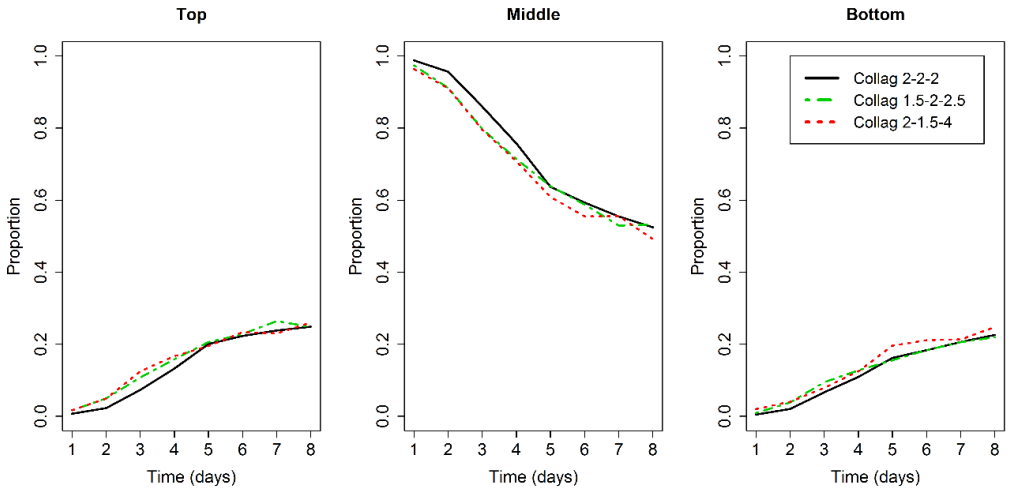

Figure 3. 8 Proportion of cells in each zone along time for the control case ([GF] = 0) of each assay.
Left: top channel, middle: middle channel, right: bottom channel.

This, together with the fact that the observed minimum and maximum values of cell proportion were in the same range for all the studied cases (Figure 3.9) suggests that the effect of collagen concentration and distribution is negligible, at least within the explored ranges. In other words, cells placed near the interfaces presented a higher probability to move towards the adjacent hydrogel, independent on its collagen concentration, than cells located in the central area of the middle channel. This implied that although cells might prefer a specific collagen concentration, the event of crossing the interface, without the influence of other cues, was purely random.

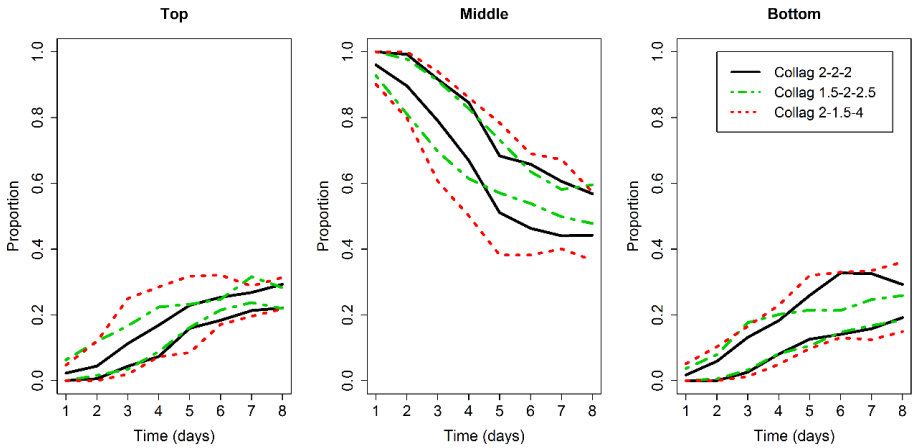

Figure 3. 9 Observed limits of the proportion of cells in each zone along time for the control case ([GF] = 0) of each assay.

A GAM model was proposed in order to confirm this hypothesis and to evaluate the interrelation between time and cell proportion in top and bottom zones. A nonlinear relationship, similar for each assay and zone, was found (Figure 3.10) indicating that quadratic $g_i(t)$ functions

should be used in the statistical model. With this idea in mind, we developed a multinomial logistic regression model to find the proportion of cells in each zone as a function of time (quadratic order), collagen concentration and step gradient with respect to the middle channel.

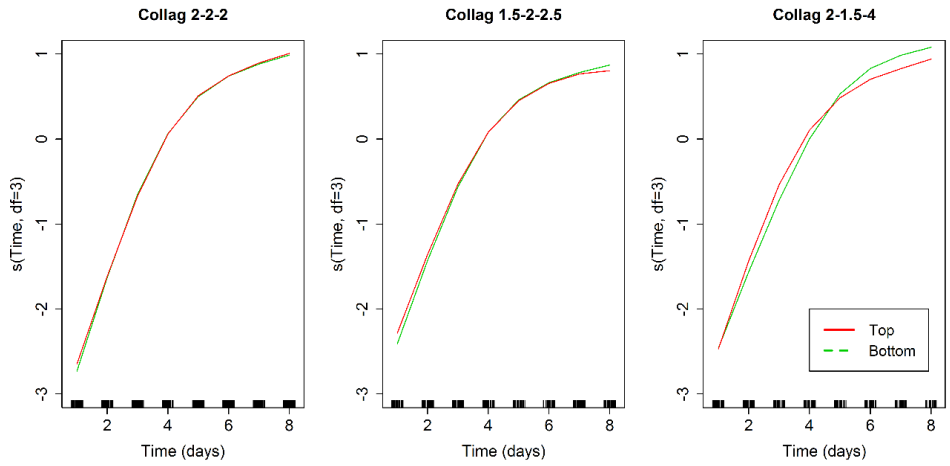

Figure 3. 10 GAM model for cell proportion in top and bottom zones.
Effect of the smoother in Time as the linear predictor of a logistic multinomial model for control experiments of each assay

A Wald test confirmed the non-significance of the covariates associated to collagen so that they can be safely eliminated from the equations. Hence, $p_1(t, x_i, ..., x_k) = p_3(t, x_i, ..., x_k)$, which finally stands as:

$$P(Y_t = 1 | x_i, \ldots, x_k) = p_1(t) = \frac{\exp(-5.13 + 1.21t - 0.0835t^2)}{1 + 2\exp(-5.13 + 1.21t - 0.0835t^2)} = P(Y_t = 3 | x_i, \ldots, x_k) \quad (3.6)$$

This equation 3.6 shows the expected proportion of cells in both top and bottom channels, which steadily increases until the 6th day and stabilizes until the 8th. Table 3.2 summarizes the adjusted model parameters.

Terms	Estimate p_1	p-value	Estimate p_3
Intercept	-5.13	0	-5.13
t	1.21	0	1.21
t^2	-0.0835	0.002	-0.0835

Table 3. 2 Multinomial logistic regression model parameters for the control conditions of each assay. p-values corresponding to the Wald Test.

3.3.2 Chemotactic effect of GFs on uniform gels (assay 1)

Specific concentrations of PDGF and VEGF were selected (see Table 3.1) based on the results obtained in previous works [126,127], to study the influence of GFs on cell migration. Hydrogels of 2 mg/ml concentration of collagen were placed in the three channels to isolate the chemotactic effect. A concentration of 5ng/ml of PDGF was found to be the strongest chemotactic stimulus for the cells, which were attracted to top zone (where the factor was applied) accumulating almost half of the population by the end of the assay (45%). About 15% of the cells, however, migrated toward bottom area, and the remaining 40% stayed in the middle zone. A higher concentration of PDGF (50 ng/ml) produced similar but less pronounced effects, achieving a final distribution of (31-44-25 %) per zone. On the other hand, the influence of VEGF was negligible compared to control, attaining a proportion of 23-55-23% respectively (Figure 3.11 first row of panels).

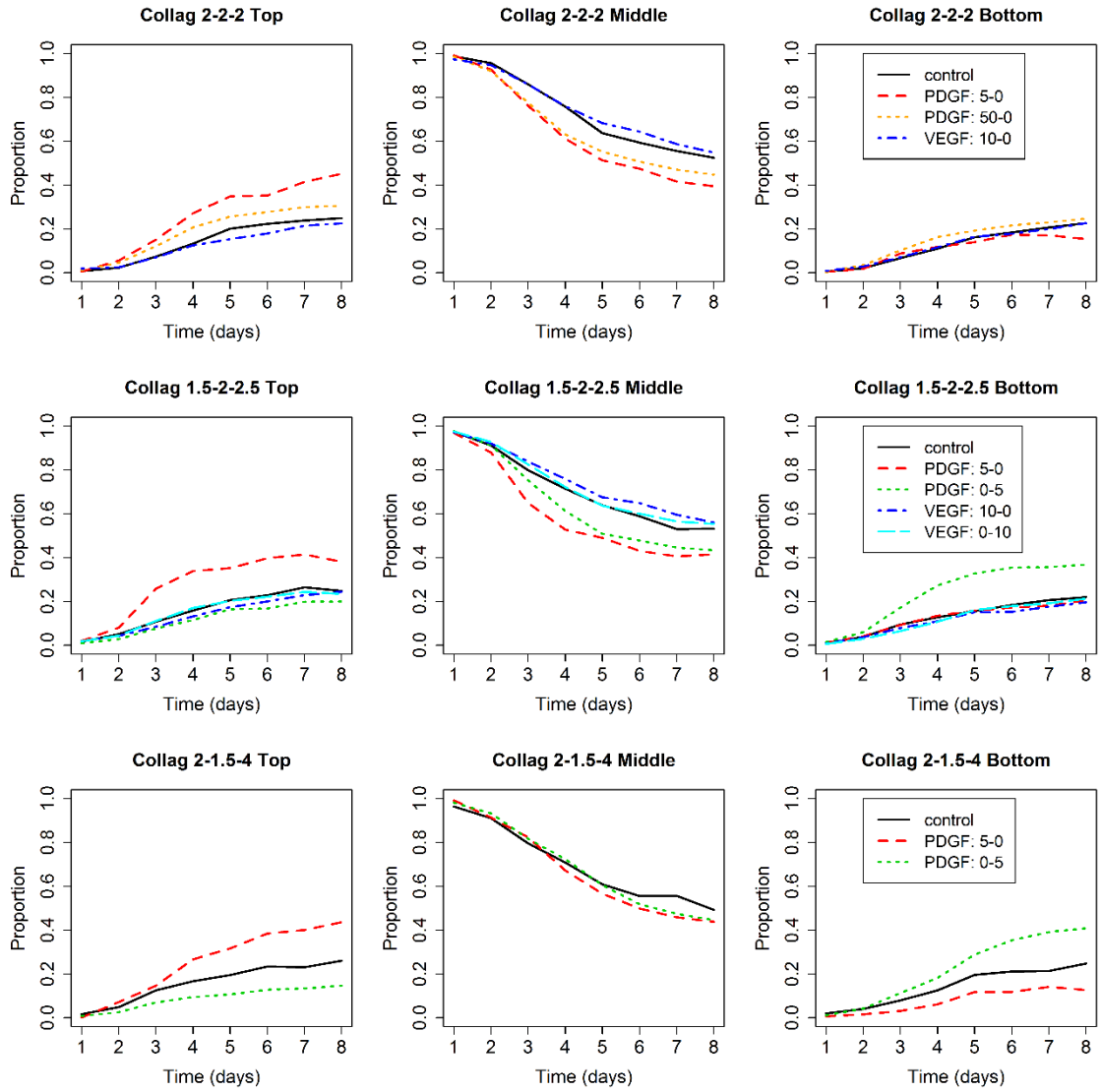

Figure 3. 11 Mean value of cell proportion evolution for each assay (rows).
Each mosaic column represents a zone/channel. Left: top channel, middle: middle channel, right: bottom channel.

Therefore, the adjusted multinomial logistic regression model for this assay, includes a quadratic effect of time with equivalent coefficients for top and bottom zones, as well as linear and quadratic effects of PDGF in top zone (denoted $[PDGF]_{Z1}$), while $[VEGF]_{Z1}$ effect is not significant. It is worth noting that the PDGF requires a quadratic term to represent the higher attractive power of lower collagen concentration (Figure 3.12).

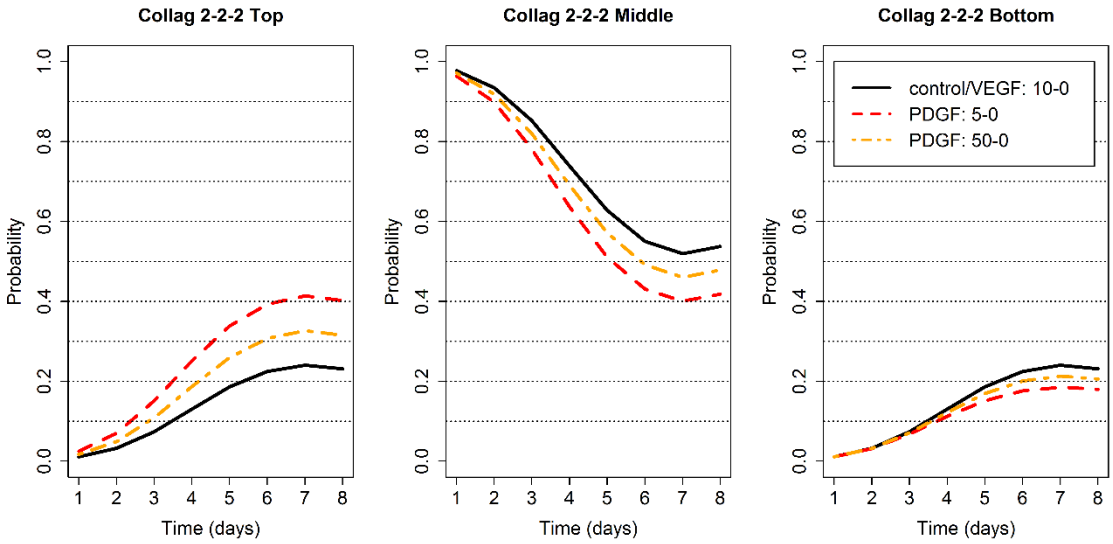

Figure 3. 12 Logistic multinomial model for assay 1. Expected proportion of cells evolution in every zone.

Adjusted parameters of the fit can be found in Table 3.3. To obtain a better idea of the net temporal effect of each GF, it is useful to plot the ratio of cell proportion in each zone between controls and GF cases. Figure 3.13 (first row) shows how the initial proportion of cells in top zone for a PDGF concentration of 5ng/ml (PDGF: 5-0) is about 2.2 times larger than the proportion of cells in such zone for the control case. This ratio decreases in time but never goes below 1.74. Similarly, a PDGF concentration of 50 ng/ml in top zone (PDGF: 50-0) presents the same effect but with lower values, reaching a maximum of 1.5 and a minimum of 1.36. Middle and bottom zones behave similarly, PDGF: 5-0 having the lower ratios.

Terms	Estimate p1	p-value	Estimate p3
Intercept	-5.76	0	-5.76
t	1.4	0	1.4
t2	-0.0981	0	-0.0981
[PDGF]Z1 (linear term)	0.178	0	0
[PDGF]Z12 (quadratic term)	-0.00338	0	0

Table 3. 3 Multinomial logistic regression model parameters for assay 1 (collagen concentration 2-2-2). p-values corresponding to the Wald Test.

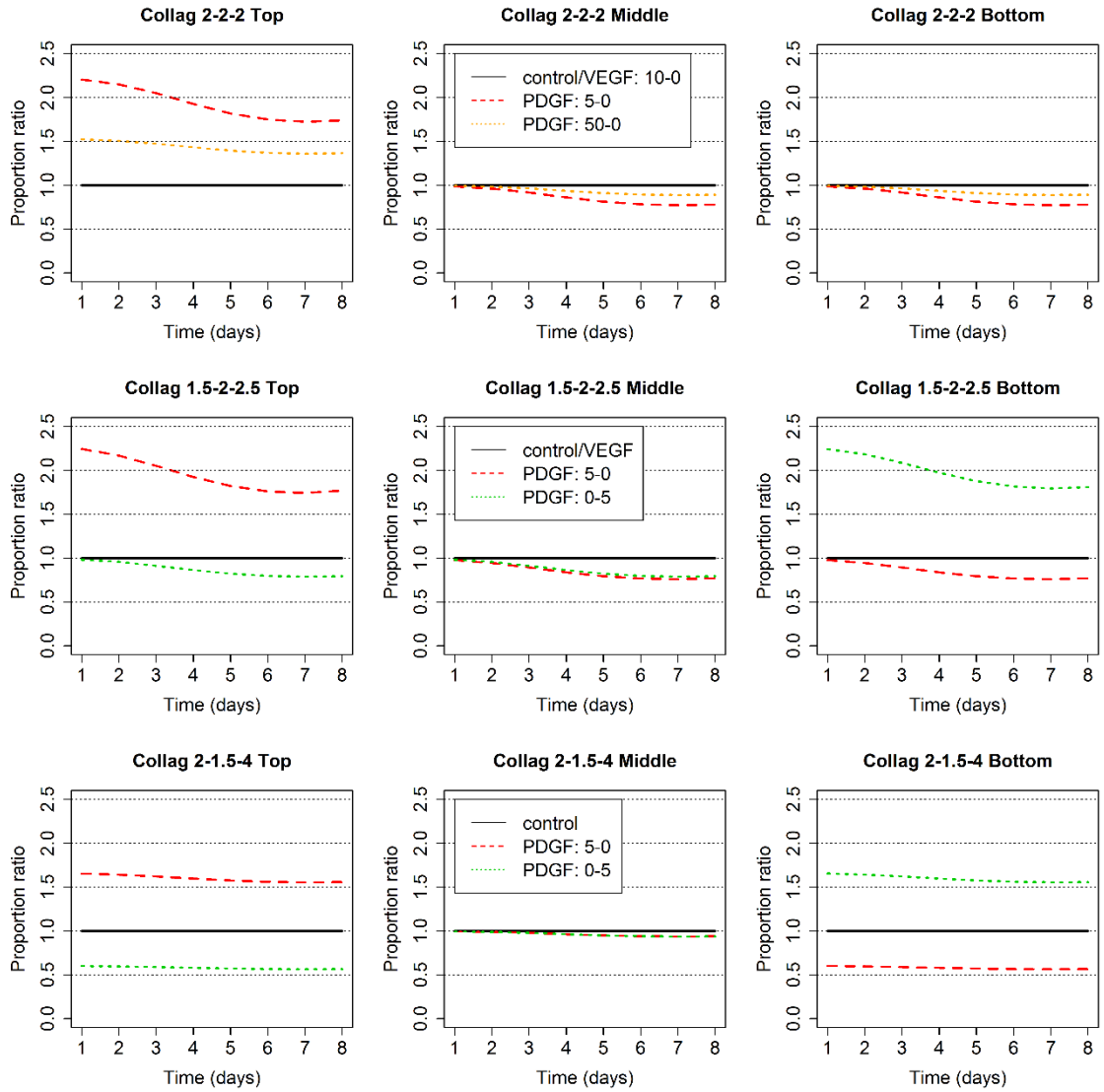

Figure 3. 13 Logistic multinomial model for assays 1 (first row), 2 (second row) and 3 (third row).
Evolution of the ratio between expected proportion of cells in each zone for each GF condition compared to control. Note that VEGF is equivalent to control since its influence is non-significant.

3.3.3 Impact of single and double step gradients of collagen concentration on chemotaxis (assays 2 and 3)

After the analysis of the effects of GFs alone, different step gradients of collagen concentration were stablished to elucidate whether these new mechanical conditions in combination with the GFs were able to alter the observed individual migratory patterns. Firstly, we used a single step gradient of 1.5, 2 and 2.5 mg/ml of collagen concentration in the top, middle and bottom chambers respectively, and secondly a double step gradient of 2, 1.5 and 4 mg/ml (see Table 3.1). In the first case (assay 2), both PDGF and VEGF were injected from both input channels separately, allowing us to study the effects of the GF gradients when applied in the same and opposite directions of the collagen concentration gradient. In assay 3, the same strategy was followed, but, based on the results from assay 2, using only PDGF.

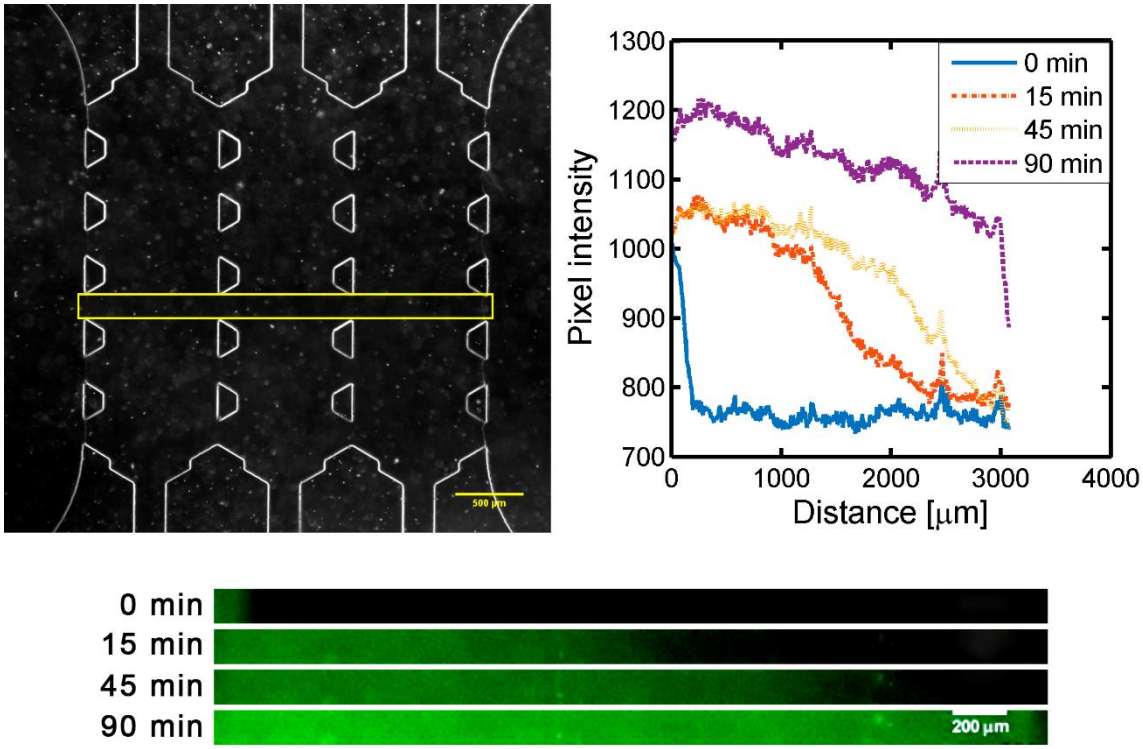

Figure 3. 14 Diffusion profile of FITC-dextran molecule (20KDa) across the chamber during the first 90 minutes. Images were captured with a 2X objective every 500 milliseconds for 3 hours. Yellow rectangle highlights the measured area

Cell ratio evolution in assay 2 was, for all the cases, practically equal compared to assay 1 where the collagen concentration was homogeneous. That is, VEGF had no influence compared to control, regardless the input channel used, and PDGF concentrations lead to similar cell proportion values: about 40% by the end of the assay in the zone were the GF was applied and 20% in the opposite zone (Figure 3.11 second row of panels). That is to say, the collagen concentration distribution had no significant effect on cell invasion, and top and bottom part could be considered almost equivalent depending on the input channel used for the GF. This symmetric behavior was also observed in assay 3, where the collagen gradients were stepper and in opposite directions. However, significant variations of cell proportion (about 44% lower than controls) in the zone opposite to the corresponding input channel were observed. Although the direction of the collagen concentration gradient does not seem to affect cell migration, the magnitude of such concentration does. A possible cause of this behavior could be the greater motility of cells in 1.5 mg/ml collagens compared to that in 2 mg/ml ones[210], explained by the differences in the structural characteristics of each collagen concentration such as mesh size or fibril diameter [221]. Compared to assays 1 and 2, more cells in assay 3 would arrive sooner to the interface of the gel in which the GF is being liberated, activating some kind of molecular signal that could be attracting more cells from middle zone, and decreasing the number of cells migrating towards the opposite zone. To discard some possible effects of the interfaces and the chip geometry on the GFs diffusion, we quantified the diffusive profile of Dextran-FITC (20KDa). Results showed that the diffusion of particles is almost the same for both hydrogels (Figure 3.14, gradient from left side of hydrogel to the right channel),

explained by the difference between particle and pore size (KDa and nm). Even though the pore size of 4mg/ml of collagen hydrogel was almost half of 2mg/ml [156], this reduction was not enough to decrease the particle movement in a significant way, therefore not affecting the diffusion of GFs.

Due to these intrinsic differences, a separated multinomial logistic regression model was adjusted for each assay (Figure 3.15).

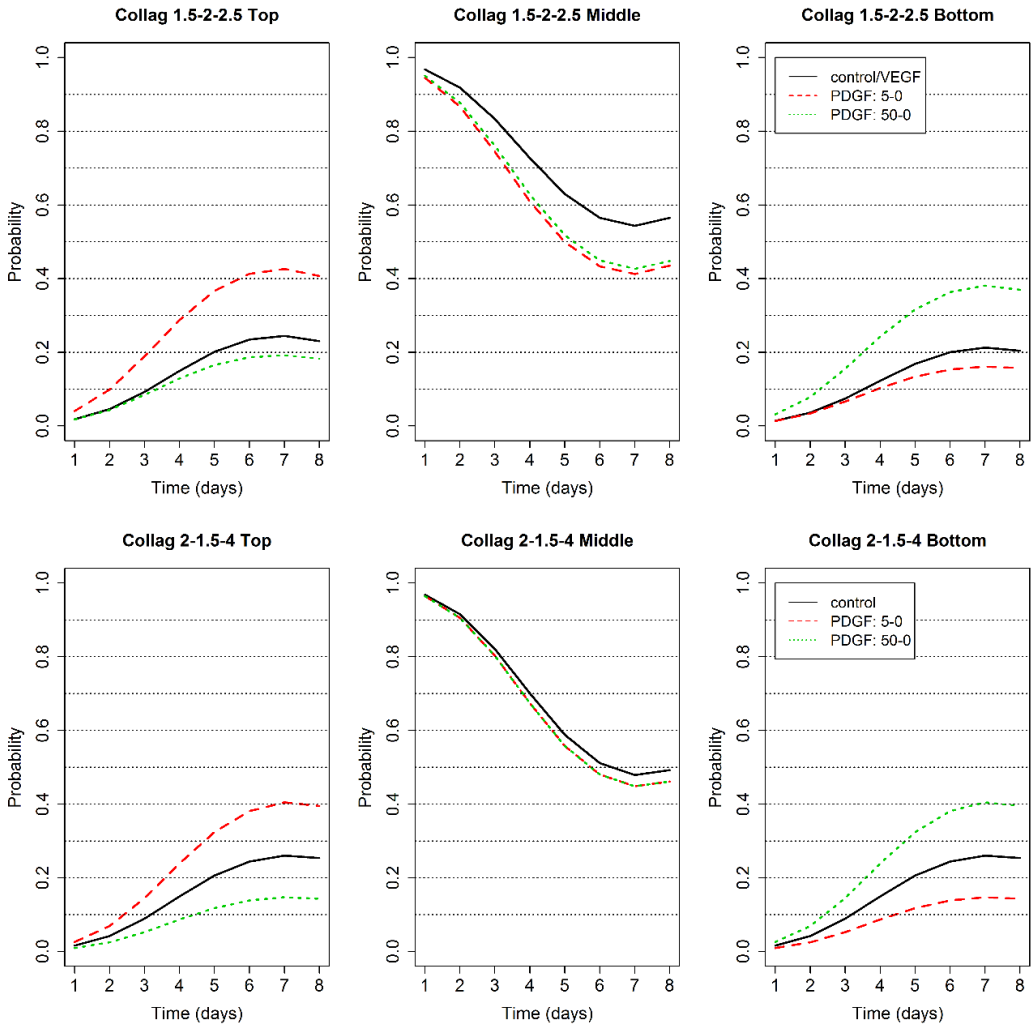

Figure 3. 15 Logistic multinomial model for assays 2 (first row) and 3 (second row).
Expected proportion of cells evolution in every zone.

Model for assay 2 is complex and includes two linear terms to account for the concentration of PDGF in top and bottom channels respectively, and four quadratic terms to account for the similar but not perfectly symmetric cell proportion temporal evolution in both zones (see Table 3.4).

Terms	Estimate p_1	p-value	Estimate p_3	p-value
Intercept	-5.14	0	-5.41	0
t	1.25	0	1.27	0
t^2	-0.0898	0.001	-0.0898	0.002
$[PDGF]_{Z1}$	0.166	0	0	-
$[PDGF]_{Z3}$	0	-	0.165	0

Table 3. 4 Multinomial logistic regression model parameters for assay 2 (collagen concentration 1.5-2-2.5). p-values corresponding to the Wald Test.

The ratio of cell proportion in each zone between controls and cases with PDGF, shows a trend practically identical to assay 1 (PDGF: 5-0) regardless the input channel used (Figure 3.13 first and second row), which confirms the little influence of the collagen gradient direction. Although model for assay 3 also includes quadratic terms independent of PDGF to account for the temporal evolution, it incorporates a term representing the difference of cell proportion between top and bottom zones, and therefore takes into account the negative effect that the PDGF has on cell population of the opposite channel (see Table 3.5). This predicts cell proportions that are about 1.5 times larger than the control in the zone where PDGF is applied and 2 times smaller in the opposite channel (Figure 3.5 third row).

Terms	Estimate p_1	p-value	Estimate p_3
Intercept	-5.34	0	-5.34
t	1.31	0	1.31
t^2	-0.0911	0.003	-0.0911
$[PDGF]_{Z1}$ - $[PDGF]_{Z3}$	0.101	0	-0.101

Table 3. 5 Multinomial logistic regression model parameters for assay 3 (collagen concentration 2-1.5-4). p-values corresponding to the Wald Test.

Both models were used to quantify the time at which the estimated probability reaches 0.2, 0.3 and 0.4 (tp_{20}, tp_{30} and tp_{40}) in top and bottom zones respectively, generating a lookup table for future studies (see Table 3.6). In control cases and those assays with VEGF, the probability 0.2 is reached at the 5th day (tp_{20} ~5) whereas the probability 0.3 is never attained (and consequently neither 0.4). On the other hand, PDGF decreases the temporal threshold, achieving the probability 0.2 in the range 3-3.5 days, even reaching 0.4 around the 6th day (tp_{40} ~6).

Regarding to the chemotactic index previously defined as the difference between the estimated proportions of cells in different zones, Table 3.6 shows its value at 7th day, when a stabilized behavior of proportions has been observed in the experiments. The total time evolution of the CI can be found in Figure 3.16. Values close to zero appear in control conditions (with no GFs) and cases with VEGF. On the other hand, the highest values correspond to PDGF at lower doses.

	Top			**Bottom**			**CI**
Collagen 2-2-2	tp_{20}	tp_{30}	tp_{40}	tp_{20}	tp_{30}	tp_{40}	
Control/ VEGF:10-0	5.09	-	-	5.09	-	-	0.00
PDGF:5-0	3.4	4.41	5.92	-	-	-	0.23
PDGF:50-0	4.04	5.57	-	5.59	-	-	0.11
Collagen 1.5-2-2.5	tp_{20}	tp_{30}	tp_{40}	tp_{20}	tp_{30}	tp_{40}	
Control/ VEGF:10-0/0-10	4.76	-	-	5.62	-	-	0.03
PDGF:5-0	3.01	4.03	5.42	-	-	-	0.26
PDGF:0-5	6.32	-	-	3.4	4.61	-	0.19
Collagen 2-1.5-4	tp_{20}	tp_{30}	tp_{40}	tp_{20}	tp_{30}	tp_{40}	
control	4.7	-	-	4.7	-	-	0.00
PDGF:5-0	3.49	4.57	6.25	-	-	-	0.26
PDGF:0-5	-	-	-	3.49	4.57	6.25	0.26

Table 3. 6 Time (days) at which the estimated probability of cells being in a certain zone reaches 0.2, 0.3 and 0.4 (tp20, tp30 and tp40 respectively).A hyphen (-) means that the probability does not attain the corresponding value at least in the studied range (8 days). Chemotactic Index (CI) is defined as the proportion of cells in the zone with GF minus the proportion of cells in the opposite zone.

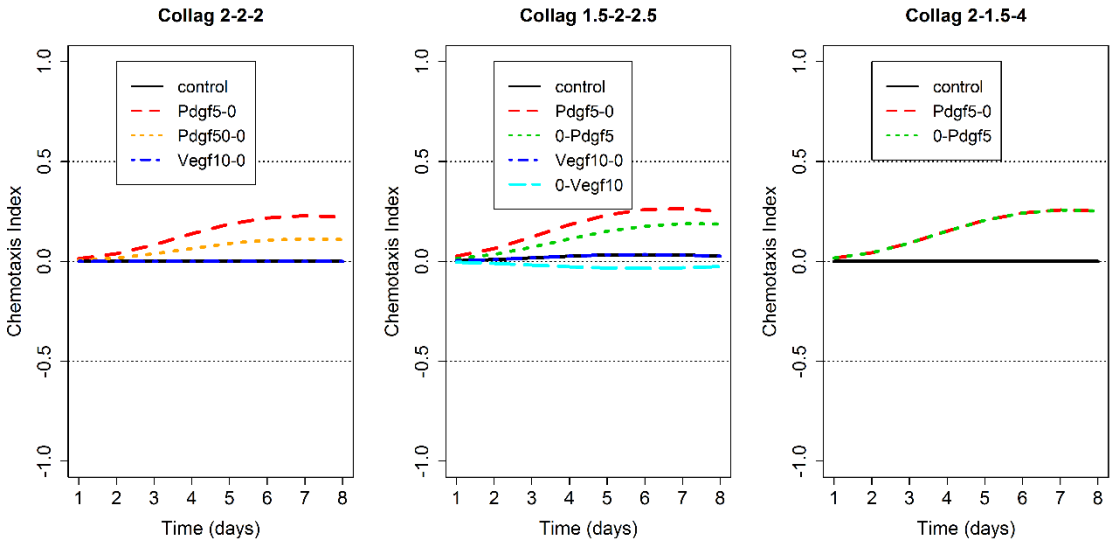

Figure 3. 16 Chemotactic index evolution for all the studied cases

3.4 Conclusions

In this work, the main proposed aims were achieved. On the one hand, a microfluidic device has been developed to quantify 3D cell migration through the interface of collagen-based gels with different concentrations in the presence of different GF gradients (namely PDGF and VEGF). The simple design of this microdevice allows an easy microscopy-based quantification via image processing and statistical analysis, which makes this chip a useful tool to perform 3D cell chemotaxis studies in different matrices. On the other hand, the results obtained from using this platform will be presented below.

A first analysis of the controls (with [PDGF] = [VEGF] = 0 ng/ml) revealed that the effects of collagen concentration and collagen gradients alone do not influence on the distribution of cells in the three channels during the individual invasion experiment, which was only dependent (quadratic order) on time.

A second exploration using the same collagen concentration in all channels (2 mg/ml) but different GF conditions, showed the strong chemo-attracting effect of PDGF at low concentrations (5 ng/ml), but weaker at higher concentrations (50 ng/ml). On the other hand, VEGF had no significant effect compared to controls, which was confirmed in a third analysis using both GFs and collagen concentration gradients.

Another third assay was performed to elucidate the role of the collagen step gradients. The results suggest that the step collagen gradient direction itself has not a direct effect on cell migration, although the magnitude of the concentration might still influence cell behavior. In fact, when the collagen step gradient is from 1.5 to 2.5 the role of the chemoattractant is similar to the case with uniform collagen density. However, if the gradient is not defined but collagen concentration is varied (2-1.5-4) there are significant negative effects (decreased cell population)

that were found in the channel opposite to the GF addition. Whether this is produced by some interaction between the GF and the collagen density, it is just a random process depending on the cell proximity to the interfaces, or it relies on some mechano-transduction signaling between the cells arriving to the interfaces and those still placed in the seeding zone is out of the scope of this work and will be explored in future studies.

To assess the reliability of our experiments, a wide statistical analysis were developed. In fact, experimental data were adjusted to different multinomial logistic regression models to elucidate the contribution and interactions between involved variables, particularly: time, collagen concentration magnitude, collagen concentration distribution (gradient) and GFs concentration. This kind of statistical modeling presents several advantages: a) it simultaneously represents the temporal evolution of the ratio of cells in the three zones, b) the model is multivariate and includes the ability to estimate the effect of one or more potential stimuli, whose statistical significance is stablished by test (e.g. study the effect of GF present in both channels simultaneously) c) the shape of GF effects or time evolution can be expressed, using adequate functions to include non-linear effects (for instance, the expected time to reach a given proportion in a certain area with GF can be easily obtained from the statistical model), d) the model can be used, without the necessity of performing new experiments, to estimate the migration response in different combinations of the considered stimuli, provided the desired GF doses fall within the current range. Apart from that, there are other advantages compared to other more commonly used methods such as the chemotactic index that is the necessity of significantly less time points for cell imaging and cell tracking measurements. However, it has also disadvantages. For example, the model could find significant statistical associations but not necessarily implying a cause-effect relationship, which should be established based on biological arguments and the adequate design of experiments.

From our study, we could conclude that our microfluidic device allows for the first time to perform 3D chemotaxis measurements for human cells through the interface of different collagen-based hydrogels. This new device can provide the basis for developing a platform for the chemotactic analysis of multiple interfaces between different biomaterials. In addition, our device can be easily extended to include more chambers, therefore increasing the number of possible conditions. This will allow testing cell migration towards specific chemo-attractants in order to characterize cell capacity to move from one matrix to another, significantly improving our understanding of how cell movement is regulated by chemotaxis and the different properties of the extracellular matrix. It is worth noting that the control over the interface formation is limited, and that some variations may arise due to the manual procedure used to insert the hydrogels into the corresponding chambers. Nevertheless, we did not observe a high variability during the experiments, cells showing a clear spatial independent pattern in their invasion from the central chamber.

In sum, the microfluidic-based chemotaxis study provided by this chip will allow tackling multiple problems in 3D cell migration, with a high control of the chemical environment and the extracellular matrix properties. In addition to the changes in ECM stiffness introduced in this Chapter

through the gradient of different collagen concentrations, it has been seen relevant to study how the disposition of the fibre network influences cell migration. Thus, in the next Chapter 4, which focuses on bone regeneration, the direct and indirect effect (ie. the disposition of ECM fibres) on cell migration will be analyzed when 3D cell culture is subjected to the application of another of the above-mentioned factors, fluid flow.

Chapter 4

Recreation of bone fracture healing microenvironment: effect of matrix architecture on 3D osteoblast migration

Abstract *

Osteoblast migration is a crucial process in bone regeneration, which is strongly regulated by interstitial fluid flow. However, the exact role that such flow exerts on osteoblast migration is still unclear. To deepen the understanding of this phenomenon, we cultured human osteoblasts on 3D microfluidic devices under different fluid flow regimes. Our results show that a slow fluid flow rate by itself is not able to alter the 3D migratory patterns of osteoblasts in collagen-based gels but that at higher fluid flow rates (increased flow velocity) may indirectly influence cell movement by altering the collagen microstructure. In fact, we observed that high fluid flow rates (1 µl/min) are able to alter the collagen matrix architecture and to indirectly modulate the migration pattern. However, when these collagen scaffolds are cross-linked with a chemical cross-linker, specifically, transglutaminase 2 (TG2), we did not find significant alterations in the scaffold architecture or in osteoblast movement. Therefore, our data suggest that high interstitial fluid flow rates can regulate osteoblast migration by means of modifying the orientation of collagen fibers. Together, these results highlight the crucial role of the matrix architecture in 3D osteoblast migration. In addition, interstitial fluid flow in conjunction with the matrix architecture seems to regulate the osteoblast morphology in 3D.

Keywords: *osteoblast migration, transglutaminase, interstitial fluid flow, fibers, collagen based matrices, cross-linkers*

This work has already been submitted to a JCR journal such as **C. Del Amo, V. Olivares, M. Cóndor, A. Blanco, J. Santolaria, J. Asín, C. Borau and JM García-Aznar. **Matrix architecture plays a pivotal role on 3D osteoblast migration: effect of interstitial fluid flow.** (Under review)*

4.1 Introduction

Previous chapters have analyzed aspects that affect cellular migration in angiogenesis or wound regeneration. This Chapter 4 is focused on the study of the cell behaviour during bone fracture healing, more specifically, the effect that one of the most relevant factors, fluid flow (and consequently matrix conformation) has on osteoblasts.

Fracture healing is a complex biological process that restores structural bone integrity [112,113]; the mechano-chemical microenvironment regulates all the steps in this process, from sequential tissue morphogenesis to a cascade of cellular and molecular events. The ability of bone to self-repair involves the coordination of cellular and mechanosensitive processes, especially cell differentiation, migration and surveillance [222–224]. This complex process is regulated by multiple microenvironmental factors that effectively determine the outcome of bone fracture healing. To unravel this complexity, experimental methodologies and computational modeling have been widely performed and combined [115,117,123–125] to improve the knowledge of this regenerative process.

Among all the microenvironmental factors that are involved in fracture healing, mechanics plays the most important role [114], and it is normally associated with the stability of the fracture gap. Indeed, primary fracture healing occurs when the fracture gap presents extreme stability and a negligible affected area, while secondary healing implies moderately affected areas and stability, occurring in the vast majority of bone injuries [112,115]. Recently, several tissue differentiation theories have been proposed, and they have been virtually tested by computers using different mechanistic-based stimuli, such as strain, pore pressure or fluid flow [110,225–228]. The theory of Lacroix and Prendergast [123] assumes that a tissue can differentiate into another specialized tissue depending on the values of two mechanical variables, namely, the deviatoric strain and the fluid flow velocity. Similarly, the theory of Gómez-Benito et al. [225] proposes a similar assumption but considers only the deviatoric strain. In a more recent work, Gonzalez-Torres et al. [110] demonstrated the relevant role of interstitial fluid flow in tissue differentiation under cyclic loading conditions. In addition, previous cell culture studies have analyzed the response of different bone cells to interstitial fluid flow (abbreviated FF) and found that interstitial FF had a stronger influence on osteocytes than on osteoblasts and preosteoblasts [229]. Moreover, the stimulation of osteoblasts by the application of fluid shear stress has suggested an increase in the release of signaling molecules such as cyclic adenosine monophosphate (cAMP) or prostaglandin E2 (PGE2) [230].

However, there is a certain lack of knowledge about how microenvironmental factors regulate cell migration during the bone healing process. In fact, the migration of osteoblasts is crucial in fracture healing and occurs both individually and collectively for the deposition of new bone [120]. Via focal adhesions, osteoblasts recognize the substrate by adhering to it and by modifying their behavior depending on the matrix component or the mechano-chemical stimuli applied [120]. Therefore, the role of the extracellular matrix in osteoblast migration is also fundamental. Type I collagen is the most abundant bone matrix protein [231,232]. The stiffness of the extracellular matrix (ECM) in the damaged area increases during the stages from callus

formation through collagen type I secretion to final bone, thus altering cell behavior during the bone healing process [121,233,234]. As a method to investigate osteoblast mechanotransduction, the substrate of the cell culture can be modified by using cross-linking methods (such as chemical cross-linkers), consequently varying the stiffness experienced by cells [229].

Other factors, such as transforming growth factor beta (TGF-β) superfamily, bone morphogenetic proteins (BMPs), and interleukins (IL-6, IL17F, and IL1β), can also play a regulatory role in bone fracture healing [99,118,119]. In addition, 3D experimental assays revealed a low chemotactic effect of growth factors on osteoblasts in terms of migration compared to the response of other cell types under similar conditions [126,235]. For instance, while fibroblasts exhibit directional migration under human platelet derived growth factor-BB (PDGF) gradients [169], osteoblast migration seems to be regulated by the ability of cells to remodel the matrix [235].

Despite the numerous 3D-culture systems and techniques already published, there are still few studies of the biomechanical response of bone cells. There are even less studies specifically about human primary osteoblasts embedded in 3D *in vitro* microenvironments since most of the bone studies have been developed with non-human cells of other animal origins, such as murine osteoblasts [236–238]. Previous studies have shown that both matrix characteristics (in terms of chemical composition) and fluid flow are important regulators of osteoblast behavior [239]. Therefore, to the best of our knowledge, the effect of these factors on osteoblast migration has yet not been experimentally explored. Hence, the main aim of this work is to understand the role of interstitial fluid flow and how extracellular matrix variations affect osteoblast migration in 3D. For this purpose, we developed a microfluidic device that allows the application of interstitial fluid flow on collagen-based gels and allows high-quality image acquisition. Thus, this system is combined with an image-based methodology to quantify not only migration parameters but also the fiber alignment and matrix porosity of collagen hydrogels. While keeping the collagen density constant, the microstructure was altered by adding the cross-linking enzyme transglutaminase 2 (TG2) [240]. TG2 is a multifunctional enzyme with Ca^{+2}-dependent protein cross-linking activity that also exhibits GTPase, cell adhesion, protein disulfide isomerase, kinase and scaffold activities [241]. This molecule is involved in apoptosis, matrix stabilization and cell adhesion in a variety of tissues, with possible involvement in bone matrix maturation and calcification [242].

Therefore, in this work, it has been quantified osteoblast migration patterns and compared them for different collagen-based architectures that were modified by varying the fluid flow conditions and using or not using cross-linkers.

4.2 Material and Methods

4.2.1 Fluid flow set-up

The fluid flow system consists of a microfluidic device lodged inside a hand-made platform fabricated by rapid prototyping and precision mechanics. The components were connected with

PTFE (polytetrafluoroethylene) tubing (inner Ø = 0.3 mm, outer Ø = 0.6 mm) through connectors [Y tube fitting PVDF (polyvinylidene fluoride), male and female luer locks and screwed connectors M6] to two syringe pumps (Harvard Apparatus Pump 11 Elite) (See Figure 4.1).

The geometry of the microfluidic devices used in these experiments was adapted from the chips described in Chapter 2 and developed by Farahat et al. (2012) with fabrication methodology [127,138]. The new design is based on a central chamber where a hydrogel is inserted to mimic the extracellular matrix. This chamber is surrounded by two channels that allow the application and control of different fluid flow conditions. The microfluidic geometry was patterned in an SU-8 wafer by soft lithography techniques, and this wafer served as a mold to cure the PDMS (poly(dimethlysiloxane)) (Sylgard 184, Dow Corning GmbH) in a 10:1 ratio) and to obtain the desired design. Plasma treatment was used for the irreversibly bonding of the PDMS device with a glass coverslip followed by coating with PDL (poly-D-lysine hydrobromide, 1 mg/ml, Sigma) to enhance hydrogel adhesion. Based on previous works, the initial flow rate applied to the cell culture in order to simulate the interstitial fluid flow was 0.1 µl/ml [243], followed later by the application of a higher flow rate (1 µl/min) in order to increase the generated shear stress. Additionally, 1 µl/min was the flow rate applied in experiments for analyzing the effect of fluid flow on the matrix architecture. Figure 4.1A describes the geometry of this chip, the disposition of the collagen-based hydrogel onto the chip (located in the central chamber) and the flow direction.

To apply fluid flow in a systematic way with the microfluidic device, we developed a flow adapter fabricated by means of additive manufacturing. Additive manufacturing or three-dimensional printing has acquired significant interest in manufacturing by directly producing 3D designs from computer-aided drawing (CAD) files [244]. As an automatic, assembly free 3D manufacturing method with fast-improving resolution and low costs, rapid prototyping (RP) has recently attracted attention for manufacturing microfluidic systems or their components [245]. The basis of this method of manufacturing is the production of parts shaped gradually and the addition of solid material [246], giving the user high versatility in terms of adaptable designs and chip geometries.

The 3D flow adapter used to perform these experiments consisted of a base with two holders, where the microfluidic device was viewed with the microscope objective, and their corresponding lids, with holes to allow the connector input (see Figure 4.1B).

The base, fabricated in aluminum, consists of two compartments. Each compartment was approximately three millimeters larger than the PDMS devices to be fitted and had a window that allows microscopic observation of the microfluidic channels.

Covers were designed to obtain a leak-proof system, and the cover elements are described below (see the corresponding element for each number in Figure 4.1). In the upper part of the cover, the following parts were distinguished: 1) four holes where the corresponding connectors of inputs and outputs of tubes are inserted, 2) a window to allow the passage of light during visualization of samples under the microscope, and 3) six holes for the locking system (six M3 screws and hexagonal nuts). The lower part of the lid, in contact with the chip, features the following elements: 4) a system that facilitates the user to fit the chip and 5) four recesses for the placement of O-rings

(silicon, inner diameter = 4 mm, thickness = 1 mm; not shown in the Figure), which ensure the leak tightness of the system and which coincide with the holes punched in the microfluidic chip. The diameter of these holes is 3 times larger than the diameter of the chip holes.

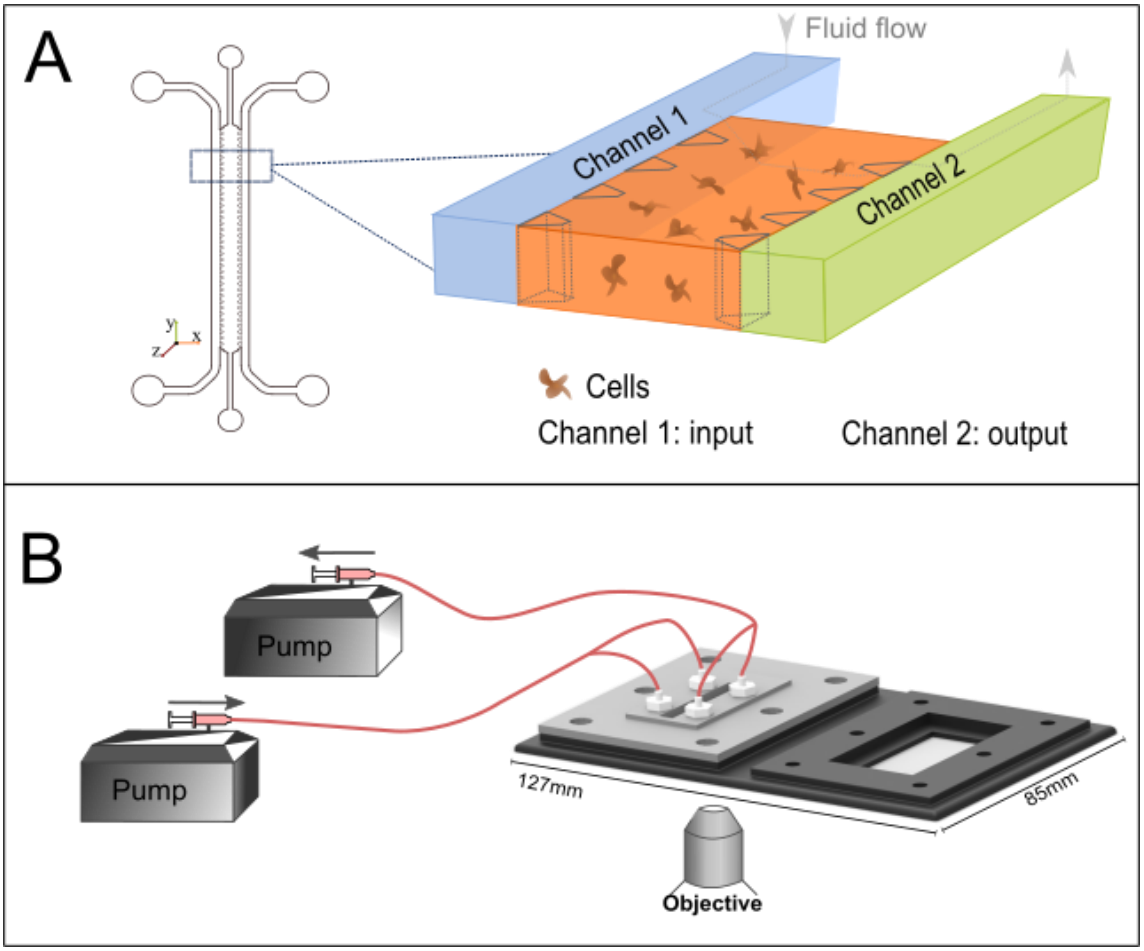

Figure 4. 1 Microfluidic device conformation and fluid flow support.
A) The general conformation of the microfluidic device and its transversal section to visualize the distribution of channels. B) A representative diagram of the fluid flow setup (1: input and output connectors; 2: microscopic visualization area; 3: screw holes for the locking system; 4: recess for microfluidic chip insertion), P201730809, property of the University of Zaragoza.

Once the prototype of the encapsulation was defined, the covers were manufactured by the 3D Object Eden 350 V printer with the material RGD525, which was found to be the most appropriate material for the conditions to which the system was to be subjected. This platform has been provisionally covered by patent P201730809, property of the University of Zaragoza, as part of the development of this thesis.

4.2.1.1 RDG 525: the optimal material for 3D printing

Considering the purpose of this system, one of the most important points was the possibility of platform sterilization, making it suitable for cell culture by autoclaving cycles. For the performance of cell migration tests, the flow system must be placed in an incubation chamber at 37°C and 5%

CO_2 under humidity conditions for at least 24 hours and must support these temperatures without deformation. Under these conditions, the materials initially chosen were RGD 720 (general purpose) and RGD 525 (high temperature). Analyses of the pieces were carried out by coordinate measurement of the pieces before and after autoclaved cycles and finite-element simulation (Abaqus) (data not shown) to quantify the deformations of the material under the high-temperature conditions previously mentioned. It was possible to conclude that with the RGD 525 material, the small deformations induced by autoclaved cycles allowed the planned test setups to be performed and had no influence on the results; therefore, this was the best material for our assays.

4.2.2 3D Cell culture and Hydrogel preparation

Human osteoblast cells (HOBs; PromoCell) were used at low passages in these experiments, and osteoblast growth medium (PromoCell) was used as the cell culture medium. In total, 40 µl of cell suspension at a density of $1 \cdot 10^6$ cells/ml was added to the collagen hydrogel by pipetting it into the central channel.

Collagen hydrogel type I (rat tail, BD Biosciences) was used at a final concentration of 4 mg/ml with DPBS 10X (Lonza), adjusting the pH to 7.4 with 0.5 M NaOH. In hydrogels crosslinked with transglutaminase 2 (rhTGM2, R&D Systems), this enzyme was added at the concentration of 25 µg/ml [235]. The polymerization of hydrogels and cell maintenance were performed in an incubator at 37°C and 5% CO_2 under humidity conditions, avoiding prepolymerization of the hydrogels.

Mechanical and microstructural characterization of 4 mg/ml collagen hydrogels was performed in a previous work by using a Haake Rheostress 1 rheometer for quantification of the hydrogel mechanical properties and a scanning electron microscope (SEM) for microarchitecture visualization (see Table 4.1) [235].

Collagen hydrogels	Storage shear modulus G' (Pa)	Maximum shear strain	Maximum G' (Pa)	Strain at maximum G
4mg/ml	121.03 ± 9.94	0.403	191.2	0.403
4mg/ml +TG2	127.90 ± 14.43	0.449	285.5	0.384

Table 4. 1 Mechanical properties of the collagen hydrogels used for the *in vitro* experiments. Three samples were analyzed for the cases without TG2 and 25 µg/ml of TG2. Data taken with permission from [235]**.**

4.2.3 Image-based quantification of hydrogel architecture

DQ-Collagen™ type I from bovine skin fluorescein conjugate (Thermo Fisher) was used to analyze the disposition of collagen fibers inside the hydrogel. The fluorescence of this reactant was used to determine the morphology of our hydrogels using a Nikon D-Eclipse C1 confocal

microscope equipped with a 40X oil objective. In total, 10 µl of DQ-Collagen was added to the collagen hydrogel (using a previously described procedure), obtaining a final concentration of 25 µg/ml [247], and softly pipetted into the microfluidic device. Then, samples were incubated overnight in an incubator and connected to the fluid system. The flow rate applied to the corresponding devices was 1 µl/min. Images were captured before and after the flow application to analyze the possible modifications caused by this mechanical stimulus.

To the best of our knowledge, this is the first time this fluorescent reactant was used for this purpose since it is normally used for measuring matrix degradation by cells [247]. Colocalization of matrix images from confocal reflection, collagen immunostaining and DQ images was performed by analyzing the ratio of detected and overlapping fibers, thus confirming the validity of this technique.

4.2.3.1 Coincident fibers by using different methodologies of collagen matrix visualization

To evaluate the coincident position of collagen fibers in all of methodologies, an algorithm to automatically obtain the true colocalization proposed for Villalta et al. was executed in MATLAB (the algorithms for the analysis of collagen matrix architecture used in this Chapter has been implemented in MATLAB by V.Olivares, M. Cóndor and PhD C.Borau) [248]. Manders overlap coefficient (R) and Pearson's correlation coefficient (r) were calculated basing on the fluorescence intensity of each pixel in a pair of images.

According to the positive, negative or null proportional contribution of pixel pairs, the correlation of images varied, being positively correlated when $r>0$, independently distributed when $r\approx0$, or negatively correlated. As the algorithm used to analyze the images allows only two simultaneous comparisons, in the case of hydrogels with DQ-Collagen, all options were cross-checked between them (confocal reflection- DQ-Collagen fluorescence – Alexa 546 immunostaining). For the case of the gel without collagen DQ, only a comparison of images was required (see Table 4.2). Figure 4.2 shows the results obtained in the analysis of coincident fibers for a pair of selected images to validate our novel method.

Based on the results from the exhaustive image and statistical analyses performed, our hypothesis of coincident collagen fibers in the case of DQ-Collagen application could be accepted. r values fluctuated between 0.36 and 0.79 and were positive in all cases, which indicates a true correlation between the images.

		Pearson	P value*	Manders Overlap	P Value*
Collagen hydrogel	*Alexa 546 +C Reflection*	0.36752287	1E-16	0.5310421	1E-16
DQ Collagen hydrogel	*Alexa 546+ DQ collagen*	0.79859203	1E-16	0.8585667	1E-16
	Alexa 546 +C Reflection	0.40916434	1E-16	0.58667082	1E-16
	DQ Collagen + C Reflection	0.44234043	1E-16	0.60646546	1E-16

Table 4. 2 Corresponding values for Manders overlap coefficient and Pearson's correlation. *P value of 0.95% indicates significant colocalization (p<0.05)

In addition, to verify that the values obtained from the correlation analysis were not coincidental, the same test was performed, but the pixels of the image were distributed in a random manner. Statistical analysis was then carried out to check that the measured values of R and r were significantly higher than those measured when there was only random overlap.

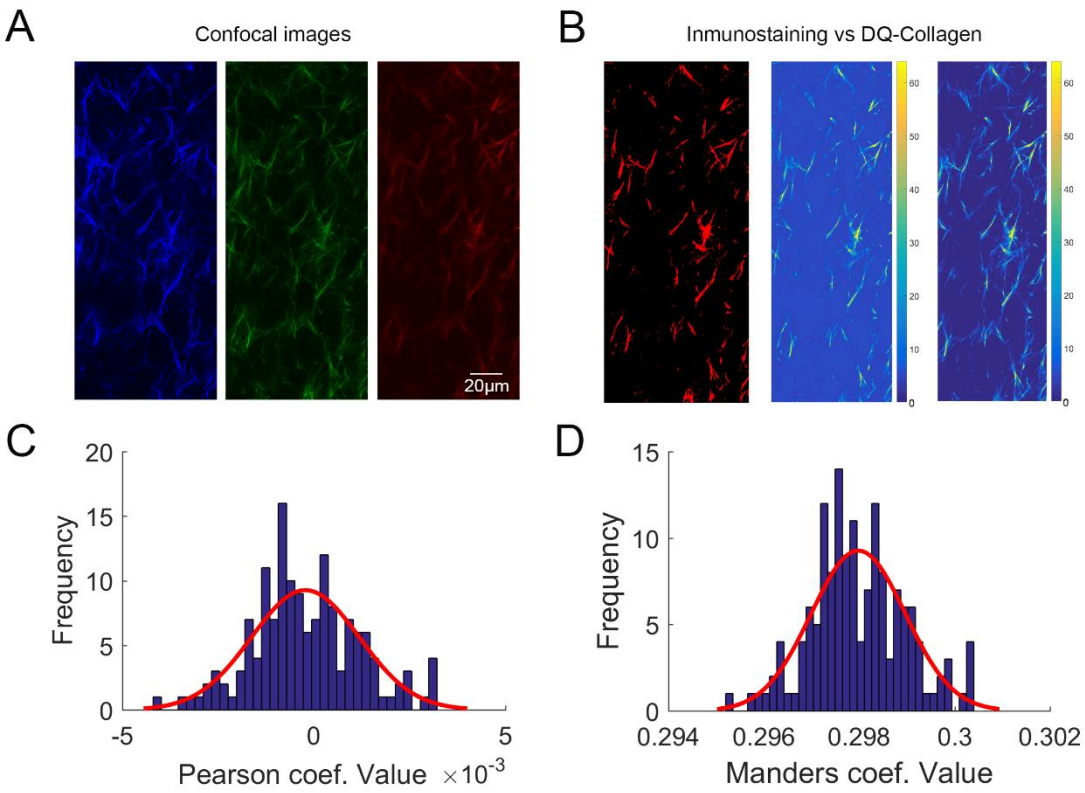

Figure 4. 2 Colocalization analysis of collagen fibers.
Confocal reflection of a collagen hydrogel, DQ-Collagen and the immunostained hydrogel images captured with a 60X oil objective are shown in A. B) Images from DQ-Collagen and inmunostained collagen was compared obtaining the colocalization mask followed by the Pearson and Manders map. Distribution of Pearson's correlation coefficient (C) and Manders overlap coefficient (D) for the fluorescence intensity of each every pixel in a pair of images

Immunostaining for collagen was also performed to confirm our hypothesis about fiber distribution. The samples were incubated with monoclonal anti-collagen type I (mouse IgG isotype) (Sigma-Aldrich, C2456) overnight at 4°C after the samples were fixed with 4% paraformaldehyde (PFA, Affymetrix) in PBS for 15 min at room temperature based on the protocol proposed by Sung et al. [249]. Following blocking with serum and washing the channels, Alexa Fluor® 546 donkey anti-mouse IgG (H+L) (Molecular Probes, A10036) was added, and the samples were incubated overnight at 4°C.

Confocal z-stack images were sequentially acquired at one point at the center of each microdevice, maintaining a constant step size of 0.5 µm and a maximum pixel dwell time. The 3D reconstruction of the cross-sectional collagen network images captured with a 40X oil objective (46 slides) was carried out by 3D skeletonization using the Ct-FIRE algorithm [250,251] and a binary stack was obtained (see Figure 4.3). Furthermore, we quantified the fiber orientation and pore size with another existing method [252]. Orientation was obtained by considering the binary matrix as a distribution of masses. The tensor of inertia for each individual fiber was calculated, and the axis of minimum inertia, which points in the direction of the fiber, was obtained through diagonalization. Pore size was evaluated by obtaining the distribution of nearest obstacle distances (NODs, defined as the Euclidean distance from a point in the liquid phase to the nearest point in the solid phase.

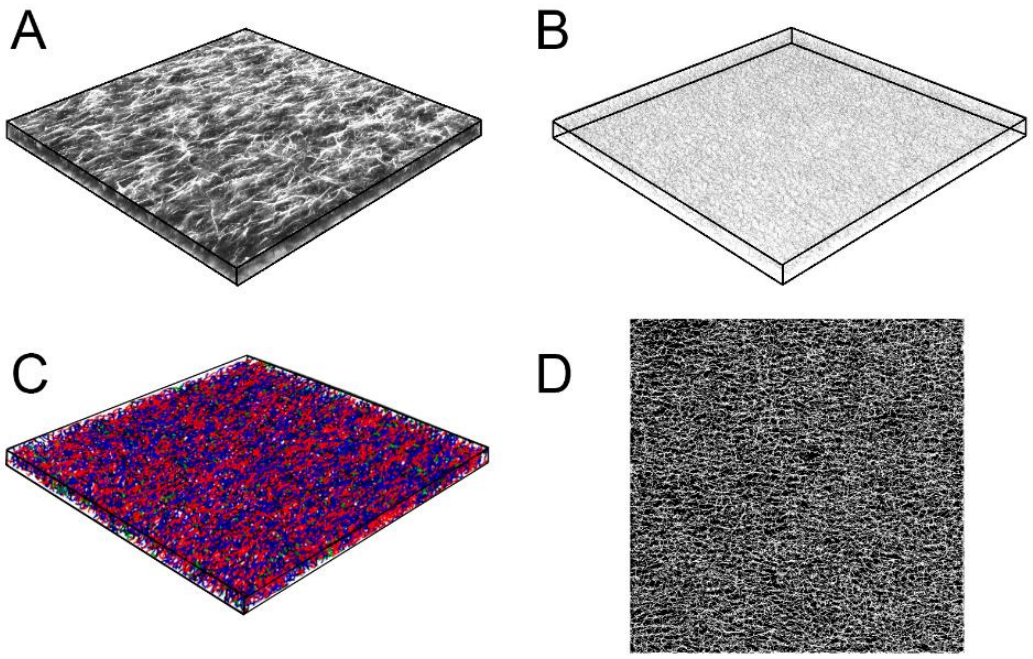

Figure 4. 3 Image processing of collagen matrix
A) Stack of confocal cross-sections. B) Binarized stack visualized with Paraview. C) Ct-Fire reconstruction of the collagen network viewed in MATLAB. D) 2D Projection of the obtained skeleton of a collagen matrix.

4.2.4 Image acquisition and cell tracking processing

The complete system with the corresponding samples and hardware for the flow application were inserted into the incubator chamber of the microscope (Nikon D-Eclipse C1, 10X objective), and the samples were maintained at 37°C, 5% CO_2 and 95% humidity. Then, time-lapse imaging was performed by choosing the focal plane in the middle along the z-axis and by acquiring phase contrast images every 20 min for 24 h. To track the cell trajectory, a hand-coded semi-automatic script implemented in MATLAB, already used in previous works, was employed [126,169,235].

ANOVA and Kruskal-Wallis tests were performed to assess statistical significance among the cell migration data sets, and statistical significance was assumed when $p < 0.001$ (***), $p < 0.01$ (**) or $p < 0.05$ (*).

4.2.5 Immunofluorescence and quantification of cell morphology

Cells arranged within the collagen fibrillar network were fixed and immunostained for vinculin and phalloidin to assess focal adhesion formation and cytoskeletal distribution. Samples were fixed by incubation with 4% paraformaldehyde for 20 min and then washed five times with PBS at room temperature (RT). Permeabilization of the cells was performed using 0.1% Triton X-100 (Calbiochem) in PBS for 10 min at RT. The cells were washed another three times and blocked with 5% BSA/PBS (Sigma) with 3% goat serum for 4 h at RT. Afterwards, mouse anti-human hVin-1 antibody (ab11194, Abcam) at 1:100 dilution in 0.5% BSA/PBS was added to the device and then incubated overnight at 4°C. After the device was washed with 0.5% BSA/PBS at least 5 times, it was incubated with Alexa Fluor® 488 goat anti-mouse antibody (A11029, Molecular Probes) at 1:100 dilution and with phalloidin-tetramethylrhodamine B isothicyanate (TRITC) (Sigma-Aldrich P1951) at 1:200 dilution for 3 h at RT in the dark, followed by three washes with 0.5% BSA/PBS and subsequent washes with PBS alone. Finally, DAPI (Invitrogen, D1306) was added at a ratio of 1:50 to stain the cell nuclei, and the samples were incubated for 1 h in the dark at RT. Then, the samples were washed again with 0.5% BSA/PBS and subsequently imaged using an Olympus Fluoview FV10i confocal microscope equipped with an UPLSAPO 60XW objective.

Additionally, quantitative analysis of the cell morphology these immunostained samples was performed by using a Nikon D-Eclipse C1 confocal microscope (40X-oil objective) to acquire images and a hand-coded script implemented in MATLAB to process them. Two main parameters were measured: cell solidity and cell major axis length. The former is calculated as the cell area divided by the area of the minimum convex polygon containing the cell. This solidity value helps to measure the irregularity or star-like shape of cells. Small values correspond to cells with thin bodies and long spread arms, and higher values relate to either spread or thin cells without protrusions (see Figure. 4.8D).

4.2.6 Quantification of interstitial fluid flow in microfluidic devices

Throughout this work, the flow rate value refers to that introduced into the pump programing. However, to determine the distribution and velocity of the fluid flow inside the hydrogel, two complementary methodologies were proposed. On the one hand, real fluid velocity was obtained by tracking fluorescent particles through the hydrogel, whereas computational simulations estimated this speed and the distribution of fluid along the channels and the central chamber. In this section, both approaches are explained, while their corresponding results are summarized in the following section.

4.2.6.1 Bead tracking

Carboxilated beads (FluoSpheres™ Carboxylate-Modified Microspheres, 0.2 µm, red fluorescent (580/605)-, Life Technologies F8887), which were previously sonicated, were used to quantify the flow velocities into the hydrogel. A hand-coded script was implemented in MATLAB (R2013a) to track the beads and obtain their velocity. To quantify the movement of beads into the collagen hydrogel, the concentration of gel selected to perform this experiment was 1.5 mg/ml in order to simplify the experimental setup. Images were captured every second during a 5 min period with a fluorescence microscope (Nikon D-Eclipse C1, Plan Fluor ELWD 40x Ph2 ADL). The distribution of fluid flow inside the 4 mg/ml hydrogel was simulated and compared to the results obtained in this experimental assay.

4.2.6.2 Computational model

Computational fluid dynamics was used to predict the flow rate inside the chamber using COMSOL Multiphysics 4.3 finite-element code (COMSOL Multiphysics). The model represents the geometry with a central channel, which lodges the hydrogel and the channels from each reservoir (see Figure 4.1A). The cell culture medium -assumed to be water- was defined as incompressible and homogenous, with a dynamic viscosity of $1 \cdot 10^{-3}$ Pa·s (common for both hydrogels). The corresponding permeability for each gel concentration was $3.19 \cdot 10^{-13}$ m^2 for the 1.5 mg/ml hydrogel and $3.82 \cdot 10^{-13}$ m^2 for the 4 mg/ml hydrogel and was experimentally calculated following a procedure published in a previous work [253].

Two inlets were defined at the entries of the left channel and the contact area between the hydrogel and the channel. The same boundary conditions were imposed for the outlets in the opposite location of the right channel. PDMS surfaces were considered impermeable walls.

The device was divided in three regions: zones 1 and 3 correspond to the lateral channels, and zone 2 corresponds to the middle channel (see Figure 4.1A; zone 1 is in blue; zone 2, in orange; and zone 3, in green). In zone 2, the inertial term was neglected following the Stokes-Brinkman equation for incompressible flow. Laminar flow was used, however, for lateral channels. Extremely fine elements were used to mesh the relevant geometry. The size of the elements ranged between $8.19 \cdot 10^{-4}$ mm and 0.143 mm, and the complete mesh consisted of 86802 elements.

4.3 Results

Several conditions have been tested to explore the role that extracellular matrix architecture and interstitial fluid flow exerts on 3D human osteoblast migration.

4.3.1 Similar flow rate estimation by different methodologies

To simplify the quantification of fluid flow into the hydrogel, a 1.5 mg/ml collagen concentration was selected for this experiment. The collagen network for this concentration presented a disposition of the fiber network that facilitated the visualization of beads inside the hydrogel. The results obtained by particle tracking and computational simulations were similar. These results allowed us to determine how fluid flow was distributed along the chambers and to extrapolate distribution for the 4 mg/ml hydrogel. Previously, the permeability of both hydrogels was determined, and the following values were obtained: $3.19 \cdot 10^{-13}$ m^2 for the 1.5 mg/ml hydrogel and $3.82 \cdot 10^{-13}$ for the 4 mg/ml hydrogel. These data were incorporated into a COMSOL model, and the velocities for a 4 mg/ml gel medium (23.47±0.7714 µm/s) and for a 1.5 mg/ml gel medium (24.238±1.0255 µm/s) were obtained. Data for each condition were taken from the area between the two posts and across the width of the gel, including the central and lateral areas of the gel (the results are summarized in Table 4.3).

Velocity 1.5 mg/ml Collagen (µm/s)		**Velocity 4 mg/ml Collagen (µm/s)**
Particle tracking	***COMSOL Multiphysics 4.3***	
26.0655±15.6797	26.86 ± 4.22	25.2453 ± 8.1634

Table 4. 3 Values of fluid speed inside the 1.5 mg/ml and 4 mg/ml collagen hydrogel.

Another flow rate applied to the osteoblast culture was 0.1 µl/min, and 2.347 µm/s was the corresponding value estimated for this case.

It is worth noting the high dispersion obtained (comparable to the mean). This effect might be caused by the high concentration of particles that were retained in the meniscus of the gel versus the long distance traveled by other groups of beads (Figure 4.4 A and B). On the other hand, the computational model showed a symmetric distribution of fluid inside the chamber when analyzing the streamline trajectories (Figure 4.4 C and D).

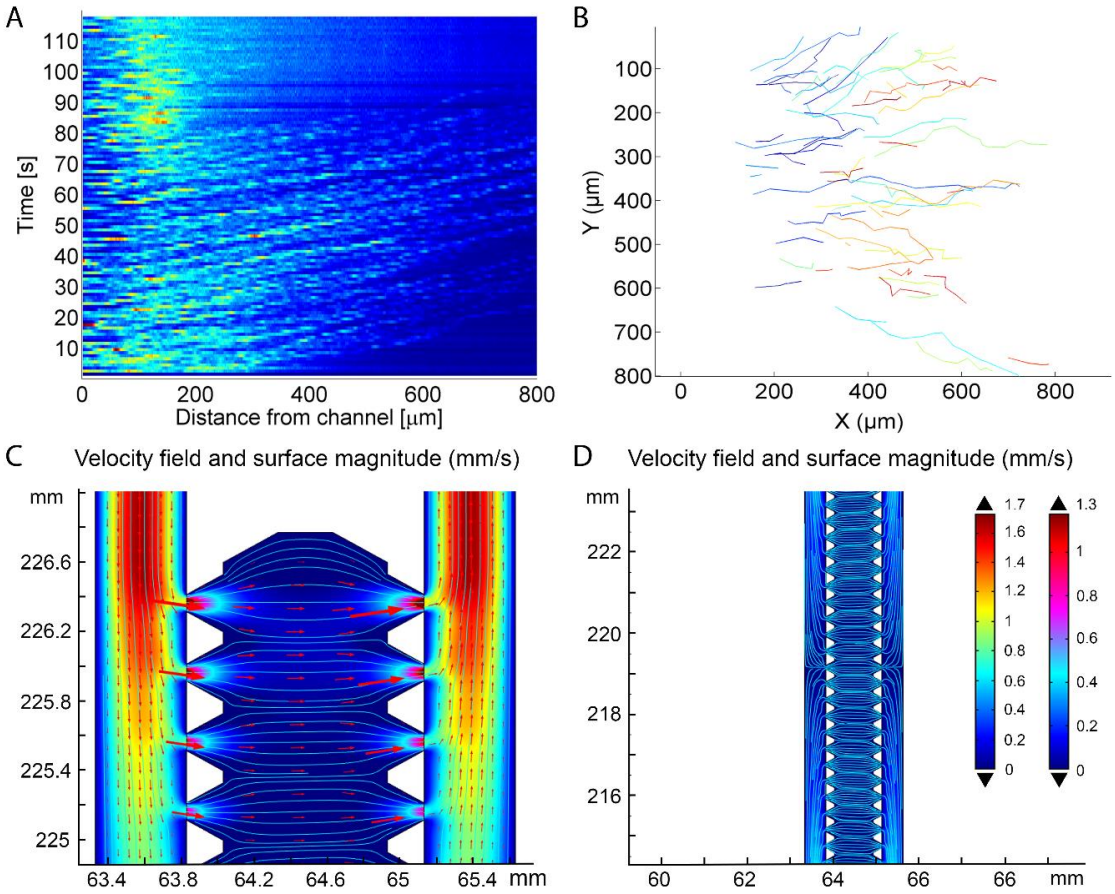

Figure 4. 4 Experimental and theoretical fluid flow estimations.
A and B: Quantification of bead movement inside the collagen hydrogel and its trajectories in the substracted (A) and merged (B) images. C and D: Estimation of fluid flow inside the chamber. COMSOL simulation of the upper chip area (C) and the central zone of the chip (D). Streamlines are represented in light blue, and the flow direction is indicated by the red arrows.

4.3.2 The application of 1 µl/min flow alters the architecture of non-crosslinked collagen-based gels

The collagen network architecture was modified by applying a rapid fluid flow but was unaffected at low flow rates or when the network was cross-linked with TG2. Microscopic images were captured before and after the application of fluid flow and then analyzed following the methodology described in the Material and methods in subsection 2.3. Experimental conditions were divided into four cases: 1) collagen hydrogel, 2) collagen + 1 µl/min of fluid flow (FF), 3) collagen reticulated with TG2 (collagen + TG2), and 4) collagen + TG2 + 1 µl/min FF. Three different experiments were performed for each condition (n=3). Note that in 1) and 3), a null flow rate was used.

To quantify the fiber orientation in 3D, a particular reference coordinate system was followed in this analysis (Figure 4.5A). Hydrogel charge into the microfluidic chamber was performed by small holes following the Y direction (axis 3), whereas the fluid movement crossed the hydrogel perpendicular to the X direction (axis 1). The Z direction represents the height of the channel (axis 13).

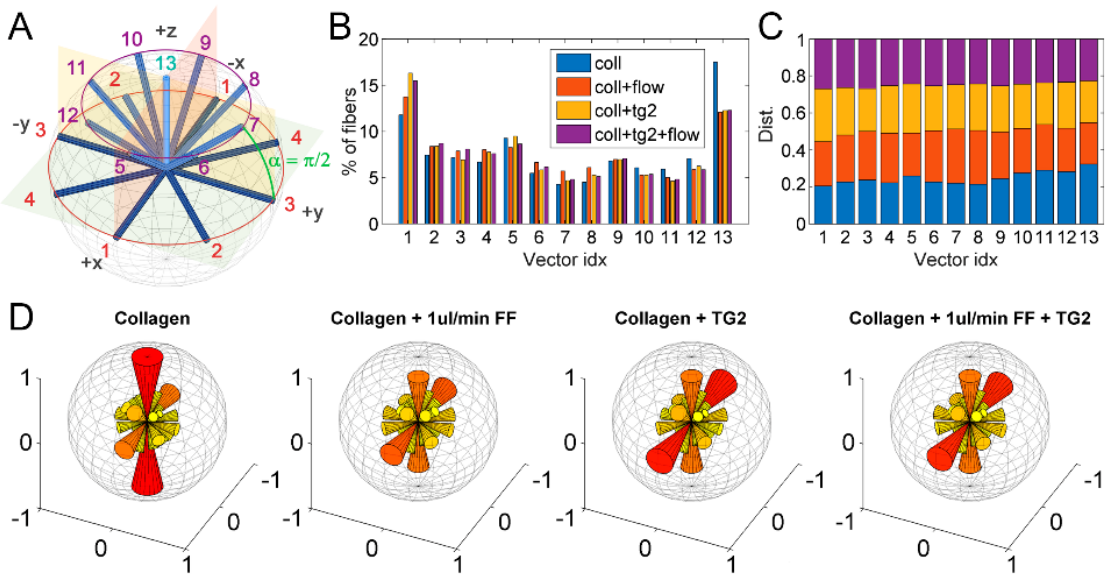

Figure 4. 5 Quantification of fibers orientation
A) Reference sphere with numeration of the divisions used to plot the spatial fiber orientation. B) 3D rose diagrams of fiber orientation for the different conditions C) Percentage of fibers in the corresponding sector for each condition D) Percentage of fibers for each condition normalized by sector.

After the reconstruction of a 3D stack, the network structure was extracted to obtain fiber alignment, porosity and pore size. To visualize fiber distribution, all the main directions of the fibers were classified into angular sectors (3D cones) whose representative vectors are shown in Figure.4.5A. Figure 4.5B shows a 3D rose diagram, scaled according to the number of fibers and normalized, revealing stronger alignment of the network mainly in the X direction and less strong alignment in the Z direction (axes 1 and 13, respectively) for all studied cases (Figure 4.5B). Alignment in Z is probably due to gravity during polymerization, while alignment in the X direction was enhanced in the presence of flow compared to case 1. The fiber distribution ratio for each sector of the sphere confirmed that 13.7% of the fibers were aligned with X in case 2 compared to 11.8% in case 1 (see Figure 4.5C). Such difference apparently comes from a reduction in the ratio of fibers aligned in Z (17.5% compared to 12.1%) and other directions with the Z component (axes 5 to 12).

In the presence of TG2, our results show that collagen network alignment was mainly unaffected (case 4 compared to case 3 in Figure 4.5B). The ratio of fibers remained practically constant for all thirteen grouping directions before and after flow (Figure 4.5D).

4.3.3 Porosity and pore size are unaffected by fluid flow

From the reconstruction of cross-sectional images obtained by confocal microscopy, the porosity and pore size between fibers were quantified (see Table 4.4).

	Pore size (µm)				Porosity	
	Means	Std error	Q90	P(radius>2.9)	Means	Std error
Collagen	2	0,386	3,43	0,20	90,787	3,237
Collagen + 1µl/min FF	1,743	0,137	2,99	0,12	91,147	3,58
Collagen + TG2	1,69	0,079	2,90	0,10	86,567	2,832
Collagen + 1µl/min FF+ TG2	1,69	0,036	2,90	0,10	87,03	2,226

Table 4. 4 Values of porosity and pore size quantified from the matrix architecture and fiber distribution.

The distribution of pore size is obtained by fitting the Rayleigh distribution for every assay, and then, the mean value and quantiles are inferred from the model. The Rayleigh distribution is asymmetrical, showing greater differences in higher quantiles. For instance, the 90th quantile of the radius (i.e., the value that is only exceeded by 10% of the values) for TG2 assays was 2.9 compared to the control, where 20% of the pores had a radius greater than this value (Table 4.5 shows the data results for other quartiles). Despite the fact that the average of the mean values of pore size in TG2 assays was similar for both conditions, the addition of this cross-linker induced greater homogeneity of the pore size.

Statistical analysis of three independent and different assays for each condition showed no significant differences between them. However, the differences between the standard error of each condition revealed interesting differences between all conditions. A high standard error value indicates the presence of large and small pore sizes, while lower values show greater uniformity of the results. Considering this, the pore size was made uniform by adding a cross-linker to the gel, and this difference was much more noticeable in the case of collagen with flow application. Interstitial fluid flow caused the standard error of the sample to be divided in half in both conditions (collagen and collagen with TG2). Therefore, the application of FF tended to make the pore size uniform. This tendency can also be observed when the gel-based matrix is cross-linked with TG2.

	Q50	Q75	Q90	Q95
Collagen	1.88	2.66	3.43	4.86
Collagen + 1µl/min FF	1.64	2.32	2.99	4.23
Collagen + TG2	1.59	2.25	2.9	4.1
Collagen + 1µl/min FF+ TG2	1.59	2.25	2.9	4.11

Table 4. 5 From the fitted distribution of data, the average of the higher quantiles for each condition was calculated and is shown in this table.

4.3.4 Fluid flow enhances the long distance migration

Effective and mean velocities were obtained for human osteoblasts cells (Figure 4.6A). Due to the large amount of data processed in this analysis, most of the cases revealed significant differences compared to control conditions (case 1). Actually, these differences were not very relevant except for non-crosslinked collagen gels under 1 µl/min flow application, which showed mean speeds with a median value approximately 40% higher and effective speeds more than twice as large as control speeds. Table 4.6 summarizes the obtained data.

These differences are also noticeable in the relative trajectories (Figure 4.7), where case 2 (collagen + 1 µl/min FF) stands out with larger and more directed paths. However, the evolution of the directionality ratio (the minimum distance between two points divided by the real covered distance; Figure 4.6B) showed few differences overall, indicating that HOB cells in these conditions tend to remain around small areas and are predominated by short and random movements.

	Vmean (µm/min)		Veffective (µm/min)	
	Means	Medians	Means	Medians
Collagen	0.0953 ±0.1143	0.0556	0.0153 ±0.0152	0.0113
Collagen + TG2	0.0990 ±0.1208	0.0560	0.0223 ±0.0212	0.0178
Collagen + 1µl/min FF	0.1276 ±0.1492	0.0792	0.0358 ±0.0447	0.0216
Collagen + 1µl/min FF+ TG2	0.0899 ±0.1051	0.0533	0.0111 ±0.0093	0.0156
Collagen + 0.1µl/min FF	0.0979 ±0.1222	0.0537	0.0220 ±0.0218	0.0082

Table 4. 6 Values obtained in the cell tracking measurements of the mean and effective velocity.

Diffusion coefficients were also calculated for each condition and indicate the purely diffusive movement (Brownian motion) of cells in the presence of only flow and without TG2 (see Table 4.7). However, in the rest of the cases, all migratory patterns corresponded to subdiffusive movement, which normally occurs under 3D migration conditions [126,127].

	Diffusivity coefficient	Alpha	Cell movement
Collagen	0.07322±0.00446	0.83 ± 0.28	Subdiffusive
Collagen + TG2	0.07884±0.00394	0.87 ± 0.25	Subdiffusive
Collagen + 1µl/min FF	0.2652±0.0107	0.97 ± 0.32	Purely diffusive (Brownian motion)
Collagen + 1µl/min FF+ TG2	0.08070±0.00531	0.89 ± 0.25	Subdiffusive
Collagen + 0.1µl/min FF	0.04419±0.00346	0.73 ± 0.24	Subdiffusive

Table 4. 7 Diffusivity coefficient of each condition and exponential adjustment parameter (alpha) obtained from the minimum square displacement (MSD) curve fitting [235,254]**.**

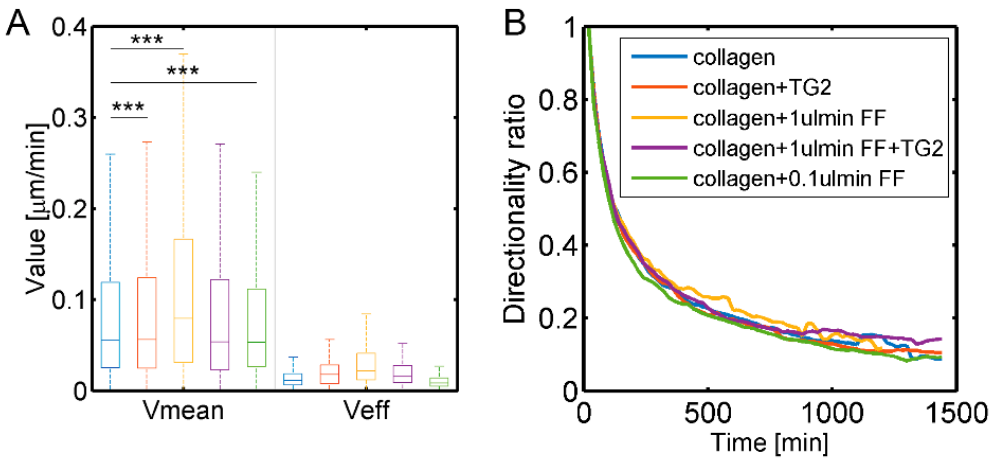

Figure 4. 6 Quantification of HOB cell displacements as well as its directionality.
A) Mean and effective speed of HOB cells [***p < 0.001, statistical analysis for Veffective revealed significant differences for all conditions]. B) Directionality ratio overtime for each condition.

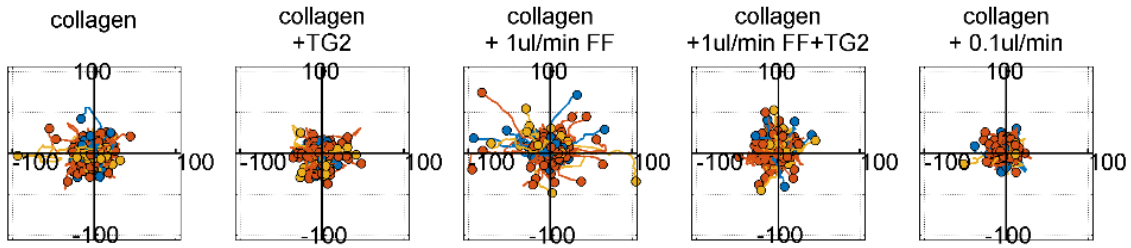

Figure 4. 7 Trajectories of cells whose starting point was centered on the coordinate origin.
The conditions analyzed were collagen or collagen + TG2 in the presence or absence of fluid flow and the cells embedded in the matrix were altered with 1 µl/min of fluid flow, presenting a higher directionality.

4.3.5 Cell morphology is regulated by the fluid flow and the matrix architecture

Flow was able to not only change fiber disposition but also affect cell shape. For instance, apparently, more focal adhesions (dyed with human vinculin 1 (HVIN1)) were observed in cells subjected to a 1 µl/min flow rate compared to controls (see Figure 4.8A). This difference is more remarkable for cells embedded in collagen gels without TG2 cross-linker addition, presenting greater alteration in the distribution of fibers under flow application. TG2 increases the strength and deformation resistance of collagen hydrogels, thus decreasing fiber alterations when the gel is subjected to shear stress and in turn causing the cell morphology to change less abruptly. The formation of thin membranes between fibers confers these properties to the hydrogel without varying its stiffness significantly, as was concluded in a previous work [235]. In hydrogels with TG2, the cells showed a lobopodial shape probably as an adaptation to the matrix architecture (see Figure 4.8).

With the quantitative study of cell morphology from immunostained samples, the cells of hydrogels cross-linked with TG2 showed higher cell solidity values that were significantly different from those of the collagen condition (also considered the control condition). For instance, the median of the hydrogel with TG2 was over the 75th quantile of cell solidity in the collagen assay). Even with flow, the median values obtained (TG2: 0.5613±0.1484; TG2+flow: 0.543±0.156) were greater than those corresponding to cases 1 and 2 (collagen: 0.515±0.1086; collagen +flow: 0.4469±0.1563). Thus, the data indicated that a relation between the fixation of fibers through cross-linkers and cell morphology may exist, with a lower number of protrusions and greater elongation presented in these cases compared to the control condition (see Figure 4.8C). Cell solidity was decreased by fluid flow application, and a more remarkable effect was observed for hydrogels without TG2 (the median of case 3 is similar to the 25th quantile of the control case).

Thus, the application of flow decreases cell solidity and increases cell major axis length for both cross-linked and non-cross-linked gels. That is, fluid flow affects cell morphology, promoting thinner bodies and star-like shapes (Figure 4.8B). On the other hand, TG2 increases solidity and decreases cell major axis length overall probably due to the higher stability of the network. Figure 4.8D represents the cell processing with the hand-coded MATLAB script.

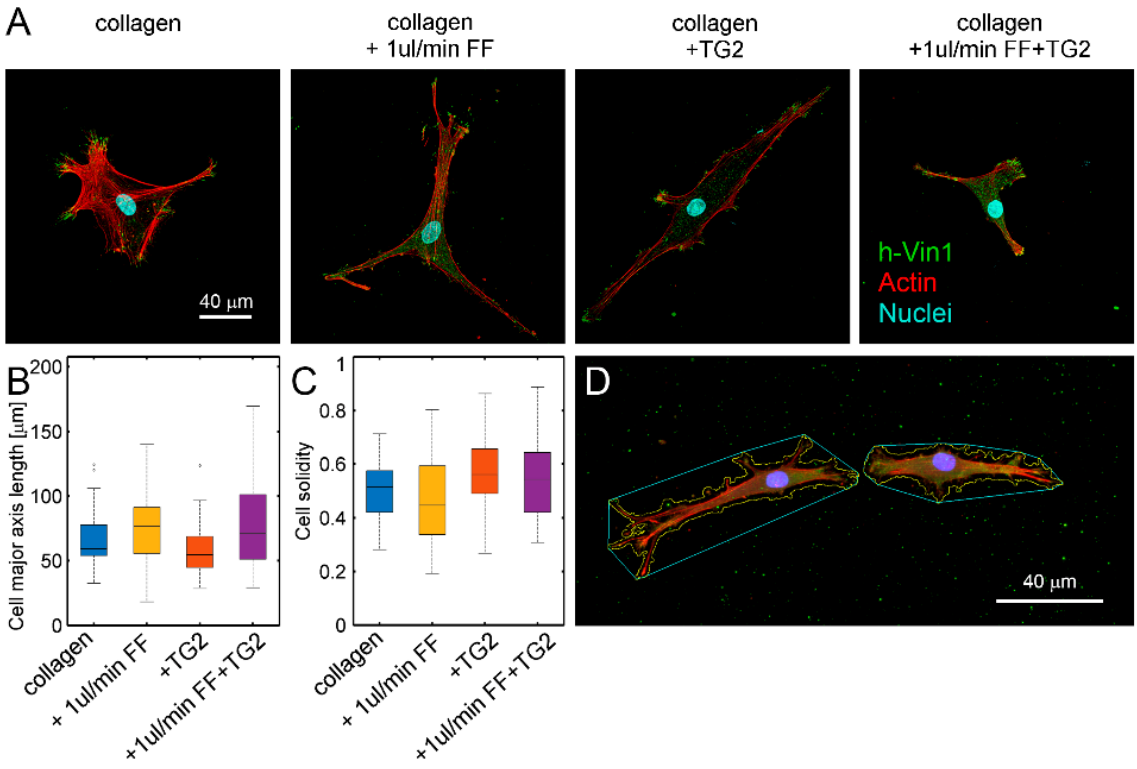

Figure 4. 8 Cell morphology analysis.
A) Examples of cell morphologies in the different mechanical conditions: Collagen, Collagen + 1 µl/min flow, Collagen+ TG2 and Collagen+ TG2+ 1 µl/min flow. Samples were fixed, stained for vinculin (green), phalloidin (actin, red) and DAPI (nuclei, blue) and imaged using an Olympus Fluoview FV10i confocal microscope with 60XW objective. B) Cell major axis length. C) Cell solidity. D) An example of cell processed with the MATLAB script (image captured using a Nikon D-Eclipse C1 confocal microscope with a 40X oil objective). N≥20 cells analyzed for each condition.

4.4 Discussion

The wide variety of mechanisms involved in cell migration are difficult to study under *in vivo* conditions due to the large number of factors involved in this process, from adjacent cells and tissues to intra- and extracellular signaling. This fact has promoted the development of new techniques that allow the re-creation of *in vivo* conditions, such as microfluidics, a fundamental technique for 3D culture providing 4D monitoring, easy re-creation of the extracellular matrix or high control of mechano-chemical gradients, among other advantages. By using microfluidic chips, we aimed to analyze the cellular behavior of human osteoblasts subjected to different mechanical factors, namely, fluid flow and ECM cross-linking. The dynamic load on the bone is fundamental for osteogenesis and maintenance of bone homeostasis, regulating the different cellular responses. The mechanosensitivity response of osteoblasts has been previously studied mainly in cells from murine species; for example, the molecular aspects involved in ion transport ,such as calcium (receptors (P2Y2)) [255] or nitric oxide release in osteoblasts, have been analyzed [256]. Additionally, the potent stimulator effect of fluid flow on ECM synthesis has been reported by other authors, who concluded that interstitial fluid flow enhances the creation of bone matrix after a few days [257].

Interstitial fluid flow through the 3D matrix, present in soft tissues, plays a fundamental role in microcirculation between blood and lymphatic vessels. This flow is altered in inflammatory processes that are triggered when an injury occurs. Previous authors have demonstrated that low interstitial flow levels are able to align collagen and to promote both human dermal fibroblast alignment in 3D cultures and cell differentiation [258,259].

In this work, the study of fluid flow effects on HOB migration in terms of mean (instantaneous) and effective velocities revealed significant differences, especially when a 1 µl/ml fluid flow rate was applied to gels without TG2. Matrix structural analysis revealed that the fiber distribution in crosslinked gels remained unaltered despite the application of flow, while significant alignment with flow occurred in non-crosslinked gels. This effect determined the different migratory pattern. In non-crosslinked gels, high rates of flow enhanced osteoblast velocity and produced changes in cell morphology, with the cells acquiring a more star-like appearance. On the other hand, migration on cross-linked gels remained unaffected despite fluid flow, while the morphology changed similar to those in non-crosslinked gels. In fact, the most important differences in cell morphology were observed with matrix cross-linking probably caused by the impediment that TG2 implies to the deformation of the gel architecture.

To understand these results, quantitative analysis of the microstructure of gels for all conditions was performed. This quantification revealed that the addition of one cross-linker to the collagen hydrogel prevented the alteration of fiber disposition when subjected to flow. Matrix architecture analysis was performed, and the pore size and porosity were estimated, revealing a more uniform distribution of the architecture when TG2 was added. While crosslinker-free collagen gel was dominated by very large or small pores, the application of fluid flow resulted in greater uniformity of the pore size, which may be directly related to differences in cell migration. In the case of gels with TG2, although the average pore size did not vary in the case of null flow, the pores were less uniform than when an interstitial flow was applied, thus favoring cell movement, although the differences found were not significant. The addition of this stabilizer intended to simulate the different matrices to which osteoblasts are subjected during endochondral ossification. Cell migration under TG2 conditions presented patterns similar to those of the control, regardless of the presence of flow. However, the interstitial fluid flow through the matrix was able to alter cell morphology without altering the architecture of the hydrogel, which produced cells with low branching (high solidity).

Other studies of the interstitial flow effect on matrix disposition have been performed. For instance, Guo & Kaufman [260] analyzed the effect of collagen fiber alignment on cell spreading and concluded that after several hours of alignment, this effect is reduced as the cell concentration is higher and with the consequent remodeling of the matrix and fiber aggregation. Hydrogels used in most of the published works presented a lower collagen concentration (2 mg/ml, 2.5 mg/ml)[258,260] compared to the collagen concentration used in this work (4 mg/ml). These differences in concentration and in the rigidity of the hydrogels can be crucial for observing a clear alignment in low-concentration gels, which are more easily modified by external stimuli. However,

in the gels used in this work, it was necessary to obtain and quantify confocal microscopic images since at first sight, the differences were not perceptible.

To better understand the three-dimensional migratory pattern of osteoblasts, apart from quantifying the trajectories followed in the assays monitored over time, cells were immunostained to analyze their morphology. With our results, we could conclude that the laxity of unmodified collagen fibers allows cells to have a larger cell body and that greater polarization was found in cells embedded in the hydrogel with TG2. Overall, fluid flow promoted the elongation of cells.

4.5 Conclusions

In conclusion, by using different strategies, our work demonstrates the crucial influence of matrix architecture on osteoblast migration. Between all the cases analyzed, we quantified significant differences in the osteoblast migration speed when collagen-based gels were exposed to interstitial fluid flow. In fact, we found that interstitial fluid flow application provokes matrix fiber alignment and homogenization of the pore size. To prevent this effect, we crosslinked collagen-based gels with TG2. Under these conditions, we found no increases in osteoblast migration speed. Therefore, these results show that the matrix architecture guides osteoblast migration in 3D.

Furthermore, we observed an alteration in osteoblast morphology when interstitial flow was applied in different collagen-based gels (crosslinked or non-crosslinked). This finding suggests that interstitial flow may help to modulate osteoblast phenotypes and drive the progression of bone regeneration. Taken together, these results have a potential use in regenerative medicine and may be useful in the design of therapeutic approaches to promote bone regeneration and prevent unsuccessful bone healing.

Chapter 5

Conclusions and Future Work

5.1 Conclusions

This chapter presents the overall conclusions of this PhD Dissertation, as well as some future lines of research that could give continuity to the work here proposed.

Throughout this work, the effect of various mechano-chemical stimuli on cell migration has been studied. In particular, it has been focused on three of the main regenerative processes that occur in the human body: wound healing, bone regeneration and formation of new blood vessels, fundamental to restore the physiology of damaged tissue. By using microtechnologies, especially microfluidic devices, the cell culture of human cells has been performed in 3D. Previously published papers have shown the influence of chemical gradients on cell polarization and migration -chemotaxis - both in 2D cultures and in cells embedded in 3D extracellular matrices [196,219,261]. On the contrary, when the created gradient is of a mechanical nature -durotaxis- there are numerous factors involved in cellular mechanotaxis. One of the main differences between chemotaxis and mechanotaxis described by Roca-Cusachs et al. involves stimulus detection pathways [32]. In contrast to chemotaxis, mechanotaxis would not require biochemical transduction to guide cell movement. Following this brief discussion, the global conclusions of this work are presented grouped by the biological process that have been recreated in the microfluidic platforms:

- **Angiogenesis**

- VEGF is one of the main regulators in angiogenic processes, producing longer sprouts more frequently. Its chemoattractant effect depends on its concentration and spatio-temporal location, having a critical impact on the sprout time evolution.

- In the case of PDGF, a null effect has been seen in the number and length of sprouts developed from the single layer of endothelial cells. This effect could be due to a non-optimal PDGF-VEGF concentration balance as well as inadequate analysis time.

- The addition of TGF-β has improved the length of sprouting in early stages, although its effect gradually disappears over time.

- With the BMP-2, the number of new sprouts was lower, with a smaller size, being BMP-2 the only growth factor with a positive evolution at longer times, where the size of these sprouts has been increased.

- **Wound regeneration**

- The microfluidic platform designed in this work has been validated to carry out combined studies of durotaxis and 3D chemotaxis in human cells. This novel microdevice combines the application of chemical gradients with the effect of collagen interfaces generated by different concentrations of this hydrogel.

- After analyzing the cell distribution inside the chip chambers over the course of a week, it has been shown that the presence of PDGF, especially at low concentrations, has caused a strong chemottractant effect on the dermal fibroblasts, independently of the collagen concentration gradient.

- The effects of VEGF on cell migration, as well as the directionality of the collagen concentration gradient, were not relevant on their own.

- **Bone regeneration**

- The support designed for the application of interstitial fluid flow has allowed the optimal development of the experiments, achieving the watertightness of the system.

- With the application of interstitial fluid flow, significant differences in the migration rate of osteoblasts in collagen hydrogels were quantified.

- The application of fluid flow causes the alignment of matrix fibers, as well as homogenization of pore size in the case of non-crosslinked collagen gels, increasing the migration rate of osteoblasts.

- The reticulation of collagen gels with TG2 has counteracted the effects of fluid flow on the migration of osteoblasts in 3D, remaining practically similar to the control case.

- Interstitial flow has promoted alterations of cell morphology, and therefore the phenotype of cells embedded in both types of matrices.

- The matrix architecture, specially the fiber distribution, plays a fundamental role in the migration of 3D osteoblasts.

5.2 Future work

In this thesis, novel techniques have been used for the study of three-dimensional cellular behaviour. Based on the conclusions obtained in this work, a series of questions have been presented that would allow us to increase knowledge.

For the recreation of injuries, both in soft and hard tissues, numerous factors are involved a well as cellular types. The simultaneous co-culture of several cell types, such as endothelial cells, with fibroblasts or osteoblasts, would let us know how the biomolecules released by these cells affect the behavior of the other cells analyzed in this work.

For this purpose, using some of the devices designed in this Thesis, a monolayer of endothelial cells, mechanically stimulated to increase the release of interleukins, cytokines and other factors that regulate tissue regeneration, could be deposited in one of the channels. Fibroblasts as well as other cell types involved in wound healing stages, such as macrophages, could be seeded in the adjacent channels. The versatility provided by the technologies used in this thesis would also allow us to increase the complexity of the design for sophisticated cocultures (see Figure 5.1). In the channels covered by a monolayer of endothelial cells, a smooth laminar flow with newly cell culture media and reusing the one from the channel would be generated simulating the flow that moves through the blood vessels. The permeability of this monolayer of cells would allow the flow of interstitial fluid as well as biomolecules through the different cell cultures being able to analyze the behavior for each cell type and their interaction.

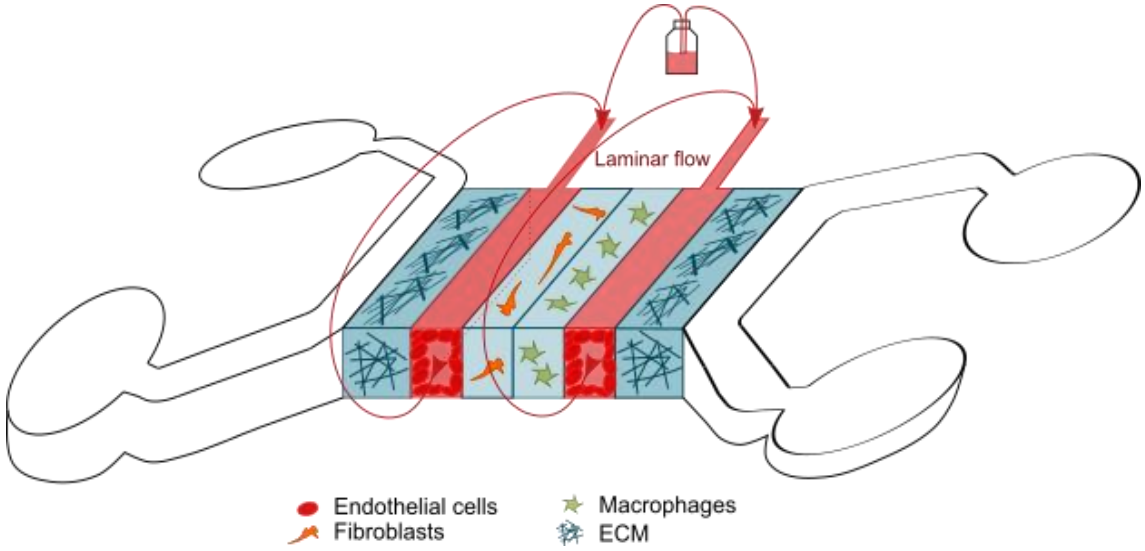

Figure 5. 1 Scheme of a new 3D coculture in a microfluidic devices combining different cell types involved in the inflammation and proliferation phases of wound healing.
A possible new geometry proposed for a complex co-culture of different cells involved in wound healing. If the chip is divided into two main zones, the lateral channels for adding cell culture media and the central channels for 3D cell culture would be differentiated. In this central area (cross-section in the illustration), the hydrogel acting as scaffold will allow the three-dimensionality and biomimetizing of the physiological cell environment.

Mechanical loading regulates cell metabolism, especially bone metabolism [107]. The mobilization of intracellular calcium (Ca^{2+}) has been reported as an effect of fluid flow on bone cells causing also alterations in the production of nitric oxide or prostaglandins [106,107]. With the use of calcium ion activity indicators such as Fluo or FURA, intracellular Ca^{2+} flows would be quantified by image analysis, all under static conditions or when mechanical factors are applied to the cells, thus continuing the work described in Chapter 4.

Another possible future line of research would be the development of organoids by using microfluidic systems. Organoids derive from pluripotent stem cells or isolated organ progenitors that differentiate to form organ-like tissue, with multiple types of cells that self-organize to form a structure no different from that of an organ. This three-dimensional, almost physiological model facilitates the study of physiopathological processes, as well as testing drugs or growth factors and the corresponding tissue response. This innovative technology requires basic cell culture techniques as well as the co-cultivation of several cell types that should be implemented in our microdevices [262,263].

Chapter 6

Conclusiones y Trabajo Futuro

6.1 Conclusiones

En este capítulo se exponen las conclusiones globales de esta tesis, así como algunas futuras líneas de investigación que podrían dar continuidad a los trabajos aquí propuestos.

A lo largo de esta tesis doctoral se ha estudiado el efecto de diversos mecanismos mecanoquímicos sobre la mecanobiología celular. Concretamente se ha enfocado hacía tres de los principales procesos regenerativos que ocurren en el cuerpo humano: regeneración de heridas, regeneración ósea y formación de vasos sanguíneos, fundamental para reestablecer la fisiología del tejido dañado. Haciendo uso de las microtecnologías se han empleado dispositivos microfluídicos que han permitido el cultivo celular en 3D de células humanas. En trabajos previamente publicados se ha visto la influencia de los gradientes de factores químicos en la polarización y migración celular –quimiotaxis- tanto en cultivos 2D como en células embebidas en matrices extracelulares. Por el contrario, cuando el gradiente creado es de naturaleza mecánica –durotaxis- son numerosos los factores implicados en la mecanotaxis celular. Una de las principales diferencias entre la quimiotaxis y la mecanotaxis descrita por Roca-Cusachs et al. recae en las vías de detección del estímulo [32]. A diferencia de la quimiotaxis, la mecanotaxis no requeriría de transducción bioquímica para dirigir el movimiento celular. A continuación de esta breve discusión, se encuentran expuestas las conclusiones globales de esta tesis doctoral agrupadas por el proceso biológico con el que se relacionan:

- **Angiogenesis**

En el estudio del efecto paracrino de factores de crecimiento comúnmente liberados por células propias de la zona dañada (ECs, fibroblastos y osteoblastos) se ha visto que el VEGF es el principal regulador en los procesos angiogénicos, produciendo *sprouts* más largos con mayor frecuencia. Además, su efecto quimioatrayente depende de la concentración y su ubicación espacio-temporal, teniendo un impacto crítico en la evolución del *sprouting* a lo largo del tiempo.

En el caso del PDGF no se ha visto un claro efecto global tanto en el número como en la longitud de los *sprouts* desarrollados desde la monocapa de células endoteliales. Este efecto podría ser debido a un balance de concentración PDGF-VEGF no-óptimo, así como a un inadecuado tiempo de análisis.

La adición del TGF-β ha mejorado la longitud del *sprout* en estadios tempranos, aunque su efecto desaparece gradualmente con el tiempo.

Con el BMP-2, el número de *sprouts* formados ha sido, en general, menor presentando a su vez un tamaño más corto, siendo el único GF con una evolución positiva a tiempos más largos, donde el tamaño de dichos *sprouts* se ha visto aumentado.

- **Regeneración de heridas**

La plataforma microfluidica diseñada en este trabajo se ha validado para realizar estudios combinados de durotaxis y quimiotaxis 3D en células humanas. Este nuevo microdispositivo combina la aplicación de gradientes químicos con el efecto de la interfaz de colágeno generado por distintas concentraciones de dicho hidrogel.

Analizada la distribución celular en el interior de las cámaras del chip a lo largo de una semana, se ha visto que la presencia de PDGF, especialmente a baja concentración, ha provocado un fuerte efecto quimioatrayente sobre los fibroblastos dermales independiente del gradiente de concentración del colágeno.

Los efectos del VEGF sobre la migración celular, así como de la direccionalidad del gradiente de concentraciones de colágeno, por sí solos no fueron relevantes.

- **Regeneración ósea**

El soporte diseñado para la aplicación de flujo de fluido intersticial ha permitido la realización óptima de los experimentos, consiguiéndose con ese diseño la estanqueidad del sistema.

Con la aplicación de flujo de fluido intersticial, se cuantificaron diferencias significativas en la velocidad de migración de los osteoblastos en los hidrogeles de colágeno.

La aplicación de flujo de fluido provoca la alineación de las fibras de la matriz, así como la homogeneización del tamaño de los poros en el caso de geles de colágeno.

La reticulación de los geles de colágeno con TG2 ha contrarrestado los efectos del flujo sobre la migración de osteoblastos en 3D, permaneciendo prácticamente similar al caso control.

El flujo intersticial provoca una alteración de la morfología celular, y por consiguiente el fenotipo de células embebidas en ambos tipos de matrices.

La arquitectura de la matriz desempeña un papel fundamental en la migración de los osteoblastos en 3D.

6.2 Trabajo futuro

En esta tesis se han utilizado novedosas técnicas para el estudio del comportamiento celular tridimensional. A partir de las conclusiones obtenidas en este trabajo, se han planteado una serie de cuestiones que permitirían ampliar el conocimiento del comportamiento celular.

Para la regeneración de una herida, tanto en tejido epitelial como óseo, son numerosos los factores involucrados, así como los tipos celulares. El cocultivo simultáneo de varios tipos celulares, como pueden ser células endoteliales, con fibroblastos u osteoblastos, nos permitiría conocer cómo las biomoléculas liberadas por dichas células afectan al comportamiento de las células analizadas en este trabajo. Para ello, utilizando algunos de los dispositivos diseñados en esta Tesis, se podría depositar en uno de los canales una monocapa de células endoteliales,

estimuladas mecánicamente para aumentar la liberación de interleuquinas, citoquinas y otros factores que regulan la regeneración tisular. Los fibroblastos, así como otros tipos de células involucradas en las etapas de cicatrización de heridas, como los macrófagos, podrían ser cocultivados en los canales adyacentes. Las versatilidades aportadas por las tecnologías utilizadas en esta tesis permitirían también aumentar la complejidad del diseño enfocado hacia cultivos complejos (ver Figura 5.1). En los canales cubiertos por una monocapa de células endoteliales, se generaría un flujo laminar suave reutilizando el medio que ha fluido por el microcanal además de añadir medio de cultivo nuevo, simulando el flujo que fluye a través de los vasos sanguíneos. La permeabilidad de esta monocapa de células permitiría el flujo de fluido intersticial y biomoléculas a través de los diferentes cultivos celulares pudiendo ser analizado el comportamiento de cada tipo celular mediante análisis de imagen.

Uno de los efectos del flujo de fluido sobre las células óseas podría estar ligado con la movilización del calcio intracelular (Ca^{2+}), causante también de alteraciones en la producción de óxido nítrico o prostaglandinas. Con el uso de indicadores de la actividad del ion calcio como Fluo o FURA, se cuantificarían los flujos de calcio intracelular mediante análisis de imagen, todo ello en condiciones estáticas o ante la aplicación de factores mecánicos a las células, continuando así el trabajo descrito en el Capítulo 4.

Otra de las posibles líneas futuras de investigación sería el desarrollo de organoides mediante sistemas de microfluídica. Los organoides derivan de células madre pluripotentes o progenitoras de órganos aislados que se diferencian para formar un tejido similar a un órgano y con múltiples tipos de células que se auto-organizan para formar una estructura no diferente a la de un órgano. Este modelo tridimensional casi fisiológico facilita el estudio de procesos fisiopatológicos, así como el testado de fármacos o factores de crecimiento y la respuesta del tejido. Esta novedosa tecnología requiere de técnicas básicas de cultivo celular, así como el cocultivo de varios tipos celulares.

Chapter 7

Nota biográfica/

Biographical note

7.1 Publicaciones obtenidas durante el desarrollo de esta Tesis Doctoral/ Publications obtained from this PhD Dissertation

C. Del Amo, V. Olivares, M. Cóndor, A. Blanco, J. Santolaria, J. Asín, C. Borau and JM García-Aznar. ***Matrix architecture plays a pivotal role on 3D osteoblast migration: effect of interstitial fluid flow.*** Under review

C. Del Amo, C. Borau, N. Movilla, J. Asín, J.M. Garcia-Aznar, ***Quantifying 3D chemotaxis in microfluidic-based chips with step gradients of collagen hydrogel concentrations***, Integrative Biology. 2017. Vol. 9. 339-349
ISSN/DOI: ISSN 1757-9694 / 10.1039/c7ib00022g

C. Del Amo, C. Borau, R. Gutiérrez, J. Asín, J.M. García-Aznar, ***Quantification of angiogenic sprouting under different growth factors in a microfluidic platform***, Journal of Biomechanics 2016. Vol.49 (8). 1340-1346
ISSN/DOI: ISSN 0021-9290 / 10.1016/j.jbiomech.2015.10.026

O. Moreno-Arotzena; J G. Meier; **C. Del Amo**; JM. García-Aznar. ***Characterization of Fibrin and Collagen Gels for Engineering Wound Healing Models***. Materials. 2015. Vol. 8 1636-1651.
ISSN/DOI: ISSN 1996-1944 / 10.3390/ma8041636

7.2 Participación en conferencias y congresos/ Participation in conferences and congresses

- Microfluidica: una aproximación in vitro al entorno celular

  C. Del Amo

  Transfiere. 7º Foro Europeo para la Ciencia, Tecnología e Innovación. (14/02/2018) Málaga. Presentación oral/ *Oral Presentation*

- Cultivos celulares en microfluidica: de migración individual a colectiva

  C. Del Amo, J. Plou, N. Movilla, M. Condor, V. Olivares, C. Borau, JM García-Aznar.

  TerCel. Red de Terapia Celular (12/01/2018) Madrid

- The effect of crosslinked collagen-based matrices on the angiogenic sprouts induced by tumor cells

C. del Amo, C. Borau, C. Valero, JM. García-Aznar

7th International Conference on Tumor-Host Interaction and Angiogenesis. University of Helsinki, University of Lausanne, University of Fribourg. (21/06/2017 – 23/06/2017), Ascona (Suiza). Póster/ *Poster presentation*

- Combining chemical gradients and material step gradients for 3D cell migration analysis

C. del Amo, C. Borau, N. Movilla, J. Asín and JM. García-Aznar

The 7th European Cell Mechanics Meeting. CellMech (21/06/2017 – 23/06/2017), Windermere, England. Póster/ *Poster presentation*

- The role of matrix mechanics on 3D cell migration: from microfluidics to numerical modeling.

JM. García-Aznar, N. Movilla, C. Valero, C. Borau. **C. del Amo**

Mechanical forces in physiology and disease. Centro Nacional de Investigaciones Cardiovasculares (CNIC) (04/11/2016 – 05/11/2016), Madrid

- Quantification of sprouting angiogenesis under the effect of different growth factors involved in the tumor microenvironment

del Amo, C.; Borau, C.; Asín, J; García-Aznar, J.M.

The Tumor Inmunobiology and Immunotherapy. American Association for Cancer Research (AACR) (20/10/2016- 23/10/2016) Boston (MA, EEUU). Póster/ *Poster presentation*

- 3D migration of human osteoblasts in microfluidic devices

N. Movilla, **C. del Amo**, C. Borau, C. Valero, JM. García-Aznar

European Orthopaedic Research Society 24th annual Meeting. EUROPEAN ORTHOPAEDIC RESEARCH SOCIETY (14/09/2017 – 16/09/2017) Bolonia, Italia

- Microfluidic-based experiments for 3D mesenchymal cell migration: im-pact of different mechano-chemical factors

C del Amo, N Movilla, C. Borau, JM García-Aznar.

EMBO Workshop. Stem cell mechanobiology in development and disease. Institute of Genetics and Biophysics (IGB). EMBO Workshop (18/10/2015 – 21/10/2015) Capri (Italia). Presentación oral/ *Oral presentation*

- Unraveling the role of different MechanoChemical conditions on 3D Cell Migration: from Microfluidics to Numerical Simulation

J.M. Garcia Aznar, O. Moreno-Artozena, F. Ribeiro, J. Escribano, M. Cóndor, I. Gonzalez, **C. del Amo**, C.Valero, C. Borau, T. Rüberg.

21st Congress of the European Society of Biomechanics, ESB 2015. European Society of Biomechanics (ESB) (05/08/2015 – 08/08/2015), Praga (República Checa)

- Angiogenesis in tissue regeneration: quantification of in vitro sprouting induced by growth factors

C. del Amo; C. Borau, R. Gutiérrez, JM García-Aznar.

International Conference on Tissue Engineering 2015. Instituto Superior Técnico (IDMEC-IST) (25/06/2015 – 27/06/2015), Lisboa (Portugal). Presentación oral/ *Oral presentation*

- Role of Growth Factors and Interstitial Fluid Flow on Angiogenesis: A Microfluidic Approach

C.del Amo, C. Borau, R. Gutiérrez, JM. García-Aznar

6th European Cell Mechanics Meeting. Institute for Bioengineering of Catalonia (IBEC) (13/05/2015 – 15/05/2015) Barcelona. Póster/ *Poster presentation*

- Microfluidics and Discrete Numerical Simulations: a framework for research in early wound healing

J.M. García-Aznar, O. Moreno-Arotzena, C. Borau, **C. del Amo**, N. Movilla

Dutch Workshop on Mathematical Modeling Wound Prevention and Treatment. 2014. Delft University of Technology (17/10/2014) Delft (Netherlands)

7.3 Patentes/ Patents

Dispositivo De Encapsulado Apto Para Aplicaciones Microfluídicas**.**

Encapsulation Device Suitable for Microfluidic Applications -

Autores/ *Authors*: José Manuel García Aznar, **Cristina Del Amo Mateos**, Alejandro Blanco Moneo, Jorge Santolaria Mazo

Número de solicitud/ *Application number*: P201730809

Fecha de presentación/ *Date of submission*: 16 Junio 2017

Universidad de Zaragoza

7.4 Estancia de Investigación/ Research stay

Proyecto*/ Project*: Estudio mecanobiológico de células endoteliales linfáticas cocultivadas con células tumorales

Mechanical-biological study of lymphatic endothelial cells co-cultured with tumor cells. **Institute for Molecular Engineering- The University of Chicago. Chicago (USA). (22/08/2016 to 24/11/2016).**

Resumen: El objetivo era aprender nuevas técnicas, algunas pioneras, empleadas en microfluidica y/o biología molecular, para la aplicación de flujo a cocultivos de células. Además, se realizaron estudios de exosomas, moléculas liberadas por las células con gran importancia biológica para la detección temprana de enfermedades como los procesos metastásicos.

Abstract:The main objective of this project was to learn new techniques, some pioneering and others commonly used in microfluidics and/or molecular biology for the application of fluid flow to the cell co-cultures. In addition, analyses of exosomes were performed, nano-molecules released by cells with great biological importance for early detection of metastatic processes.

Beca/ *Grant*: Ministerio de Educación, Cultura y Deporte. Ayudas a la movilidad para estancias breves y traslados temporales (EST15/00695).

7.5 Docencia/ Teaching activities

- **Asignatura/ Subject: Biología General/ *General Biology*** (Grado en Biotecnología/ *Degree in Biotechnology*). Departmento Bioquímica y Biología Molecular. Facultad de Ciencias. Curso Académico / *Academic year:* 2016-2017: 36h

- **Asignatura/ Subject: Mecánica/ *Mechanics*** (Grado en Ingeniería Mecánica). Departamento Ingeniería Mecánica (*Degree in Mechanical Engineering)* / EINA.
  Curso Académico / *Academic year:* 2016-2017: 24h,
  Curso Académico / *Academic year:* 2015-2016: 60h

- **Codirección de trabajos final de grado (TFG)/ Supervision of undergraduate Master Theses**
  - 2014/15. Estudiante/ Student: Alejandro Blanco Moneo. *Design, manufacturing and simulation of encapsulated obtained by additive fabrication for microfluidic applications*.
  - 2014/15. Estudiante/ Student: Raquel Gutiérrez Arnau. *Study of cell behavior in three-dimensional matrix in microfluidics platforms for regenerative medicine applications*.

Appendix

A1. ELISAs for estimation of GF concentration

Dynamic regulation of cell proliferation and differentiation, allows cells to form more complex structures such as tissues and organs [264]. Cells that conform these tissues are subjected to various stimuli, such as the extracellular matrix in which they are embedded [265]. On the other hand, there are numerous molecules that act in the cell niche, either released by these same cells or others from other adjacent tissues, or added to the system (e.g. drugs or growth factors). Cell-matrix interactions involve the chemical composition and structural organization of the ECM, in addition to its mechanical properties.

Microfluidic devices have been an excellent tool to represent the cell microenvironment by adding biomimetic hydrogels and generating controlled mechanochemical gradients. Matrix architecture plays a crucial role on the molecules distribution through the hydrogel. As purely diffusive factor in fluid, biomolecules interact directly with cells embedded in the matrix as well as by bounding to the matrix fibers [158].

The design of microfluidic assays with chemical gradients proposed in this thesis has required the analysis of the molecule transport along these platforms. In chapter 3 was shown how molecules diffuse in our microdevices by using a fluorescent reactant. However, this section is focused on the quantification of protein in the channel opposite to the additive channel. Considering that the initial concentration of GF was added in one of the channels, diffusing through the hydrogel to the opposite channel, the aim of this study was to quantify the final concentration after 24h of incubation (at 37°C and 5% of CO_2). Specific enzyme-linked immunosorbent assays (ELISA) were performed for two different GFs: PDGF and BMP-2. As a technique for detecting and quantifying substances such as peptides, proteins, antibodies and hormones, ELISA consists of 96 well plate coated with a specific antibody able to immobilize the antigen. For detecting the sample, an antibody linked to an enzyme is added and incubated with a substrate which produces a measureable product. Then, the enzyme activity can be measured with a plate reader. The protocols followed in this thesis will be presented below.

- ## Microfluidic-based assay procedure

In order to simplify the analysis and considering that the geometry of the central channel is preserved in all our designs, these experiments have been performed on the devices shown in the Figure A1 (previously published by Moreno-Arotzena et al. [158]). Consisting of two lateral channels, one of addition (named channel 1) and its opposite channel (channel 2), and a central channel where the hydrogel was introduced, the factor to study was added in channel 1. After 24h of incubation, the concentration of factor present in both channels has been analyzed so we can know how much protein has spread through the hydrogel and make sure that the stimulus is reaching our cells. It should be mentioned that the hydrogel selected for these experiments was 2mg/ml-Collagen type I rat tail following the procedure described in previous chapters.

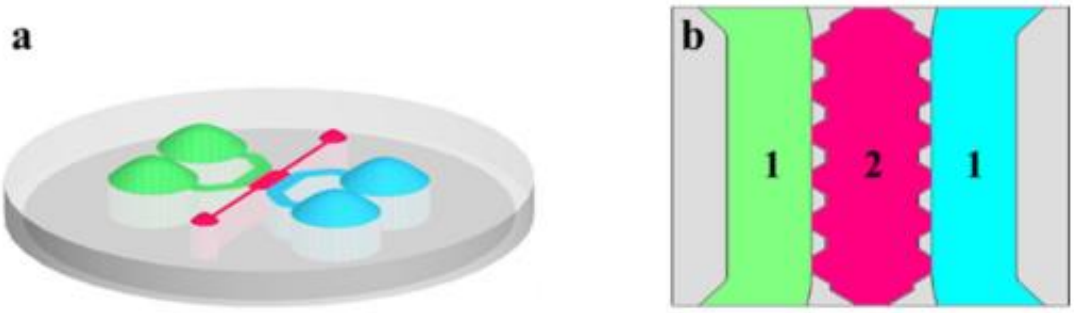

Figure A 1. Geometry of the microfluidic device.
A general view of the microdevice is shown in picture (a). The central area is demonstrated as a top view in picture (b), in which the geometry and nomenclature of the compartments are detailed: the channel (1) and the hydrogel (2) compartments. The hydrogel is injected into the central cavity (pink), whose dimensions are 2.5 x 1.3mm; the main channels (green and blue) are filled with culture media or PBS. When a GF or dextran is added in order to establish a chemical gradient, it is included in the addition channel (green) and diffuses through the hydrogel towards the opposite channel (blue). Figure and caption taken from [210]

- **Protocol for ELISA assays**

Factor addition: Human PDGF-BB (Elisa Kit, Sigma Aldrich, RAB0398)/ Human BMP2 (Elisa Kit, Sigma Aldrich, RAB0028) was added 24h after hydrogels preparation in only one of the reservoir channels of the microfluidic devices (channel 1) to study the diffusion of the factor to the other channel.

Preparation of Reagents:

Considering that the ELISA kit must be stored at -20°C, all reagents and samples should be brought to room temperature before use. Gently mix all liquid reagents prior to use.

The obtaining of the sample was performed 24h (aprox) after factors addition. First, medium from the reservoirs was discarded by vacuum aspiration taken only the medium from the channels in direct contact with. Samples were centrifuged at 1000g for 10min before use to eliminate any residues. The corresponding dilution samples should be performed in Standard Diluent Buffer to obtain samples in the range of pg/ml.

Preparation of the standard curve for each factor according to the corresponding protocol indicated by the supplier. Samples were running at least in duplicate. Likewise, the other reagents have been also prepared. For instance, Wash Buffer Concentrate (25X) was diluted in distilled water to obtain a working Wash Buffer solution 1X, mixing gently to dissolve the crystals. Store both solutions at 4ºC. The diluted buffer should be used within 14 days. In the same way, streptavidin-HRP or detection antibody vial was also diluted according to the technical bulletin of the product.

Methodology:

- Considering that all standards and samples should be run at least in duplicate, 100 µL of each standard and samples (after extraction) was added to the appropriate microtiter wells. 96-well plate was covered and incubated overnight at 4°C with gently shaking.
- After the incubation, the solution was discarded and wells washed (4 times) with 1x wash solution by filling each well with 300 µl of this buffer. Plate should be dried of liquid to good performance. After the last wash, remove any remaining buffer by inverting the plate and blotting it against clean paper towels.
- 100 µL of 1x biotinylated detection antibody (Biotin Conjugate) solution was added into each well. The plate was covered again and incubated for 1 h at room temperature with gentle shaking.
- The second step was repeated to wash properly the plate and to complete removal of liquid. Added 100 µl Streptavidin-HRP Working Solution to each well and incubated for 30 min at room temperature.
- Discard the solution. Repeat the wash as in second step described above.
- Added 100 µl of ELISA colorimetric TMB reagent to each well and incubated for 30 min at room temperature in the dark. Then, 100 µl of Stop Solution was added to each well.
- Read the absorbance of each well at 450 nm immediately after adding the Stop Solution.
- Absorbance data obtained in the plate reader were plotted along with the known values of the standard curve. Performing the best fitted adjustment of these data, with the equation obtained, the concentrations were estimated by interpolation for the rest of the samples. The dilution factor applied to the samples should be consider to calculate the factor concentration in the results.

• Results and conclusion

The results obtained for the GF analyzed in these tests have confirmed our initial hypothesis about the molecule distribution. After 24 h incubation, approximately half of the initial solution added to the device has diffused across the hydrogel to the opposite channel. Figure A2 shows the results of ELISA immunoassay for BMP-2 and PDGF factors. The difference between the initial concentration added and the total concentration estimated may be due to pipetted error as well as the evaporation and its consequent concentration of the sample.

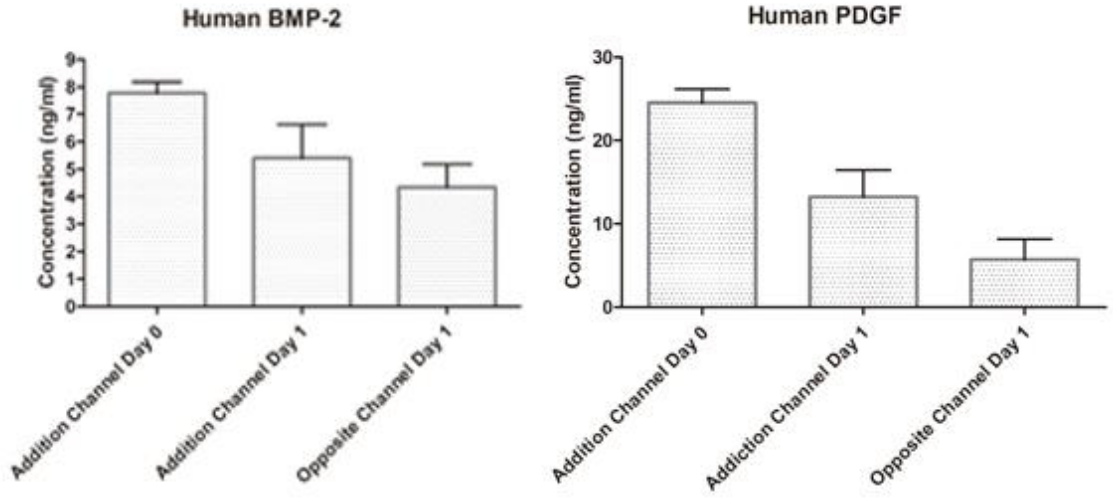

Figure A 2. BMP-2 and PDGF-BB concentration estimated by using ELISA techniques.

Samples were obtained after 24h incubation at 37ºC and 5% CO_2.

Despite results obtained in this experiment were coherent with previous published work where an experimental and numerical model described the transport of GFs. The molecule size and behavior, directly related to the formation of aggregates characteristic from some proteins, could affect to its spatial distribution. The binding of GFs to the collagen hydrogel is more significant compared to other types of hydrogels [158], directly involved in haptotactic cues.

To conclude, the microfluidic platforms with their versatile technology to biomimetize the cellular microenvironment, have been a great instrument for the application of chemical gradients in a controlled manner. In this work it has been demonstrated how the factor is able to move by diffusing all over the chip towards the opposite channel. This would confirm the possible stimulation of cells mediated by added GF, in addition to other mechanical and chemical signals from the environment.

A2. Evolution of fluid flow set-up

One of the most important research lines to be developed throughout this thesis has been the application of interstitial fluid flow to three-dimensional cell culture. The difficulties found during this work in setting up an optimal flow application system in which leaks, bubbles and rupture of the hydrogels were minimized resulted in numerous designs up to the one finally used. Some of these attempts as well as the methodology finally used have been shown in Figure A3.

In the first experiments of flow application, connectors were placed directly in the reservoirs of the chip. The pressure to introduce them produced the rupture of the hydrogels. In order to absorb the flow shocks, falcon tubes were added to the system, which would release the pressure of the flow before getting to the chip chamber, which did not give good results either. In view of this fact, several alternatives were proposed, the use of glass needles and tubes, such as those used in previously published permeability tests [253]. One of the biggest disadvantages of these glass tubes was their openness to the exterior and the difficulty of viewing the microfluidic chips under the microscope. As an improvement of these systems, we saw the need to design a new model of application, in which on the one hand we preserve the watertightness of the system and on the other hand we avoid the breakage of the gels, as well as the entry of bubbles. The final design consisted of a base and a cover, which were joined together by means of screw joints, with o-rings that guarantee the watertightness of the system. The connectors for the inlet and outlet will be screwed without touching the microfluidic chip. This means that tensions are not concentrated in the reservoir area, but are distributed throughout the pdms, thus avoiding rupture of the hydrogel

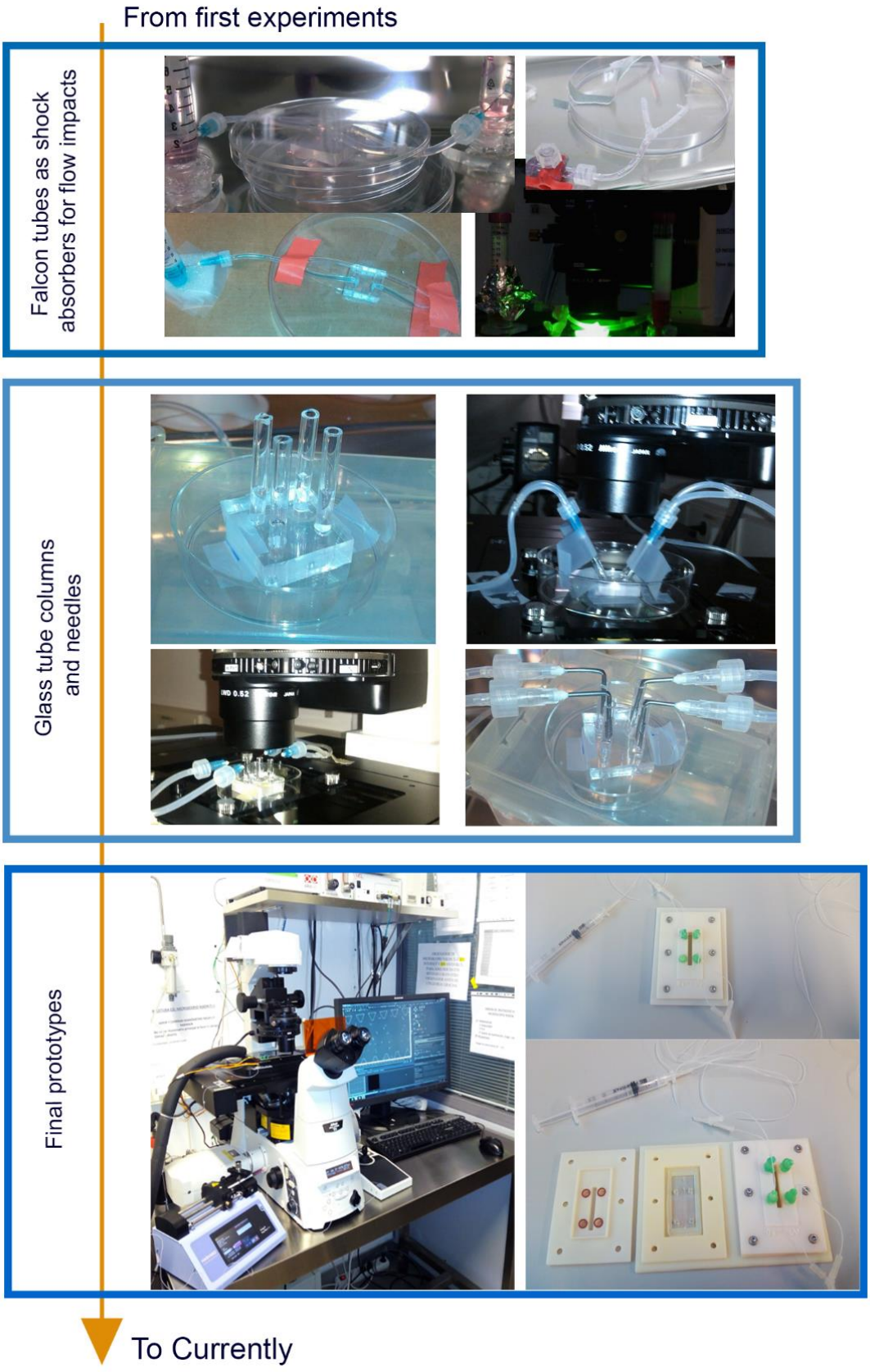

Figure A 3. Evolution of fluid set up.
With the development of the final prototype, the initial problems were solved and the interstitial flow could be successfully applied to three-dimensional cell cultures.

References

[1] D. Huh, G.A. Hamilton, D.E. Ingber, From 3D cell culture to organs-on-chips, Trends Cell Biol. 21 (2011) 745–754. doi:10.1016/j.tcb.2011.09.005.

[2] I. Meyvantsson, D.J. Beebe, Cell Culture Models in Microfluidic Systems, Annu. Rev. Anal. Chem. 1 (2008) 423–449. doi:10.1146/annurev.anchem.1.031207.113042.

[3] A. Aziz, C. Geng, M. Fu, X. Yu, K. Qin, B. Liu, The Role of Microfluidics for Organ on Chip Simulations, Bioengineering. 4 (2017) 39. doi:10.3390/bioengineering4020039.

[4] A. Khademhosseini, R. Langer, J. Borenstein, J.P. Vacanti, Microscale technologies for tissue engineering and biology., Proc. Natl. Acad. Sci. U. S. A. 103 (2006) 2480–7. doi:10.1073/pnas.0507681102.

[5] J. Voldman, M.L. Gray, M.A. Schmidt, Microfabrication in biology and medicine, Annu. Rev. Biomed. Eng. 1 (1999) 401–425. doi:10.1021/bp980203f.

[6] E.W.K. Young, D.J. Beebe, Fundamentals of microfluidic cell culture in controlled microenvironments, Chem. Soc. Rev. 39 (2010) 1036. doi:10.1039/b909900j.

[7] Y. Shin, S. Han, J.S. Jeon, K. Yamamoto, I.K. Zervantonakis, R. Sudo, R.D. Kamm, S. Chung, Microfluidic assay for simultaneous culture of multiple cell types on surfaces or within hydrogels, Nat Protoc. 7 (2012) 1247–1259. doi:10.1038/nprot.2012.051.

[8] E.W.K. Young, D.J. Beebe, Fundamentals of microfluidic cell culture in controlled microenvironments, Chem Soc Rev. 39 (2010) 1036–1048. doi:10.1039/b909900j.Fundamentals.

[9] Z. Pujic, D. Mortimer, J. Feldner, G.J. Goodhill, Assays for eukaryotic cell chemotaxis., Comb. Chem. High Throughput Screen. 12 (2009) 580–588. doi:10.2174/138620709788681952.

[10] P. Gravesen, J. Branebjerg, O.S. Jensen, Microfluidics-a review, J. Micromech. Microeng. 3 (1993) 168–182.

[11] W.J. Polacheck, R. Li, S.G.M. Uzel, R.D. Kamm, Microfluidic platforms for mechanobiology, Lab Chip. 13 (2013) 2252–2267. doi:10.1039/c3lc41393d.

[12] A. Boussommier-Calleja, R. Li, M.B. Chen, S.C. Wong, R.D. Kamm, Microfluidics: A new tool for modeling cancer-immune interactions, Trends Cancer. 2 (2016) 6–19. doi:10.1097/ACI.0000000000000108.Anti-Interleukin.

[13] D.S. Kong, T.A. Thorsen, J. Babb, S.T. Wick, J.J. Gam, R. Weiss, P.A. Carr, Open-source, community-driven microfluidics with Metafluidics, Nat. Biotechnol. 35 (2017) 523–529. doi:10.1038/nbt.3873.

[14] S. Halldorsson, E. Lucumi, R. Gómez-Sjöberg, R.M.T. Fleming, Advantages and challenges of microfluidic cell culture in polydimethylsiloxane devices, Biosens. Bioelectron. 63 (2015) 218–231. doi:10.1016/j.bios.2014.07.029.

[15] V. van Duinen, S.J. Trietsch, J. Joore, P. Vulto, T. Hankemeier, Microfluidic 3D cell culture: From tools to tissue models, Curr. Opin. Biotechnol. 35 (2015) 118–126. doi:10.1016/j.copbio.2015.05.002.

[16] George M. Whitesides, The origins and the future of microfluidics, Nature. 442 (2006) 368–373. doi:10.1038/nature05058.

[17] Ashleigh B. Theberge, Jiaquan Yu, Edmond W. K. Young, William A. Ricke, Wade Bushman, David J. Beebe, Microfluidic multiculture assay to analyze biomolecular signaling in angiogenesis, Anal Chem. 87 (2015) 3239–3246. doi:10.1021/ac503700f.

[18] D.E. Ingber, Reverse Engineering Human Pathophysiology with Organs-on-Chips, Cell. 164 (2016) 1105–1109. doi:10.1016/j.cell.2016.02.049.

[19] S.N. Bhatia, D.E. Ingber, Microfluidic organs-on-chips, Nat. Biotechnol. 32 (2014). doi:10.1038/nbt.2989.

[20] S.F. Moussavi-Haramic, H.M. Pezzi, A. Huttenlocher, D.J. Beebe, Simple Microfluidic Device For Studying Chemotaxis In Response To Dual Gradients, Biomed Microdevices. 17 (2015) 9955.

[21] L.J. Barkal, E. Berthier, A.B. Theberge, N.P. Keller, D.J. Beebe, Multikingdom microscale models, Plos Pathog. 13 (2018) e1006424. doi:10.1371/journal.ppat.1006424.

[22] J.N. Lee, C. Park, G.M. Whitesides, Solvent Compatibility of Poly(dimethylsiloxane)-Based Microfluidic Devices, Anal. Chem. 75 (2003) 6544–6554. doi:10.1021/ac0346712.

[23] S.K. Sia, G.M. Whitesides, Microfluidic devices fabricated in Poly(dimethylsiloxane) for biological studies, Electrophoresis. 24 (2003) 3563–3576. doi:10.1002/elps.200305584.

[24] C. Kim, J. Kasuya, J. Jeon, S. Chung, R.D. Kamm, A quantitative microfluidic angiogenesis

screen for studying anti-angiogenic therapeutic drugs, Lab Chip. (2014). doi:10.1039/C4LC00866A.

[25] I.K. Zervantonakis, S.K. Hughes-Alford, J.L. Charest, J.S. Condeelis, F.B. Gertler, R.D. Kamm, Three-dimensional microfluidic model for tumor cell intravasation and endothelial barrier function, PNAS. 109 (2012) 13515–13520. doi:10.1073/pnas.1210182109.

[26] J.S. Jeon, I.K. Zervantonakis, S. Chung, R.D. Kamm, J.L. Charest, In vitro model of tumor cell extravasation., PLoS One. 8 (2013) e56910. doi:10.1371/journal.pone.0056910.

[27] G. Adriani, D. Ma, A. Pavesi, R.D. Kamm, E.L.K. Goh, A 3D neurovascular microfluidic model consisting of neurons, astrocytes and cerebral endothelial cells as a blood–brain barrier, Lab Chip. 12 (2017) 169–182. doi:10.1039/C6LC00638H.

[28] P. Galie, M. Russell, M. Westfall, J. Stegemann, Interstitial fluid flow and cyclic strain differentially regulate cardiac fibroblast activation via AT1R and TGF-β1, Exp Cell Res. 318 (2012) 75–84. doi:10.1016/j.yexcr.2011.10.008.Interstitial.

[29] Y. Qu, F. An, Y. Luo, Y. Lu, T. Liu, W. Zhao, B. Lin, A nephron model for study of drug-induced acute kidney injury and assessment of drug-induced nephrotoxicity, Biomaterials. (2017). doi:10.1016/j.biomaterials.2017.11.010.

[30] G.A. Wright, L. Costa, A. Terekhov, D. Jowhar, W. Hofmeister, C. Janetopoulos, On-Chip Open Microfluidic Devices for Chemotaxis Studies, Microsc Microanal. 18 (2012) 816–828. doi:10.1017/S1431927612000475.On-Chip.

[31] S. Toetsch, P. Olwell, A. Prina-Mello, Y. Volkov, The evolution of chemotaxis assays from static models to physiologically relevant platforms, Integr. Biol. 1 (2009) 170–181. doi:10.1039/B814567A.

[32] P. Roca-Cusachs, R. Sunyer, X. Trepat, Mechanical guidance of cell migration: Lessons from chemotaxis, Curr. Opin. Cell Biol. 25 (2013) 543–549. doi:10.1016/j.ceb.2013.04.010.

[33] A.J. Ridley, Cell Migration: Integrating Signals from Front to Back, Science (80-.). 302 (2003) 1704–1709. doi:10.1126/science.1092053.

[34] J. Li, F. Lin, Microfluidic devices for studying chemotaxis and electrotaxis, Trends Cell Biol. 21 (2011) 489–497. doi:10.1016/j.tcb.2011.05.002.

[35] M. Dudaie, D. Weihs, F.J. Vermolen, A. Gefen, Modeling migration in cell colonies in two and three dimensional substrates with varying stiffnesses, Silico Cell Tissue Sci. 2 (2015) 1–14. doi:10.1186/s40482-015-0005-9.

[36] P. Rørth, Whence Directionality: Guidance Mechanisms in Solitary and Collective Cell Migration, Dev. Cell. 20 (2011) 9–18. doi:10.1016/j.devcel.2010.12.014.

[37] R. Sunyer, V. Conte, J. Escribano, A. Elosegui-artola, A. Labernadie, L. Valon, D. Navajas, J.M. García-aznar, J.J. Muñoz, P. Roca-Cusachs, X. Trepat, Collective cell durotaxis emerges from long-range intercellular force transmission, Science (80-.). 353 (2016) 1157–1161. doi:10.5061/dryad.r8h3n.

[38] C.M. Lo, H.B. Wang, M. Dembo, Y.L. Wang, Cell movement is guided by the rigidity of the substrate., Biophys. J. 79 (2000) 144–152. doi:10.1016/S0006-3495(00)76279-5.

[39] L. Bollmann, D.E. Koser, R. Shahapure, H.O.B. Gautier, G.A. Holzapfel, G. Scarcelli, M.C. Gather, E. Ulbricht, K. Franze, Microglia mechanics: immune activation alters traction forces and durotaxis, Front. Cell. Neurosci. 9 (2015). doi:10.3389/fncel.2015.00363.

[40] S.L. Lin, J.C. Yang, K.N. Ho, C.H. Wang, C.W. Yeh, H.M. Huang, Effects of compressive residual stress on the morphologic changes of fibroblasts, Med. Biol. Eng. Comput. 47 (2009) 1273–1279. doi:10.1007/s11517-009-0512-6.

[41] J. Bueno, Y. Bazilevs, R. Juanes, H. Gomez, Droplet motion driven by tensotaxis, Extrem. Mech. Lett. 13 (2017) 10–16. doi:10.1016/j.eml.2017.01.004.

[42] S. Li, P. Butler, Y. Wang, Y. Hu, D. Cho Han, S. Usami, J.-L. Guan, S. Chien, C.B. by Yuan-Cheng Fung, The role of the dynamics of focal adhesion kinase in the mechanotaxis of endothelial cells, PNAS. 99 (2002) 3546–3551.

[43] R. Hernández Vera, E. Genové, L. Alvarez, S. Borrós, R. Kamm, D. Lauffenburger, C.E. Semino, Interstitial fluid flow intensity modulates endothelial sprouting in restricted Src-activated cell clusters during capillary morphogenesis., Tissue Eng. Part A. 15 (2009) 175–85. doi:10.1089/ten.tea.2007.0314.

[44] P.A. Galie, D.-H.T. Nguyen, C.K. Choi, D.M. Cohen, P.A. Janmey, C.S. Chen, Fluid shear stress threshold regulates angiogenic sprouting., PNAS. 111 (2014) 7968–73. doi:10.1073/pnas.1310842111.

[45] V. Vickerman, R.D. Kamm, Mechanism of a flow-gated angiogenesis switch: Early signaling events at cell-matrix and cell-cell junctions, Integr. Biol. 4 (2012) 863–874. doi:10.1039/b000000x/Vickerman.

[46] V. Vickerman, J. Blundo, S. Chung, R.D. Kamm, Desing, Fabrication and Implementation of a Novel MultiParameter Control Microfluidic Platform for Three-Dimensional Cell Culture and Real-Time Imaging, Lab Chip. 8 (2008) 1468–1477. doi:10.1039/b802395f.Design.

[47] J.W. Song, L.L. Munn, Fluid forces control endothelial sprouting, PNAS. 108 (2011) 15342–15347. doi:10.1073/pnas.1105316108/-/DCSupplemental.www.pnas.org/cgi/doi/10.1073/pnas.1105316108.

[48] W.J. Polacheck, A.E. German, A. Mammoto, D.E. Ingber, R.D. Kamm, Mechanotransduction of fluid stresses governs 3D cell migration., Proc. Natl. Acad. Sci. U. S. A. 111 (2014) 2447–52. doi:10.1073/pnas.1316848111.

[49] P. Domachuk, K. Tsioris, F.G. Omenetto, D.L. Kaplan, Bio-microfluidics: Biomaterials and biomimetic designs, Adv. Mater. 22 (2010) 249–260. doi:10.1002/adma.200900821.

[50] S.K. Sia, G.M. Whitesides, Microfluidic devices fabricated in poly(dimethylsiloxane) for biological studies, Electrophoresis. 24 (2003) 3563–3576. doi:10.1002/elps.200305584.

[51] J. Shemesh, I. Jalilian, A. Shi, G. Heng Yeoh, M.L. Knothe Tate, M. Ebrahimi Warkiani, Flow-induced stress on adherent cells in microfluidic devices, Lab Chip. 15 (2015) 4114–4127. doi:10.1039/C5LC00633C.

[52] S. Lee, J. Sung, Microtechnology-Based Multi-Organ Models, Bioengineering. 4 (2017) 46. doi:10.3390/bioengineering4020046.

[53] M. Mehling, S. Tay, Microfluidic cell culture, Curr. Opin. Biotechnol. 25 (2014) 95–102. doi:10.1016/j.copbio.2013.10.005.

[54] J. Tien, L. Li, O. Ozsun, K.L. Ekinci, Dynamics of Interstitial Fluid Pressure in Extracellular Matrix Hydrogels in Microfluidic Devices, J. Biomech. Eng. 137 (2015) 91009. doi:10.1115/1.4031020.

[55] L. Van De Water, S. Varney, J.J. Tomasek, Mechanoregulation of the Myofibroblast in Wound Contraction, Scarring, and Fibrosis: Opportunities for New Therapeutic Intervention., Adv. Wound Care. 2 (2013) 122–141. doi:10.1089/wound.2012.0393.

[56] J. Schwarz, V. Bierbaum, J. Merrin, T. Frank, R. Hauschild, T. Bollenbach, S. Tay, M. Sixt, M. Mehling, A microfluidic device for measuring cell migration towards substrate- bound and soluble chemokine gradients, Sci. Rep. 6 (2016). doi:10.1038/srep36440.

[57] W. Risau, Mechanisms Of Angiogenesis, Nature. 386 (1997) 671–674. doi:10.1146/annurev.physiol.49.1.453.

[58] P. Carmeliet, Angiogenesis in health and disease, Nat. Med. 9 (2003) 653–660. doi:10.1016/S0306-3623(01)00111-2.

[59] J. Folkman, P.A. D'Amore, Blood vessel formation: What is its molecular basis?, Cell. 87

(1996) 1153–1155. doi:10.1016/S0092-8674(00)81810-3.

[60] W. Risau, I. Flamme, Vasculogenesis, Annu. Rev. Cell Dev. Biol. 11 (1995) 73–91.

[61] Christopher W Pugh, Peter J Ratcliffe, Regulation of angiogenesis by hypoxia: role of the HIF system, Nat. Med. 9 (2003) 677–684.

[62] C. a Reinhart-King, Endothelial cell adhesion and migration., Methods Enzymol. 443 (2008) 45–64. doi:10.1016/S0076-6879(08)02003-X.

[63] D. Ribatti, E. Crivellato, "Sprouting angiogenesis", a reappraisal, Dev. Biol. 372 (2012) 157–165. doi:10.1016/j.ydbio.2012.09.018.

[64] P. Rørth, Collective Cell Migration, Annu. Rev. Cell Dev. Biol. 25 (2009) 407–29. doi:10.1146/annurev.cellbio.042308.113231.

[65] K.-A. Norton, A.S. Popel, Effects of endothelial cell proliferation and migration rates in a computational model of sprouting angiogenesis, Nat. Publ. Gr. (2016). doi:10.1038/srep36992.

[66] H.G. Augustin, G. Young Koh, G. Thurston, K. Alitalo, Control of vascular morphogenesis and homeostasis through the angiopoietin–Tie system, Nat. Rev. Mol. Cell Biol. 10 (2009) 165–177. doi:10.1038/nrm2639.

[67] S.A. Eming, B. Brachvogel, T. Odorisio, M. Koch, Regulation of angiogenesis: Wound healing as a model, Prog. Histochem. Cytochem. 42 (2007) 115–170. doi:10.1016/j.proghi.2007.06.001.

[68] G.J. Pettet, H.M. Byrne, D.L.S. Mcelwain, J. Norbury, A model of wound-healing angiogenesis in soft tissue, Math. Biosci. 136 (1996) 35–63. doi:10.1016/0025-5564(96)00044-2.

[69] M.G. Tonnesen, X. Feng, R. a F. Clark, Angiogenesis in wound healing, J. Investig. Dermatology Symp. Proc. 5 (2000) 40–46. doi:10.1046/j.1087-0024.2000.00014.x.

[70] P. Bao, A. Kodra, M. Tomic-Canic, M.S. Golinko, H.P. Ehrlich, H. Brem, The Role of Vascular Endothelial Growth Factor in Wound Healing, J. Surg. Res. 153 (2009) 347–358. doi:10.1016/j.jss.2008.04.023.

[71] D.O. Bates, R.O.P. Jones, The role of vascular endothelial growth factor in wound healing., Int. J. Low. Extrem. Wounds. 2 (2003) 107–20. doi:10.1177/1534734603256626.

[72] K.E. Johnson, T. a Wilgus, Vascular Endothelial Growth Factor and Angiogenesis in the Regulation of Cutaneous Wound Repair, Adv. Wound Care. 3 (2014) 647–661.

doi:10.1089/wound.2013.0517.

[73] M. Pakyari, A. Farrokhi, M.K. Maharlooei, A. Ghahary, Critical Role of Transforming Growth Factor Beta in Different Phases of Wound Healing., Adv. Wound Care. 2 (2013) 215–224. doi:10.1089/wound.2012.0406.

[74] F. Arnold, D.C. West, Angiogenesis in wound healing, Pharmac Ther. 52 (1991) 407–422.

[75] E.J. Battegay, J. Rupp, L. Iruela-Arispe, E.H. Sage, M. Pech, PDGF-BB Modulates Endothelial Proliferation and Angiogenesis In Vitro via PDGF B-Receptors, J. Cell Biol. 125 (1994) 917–928.

[76] R.A.D. Carano, E.H. Filvaroff, Angiogenesis and bone repair, Drug Discov. Today. 8 (2003) 980–989. doi:10.1016/S1359-6446(03)02866-6.

[77] K.D. Hankenson, M. Dishowitz, C. Gray, M. Schenker, Angiogenesis in bone regeneration, Injury. 42 (2011) 556–561. doi:10.1016/j.injury.2011.03.035.

[78] L. Geris, A. Gerisch, J. Vander Sloten, R. Weiner, H. Van Oosterwyck, Angiogenesis in bone fracture healing: A bioregulatory model, J. Theor. Biol. 251 (2008) 137–158. doi:10.1016/j.jtbi.2007.11.008.

[79] K. Taguchi, R. Ogawa, M. Migita, H. Hanawa, H. Ito, H. Orimo, The role of bone marrow-derived cells in bone fracture repair in a green fluorescent protein chimeric mouse model, Biochem. Biophys. Res. Commun. 331 (2005) 31–36. doi:10.1016/j.bbrc.2005.03.119.

[80] J. Kleinheinz, U. Stratmann, U. Joos, H.P. Wiesmann, VEGF-activated angiogenesis during bone regeneration, J. Oral Maxillofac. Surg. 63 (2005) 1310–1316. doi:10.1016/j.joms.2005.05.303.

[81] J. Street, M. Bao, L. DeGuzman, S. Bunting, F. V Peale, N. Ferrara, H. Steinmetz, J. Hoeffel, J.L. Cleland, A. Daugherty, N. van Bruggen, H.P. Redmond, R.A.D. Carano, E.H. Filvaroff, Vascular endothelial growth factor stimulates bone repair by promoting angiogenesis and bone turnover., PNAS. 99 (2002) 9656–9661. doi:10.1073/pnas.152324099.

[82] U. Mayr-Wohlfart, J. Waltenberger, H. Hausser, S. Kessler, K.-P.G. Nther, C. Dehio, W. Puhl, A.R.E. Brenner, Vascular Endothelial Growth Factor Stimulates Chemotactic Migration of Primary Human Osteoblasts, Bone. 30 (2002) 472–477.

[83] M.M.L. Deckers, M. Karperien, C. Van Der Bent, T. Yamashita, S.E. Papapoulos, C.W.G.M.L. Wik, Expression of Vascular Endothelial Growth Factors and Their Receptors during Osteoblast Differentiation, Endocrinology. 141 (2000) 1667–1674.

[84] Hairong Peng, Vonda Wright, Arvydas Usas, Brian Gearhart, Hsain-Chung Shen, James Cummins, Johnny Huard, Synergistic enhancement of bone formation and healing by stem cell–expressed VEGF and bone morphogenetic protein-4, J Clin Invest. 110 (2002) 751–759. doi:10.1172/JCI200215153.

[85] J. Street, M. Bao, L. deGuzman, S. Bunting, F. V Peale, N. Ferrara, H. Steinmetz, J. Hoeffel, J.L. Cleland, A. Daugherty, N. van Bruggen, H.P. Redmond, R.A.D. Carano, E.H. Filvaroff, Vascular endothelial growth factor stimulates bone repair by promoting angiogenesis and bone turnover., Proc. Natl. Acad. Sci. 99 (2002) 9656–9661. doi:10.1073/pnas.152324099.

[86] M.M.L. Deckers, R.L. Van Bezooijen, G. Van Der Horst, J. Hoogendam, C. Van Der Bent, S.E. Papapoulos, C.W.G.M. LöWik, Bone Morphogenetic Proteins Stimulate Angiogenesis through Osteoblast-Derived Vascular Endothelial Growth Factor A, Endocrinology. 143 (2002) 1545–1553.

[87] H. Eckardt, M. Ding, M. Lind, E.S. Hansen, K.S. Christensen, I. Hvid, Recombinant human vascular endothelial growth factor enhances bone healing in an experimental nonunion model., J. Bone Joint Surg. Br. 87 (2005) 1434–1438. doi:10.1302/0301-620X.87B10.16226.

[88] J.A. Flegg, S.N. Menon, P.K. Maini, D.L.S. McElwain, On the mathematical modeling of wound healing angiogenesis in skin as a reaction-transport process, Front. Physiol. 6 (2015) 1–17. doi:10.3389/fphys.2015.00262.

[89] G. Broughton, J.E. Janis, C.E. Attinger, The Basic Science of Wound Healing, Plast. Reconstr. Surg. 117 (2006) 12S–34S. doi:10.1097/01.prs.0000225430.42531.c2.

[90] S.A. Eming, P. Martin, M. Tomic-canic, H. Park, R. Medicine, Wound repair and regeneration: mechanism, signaling and translation, Sci Transl Med. 6 (2014) 1–36. doi:10.1126/scitranslmed.3009337.Wound.

[91] S. Guo, L.A. DiPietro, Factors Affecting Wound Healing, J. Dent. Res. 89 (2010) 219–229. doi:10.1177/0022034509359125.

[92] M.B. Witte, A. Barbul, General Principles of Wound Healing, Surg. Clin. North Am. 77 (1997) 509–528. doi:10.1016/S0039-6109(05)70566-1.

[93] B.K. Sun, Z. Siprashvili, P.A. Khavari, Advances in skin grafting and treatment of cutaneous wounds, Science (80-.). 346 (2014) 941–945. doi:10.1126/science.1253836.

[94] A.J. Singer, R.C. AF, Cutaneous Wound Healing, N. Engl. J. Med. (1999).

[95] V. Falanga, Wound healing and its impairment in the diabetic foot, Lancet. 366 (2005)

1736–1743. doi:10.1016/S0140-6736(05)67700-8.

[96] C.L. Baum, C.J. Arpey, Normal cutaneous wound healing: clinical correlation with cellular and molecular events, Dermatol. Surg. 31 (2005) 674–86; discussion 686. doi:10.1111/j.1524-4725.2005.31612.

[97] C. Wittkowske, G.C. Reilly, D. Lacroix, C.M. Perrault, In Vitro Bone Cell Models: Impact of Fluid Shear Stress on Bone Formation, Front. Bioeng. Biotechnol. 4 (2016). doi:10.3389/fbioe.2016.00087.

[98] R. Florencio-Silva, G.R.D.S. Sasso, E. Sasso-Cerri, M.J. Simões, P.S. Cerri, Biology of Bone Tissue: Structure, Function, and Factors That Influence Bone Cells, Biomed Res. Int. 2015 (2015) 1–17. doi:10.1155/2015/421746.

[99] U. Saran, S.G. Piperni, S. Chatterjee, Role of angiogenesis in bone repair, Arch. Biochem. Biophys. 561 (2014) 109–117. doi:10.1016/j.abb.2014.07.006.

[100] A. Spyropoulou, K. Karamesinis, E.K. Basdra, Mechanotransduction pathways in bone pathobiology., Biochim. Biophys. Acta. 1852 (2015) 1700–1708. doi:10.1016/j.bbadis.2015.05.010.

[101] S. Harada, G.A. Rodan, Control of osteoblast function and regulation of bone mass., Nature. 423 (2003) 349–355. doi:10.1038/nature01660.

[102] D. Golden, E.A. Saria, M.F. Hansen, Regulation of Osteoblast Migration Involving Receptor Activator of Nuclear Factor-kappa B (RANK) Signaling, J. Cell. Physiol. 230 (2015) 2951–2960. doi:10.1002/jcp.25024.

[103] Y.-X. Qin, M. Hu, Mechanotransduction in Musculoskeletal Tissue Regeneration: Effects of Fluid Flow, Loading, and Cellular-Molecular Pathways, Biomed Res. Int. 2014 (2014) 1–12. doi:10.1155/2014/863421.

[104] P.P. Eleniste, S. Huang, K. Wayakanon, H.W. Largura, A. Bruzzaniti, Osteoblast differentiation and migration are regulated by Dynamin GTPase activity, Int J Biochem Cell Biol. Int J Biochem Cell Biol. 46 (2014) 9–18. doi:10.1016/j.biocel.2013.10.008.

[105] S.P. Fritton, S. Weinbaum, Fluid and Solute Transport in Bone: Flow-Induced Mechanotransduction, Annu Rev Fluid Mech. 41 (2009) 347–374. doi:10.1146/annurev.fluid.010908.165136.

[106] H. Wang, W. Sun, J. Ma, Y. Pan, L. Wang, W. Zhang, Polycystin-1 mediates mechanical strain-induced osteoblastic mechanoresponses via potentiation of intracellular calcium

and Akt/β-catenin pathway, PLoS One. 9 (2014). doi:10.1371/journal.pone.0091730.

[107] J. You, G.C. Reilly, X. Zhen, C.E. Yellowley, Q. Chen, H.J. Donahue, C.R. Jacobs, Osteopontin Gene Regulation by Oscillatory Fluid Flow via Intracellular Calcium Mobilization and Activation of Mitogen-activated Protein Kinase in MC3T3-E1 Osteoblasts, J. Biol. Chem. 276 (2001) 13365–13371. doi:10.1074/jbc.M009846200.

[108] J.J. Fredberg, D. Discher, C. Dong, F. Guilak, D. Ingber, P. Janmey, R.D. Kamm, G.W. Schmid-Schönbein, S. Weinbaum, Biomechanics: cell research and applications for the next decade, Ann Biomed Eng. 37 (2009) 847–859. doi:10.1007/s10439-009-9661-x.

[109] K.M. Reich, C. V. Gay, J.A. Frangos, Fluid shear stress as a mediator of osteoblast cyclic adenosine monophosphate production, J. Cell. Physiol. 143 (1990) 100–104. doi:10.1002/jcp.1041430113.

[110] L.A. González-Torres, M.J. Gómez-Benito, M. Doblaré, J.M. García-Aznar, Influence of the frequency of the external mechanical stimulus on bone healing: a computational study, Med. Eng. Phys. 34 (2010) 363–371.

[111] J. Martínez-Reina, I. Reina, J. Domínguez, J.M. García-Aznar, A bone remodelling model including the effect of damage on the steering of BMUs, J. Mech. Behav. Biomed. Mater. 32 (2014) 99–112. doi:10.1016/j.jmbbm.2013.12.025.

[112] P. V Giannoudis, T.A. Einhorn, D. Marsh, Fracture healing: the diamond concept, Injury. (2007) 3–6.

[113] T.A. Einhorn, L.C. Gerstenfeld, Fracture healing: mechanisms and interventions, Nat Rev Rheumatol. 11 (2015) 45–54. doi:10.1038/nrrheum.2014.164.

[114] M.S. Ghiasi, J. Chen, A. Vaziri, E.K. Rodriguez, A. Nazarian, Bone fracture healing in mechanobiological modeling: A review of principles and methods, Bone Reports. 6 (2017) 87–100. doi:10.1016/j.bonr.2017.03.002.

[115] A. Bailón-Plaza, M.C.H. Van Der Meulen, A Mathematical Framework to Study the Effects of Growth Factor Influences on Fracture Healing, J. Theor. Biol. 212 (2001) 191–209. doi:10.1006/jtbi.2001.2372.

[116] Y. Lu, T. Lekszycki, Modeling of an initial stage of bone fracture healing, Contin. Mech. Thermodyn. 27 (2015). doi:10.1007/s00161-014-0380-7.

[117] M. Doblaré, J.M. García, M.J. Gómez, Modelling bone tissue fracture and healing: A review, Eng. Fract. Mech. 71 (2004) 1809–1840. doi:10.1016/j.engfracmech.2003.08.003.

[118] R. Marsell, T.A. Einhorn, The biology of fracture healing, Injury. 42 (2012) 551–555. doi:10.1016/j.injury.2011.03.031.THE.

[119] L. Claes, S. Recknagel, A. Ignatius, Fracture healing under healthy and inflammatory conditions, Nat. Rev. Rheumatol. 8 (2012) 133–143. doi:10.1038/nrrheum.2012.1.

[120] A. Thiel, M.K. Reumann, A. Boskey, J. Wischmann, R. von Eisenhart-Rothe, P. Mayer-Kuckuk, Osteoblast migration in vertebrate bone, Biol. Rev. 49 (2017). doi:10.1111/brv.12345.

[121] P. Augat, U. Simon, A. Liedert, L. Claes, Mechanics and mechano-biology of fracture healing in normal and osteoporotic bone, Osteoporos. Int. 16 (2005) 36–43. doi:10.1007/s00198-004-1728-9.

[122] V. Sathyendra, M. Darowish, Basic science of bone healing, Hand Clin. 29 (2013). doi:10.1016/j.hcl.2013.08.002.

[123] D. Lacroix, P.J. Prendergast, G. Li, D. Marsh, Biomechanical model to simulate tissue differentiation and bone regeneration: application to fracture healing., Med. Biol. Eng. Comput. 40 (2002) 14–21. doi:10.1007/BF02347690.

[124] S.J. Shefelbine, P. Augat, L. Claes, U. Simon, Trabecular bone fracture healing simulation with finite element analysis and fuzzy logic, J. Biomech. 38 (2005) 2440–2450. doi:10.1016/j.jbiomech.2004.10.019.

[125] L. Claes, C.A.C.A. Heigele, C. Neidlinger-Wilke, D. Kaspar, W. Seidl, K.J.K.J. Margevicius, P. Augat, Effects of Mechanical Factors on the Fracture Healing Process, Clin. Orthop. Relat. Res. 355S (1998) S132–S147. doi:10.1097/00003086-199810001-00015.

[126] O. Moreno-Arotzena, C. Borau, N. Movilla, M. Vicente-Manzanares, J.M. García-Aznar, Fibroblast Migration in 3D is Controlled by Haptotaxis in a Non-muscle Myosin II-Dependent Manner, Ann. Biomed. Eng. (2015). doi:10.1007/s10439-015-1343-2.

[127] C. Del Amo, C. Borau, R. Gutiérrez, J. Asín, J.M. García-Aznar, Quantification of angiogenic sprouting under different growth factors in a microfluidic platform, J. Biomech. 49 (2016) 1340–1346. doi:10.1016/j.jbiomech.2015.10.026.

[128] O. Huttala, H. Vuorenpää, T. Toimela, J. Uotila, H. Kuokkanen, T. Ylikomi, J.-R. Sarkanen, T. Heinonen, Human Vascular Model with Defined Stimulation Medium – A Characterization Study, ALTEX. 32 (2015) 125–136.

[129] S. Chung, R. Sudo, V. Vickerman, I.K. Zervantonakis, R.D. Kamm, Microfluidic Platforms for

Studies of Angiogenesis , Cell Migration , and Cell – Cell Interactions Accessed, Biomed. Eng. Soc. (2014).

[130] J.T. Daub, R.M.H. Merks, A cell-based model of extracellular-matrix-guided endothelial cell migration during angiogenesis., Bull. Math. Biol. 75 (2013) 1377–99. doi:10.1007/s11538-013-9826-5.

[131] S. Jung, J. Kleinheinz, Angiogenesis : the fundament of osseous regeneration, Hard Tissue. 2 (2013) 1–4.

[132] Y.K. Park, T.-Y. Tu, S.H. Lim, I.J.M. Clement, S.Y. Yang, R.D. Kamm, In Vitro Microvessel Growth and Remodeling within a Three-dimensional Microfluidic Environment., Cell. Mol. Bioeng. 7 (2014) 15–25. doi:10.1007/s12195-013-0315-6.

[133] K. Bentley, G. Mariggi, H. Gerhardt, P. a Bates, Tipping the balance: robustness of tip cell selection, migration and fusion in angiogenesis., PLoS Comput. Biol. 5 (2009) e1000549. doi:10.1371/journal.pcbi.1000549.

[134] A. Shamloo, N. Ma, M.-M. Poo, L.L. Sohn, S.C. Heilshorn, Endothelial cell polarization and chemotaxis in a microfluidic device., Lab Chip. 8 (2008) 1292–1299. doi:10.1039/b719788h.

[135] M.L. Decaris, C.I. Lee, M.C. Yoder, A.F. Tarantal, J.K. Leach, Influence of the oxygen microenvironment on the proangiogenic potential of human endothelial colony forming cells, Angiogenesis. 12 (2009) 303–311. doi:10.1007/s10456-009-9152-6.

[136] P. Vempati, A.S. Popel, F. Mac Gabhann, Extracellular regulation of VEGF: isoforms, proteolysis, and vascular patterning., Cytokine Growth Factor Rev. 25 (2014) 1–19. doi:10.1016/j.cytogfr.2013.11.002.

[137] X. Feng, M.G. Tonnesen, S. a Mousa, R. a F. Clark, Fibrin and collagen differentially but synergistically regulate sprout angiogenesis of human dermal microvascular endothelial cells in 3-dimensional matrix., Int. J. Cell Biol. 2013 (2013) 231279. doi:10.1155/2013/231279.

[138] W.A. Farahat, L.B. Wood, I.K. Zervantonakis, A. Schor, S. Ong, D. Neal, R.D. Kamm, H.H. Asada, Ensemble analysis of angiogenic growth in three-dimensional microfluidic cell cultures., PLoS One. 7 (2012) e37333. doi:10.1371/journal.pone.0037333.

[139] R. Blanco, H. Gerhardt, VEGF and Notch in tip and stalk cell selection, Cold Spring Harb. Perspect. Med. 3 (2013) 1–19. doi:10.1101/cshperspect.a006569.

[140] E. Cenni, F. Perut, N. Baldini, In vitro models for the evaluation of angiogenic potential in bone engineering., Acta Pharmacol. Sin. 32 (2011) 21–30. doi:10.1038/aps.2010.143.

[141] S.-Y. Park, K.-H. Kim, S.-Y. Shin, K.-T. Koo, Y.-M. Lee, Y.-J. Seol, Dual delivery of rhPDGF-BB and bone marrow mesenchymal stromal cells expressing the BMP2 gene enhance bone formation in a critical-sized defect model., Tissue Eng. Part A. 19 (2013) 2495–505. doi:10.1089/ten.tea.2012.0648.

[142] A. Banfi, G. von Degenfeld, R. Gianni-Barrera, S. Reginato, M.J. Merchant, D.M. McDonald, H.M. Blau, Therapeutic angiogenesis due to balanced single-vector delivery of VEGF and PDGF-BB., FASEB J. 26 (2012) 2486–97. doi:10.1096/fj.11-197400.

[143] E. Pardali, P. Ten Dijke, TGFβ signaling and cardiovascular diseases., Int. J. Biol. Sci. 8 (2012) 195–213. doi:10.7150/ijbs.3805.

[144] F.O. Ribeiro, M.J. Gómez-Benito, J. Folgado, P.R. Fernandes, J.M. García-Aznar, In silico Mechano-Chemical Model of Bone Healing for the Regeneration of Critical Defects: The Effect of BMP-2, PLoS One. 10 (2015) e0127722. doi:10.1371/journal.pone.0127722.

[145] Y. Shin, J.S. Jeon, S. Han, G.-S. Jung, S. Shin, S.-H. Lee, R. Sudo, R.D. Kamm, S. Chung, In vitro 3D collective sprouting angiogenesis under orchestrated ANG-1 and VEGF gradients., Lab Chip. 11 (2011) 2175–2181. doi:10.1039/c1lc20039a.

[146] J.M. Chan, I.K. Zervantonakis, T. Rimchala, W.J. Polacheck, J. Whisler, R.D. Kamm, Engineering of In Vitro 3D Capillary Beds by Self-Directed Angiogenic Sprouting, PLoS One. 7 (2012) 1–11. doi:10.1371/journal.pone.0050582.

[147] C. Kim, J. Kasuya, J. Jeon, S. Chung, R.D. Kamm, A quantitative microfluidic angiogenesis screen for studying anti-angiogenic therapeutic drugs., Lab Chip. 15 (2015) 301–10. doi:10.1039/c4lc00866a.

[148] K.E. Johnson, T.A. Wilgus, Vascular Endothelial Growth Factor and Angiogenesis in the Regulation of Cutaneous Wound Repair., Adv. Wound Care. 3 (2014) 647–661. doi:10.1089/wound.2013.0517.

[149] R. Rong, Y.-C. Wang, L.-Q. Hu, Q.-Q. He, X.-F. Zhou, T.-H. Wang, P.-L. Bu, Role of endogenous PDGF-BB in cultured cardiomyocytes exposed to hypoxia., Neuropeptides. 50 (2015) 43–9. doi:10.1016/j.npep.2014.12.001.

[150] A.A. Ucuzian, A.A. Gassman, A.T. East, P. Greisler, Molecular Mediators of Angiogenesis, Burn Care Res. 31 (2010) 1–28. doi:10.1097/BCR.0b013e3181c7ed82.Molecular.

[151] P.A. Suwanadabol, S.M. Seedial, X. Shi, F. Zhang, D. Yamanouchi, D. Roenneburg, B. Liu, K. Craig kent, TGF-B increases vascular smooth muscle cell proliferation through the Smad3 and ERK MAPK pathways., J. Vasc. Surg. 56 (2012) 446–454. doi:10.1016/j.jvs.2011.12.038.TGF-.

[152] R.N. Willette, J.L. Gu, P.G. Lysko, K.M. Anderson, H. Minehart, T. Yue, BMP-2 gene expression and effects on human vascular smooth muscle cells., J. Vasc. Res. 36 (1999) 120–5. doi:25634.

[153] A.B. Theberge, J. Yu, E.W.K. Young, W.A. Ricke, W. Bushman, D.J. Beebe, Microfluidic multiculture assay to analyze biomolecular signaling in angiogenesis., Anal. Chem. 87 (2015) 3239–46. doi:10.1021/ac503700f.

[154] Lodish H, Berk A, Zipursky SL, et al. Collagen: The Fibrous Proteins of the Matrix, in: Mol. Cell Biol. 4th Ed., 2000.

[155] E.E. Antoine, P.P. Vlachos, M.N. Rylander, Review of collagen I Hydrogels for bioengineered tissue microenvironments: characterization of mechanics, structure and transport, Tissue Eng. Part B. Rev. 20 (2014) 683–96.

[156] M. Miron-Mendoza, J. Seemann, F. Grinnell, The differential regulation of cell motile activity through matrix stiffness and porosity in three dimensional collagen matrices, Biomaterials. 31 (2010) 6425–6435. doi:10.1016/j.biomaterials.2010.04.064.THE.

[157] J.M. Zuidema, C.J. Rivet, R.J. Gilbert, F. a. Morrison, A protocol for rheological characterization of hydrogels for tissue engineering strategies, J. Biomed. Mater. Res. - Part B Appl. Biomater. 102 (2014) 1063–1073. doi:10.1002/jbm.b.33088.

[158] O. Moreno-Arotzena, G. Mendoza, M. Cóndor, T. Rüberg, J.M. García-Aznar, Inducing chemotactic and haptotactic cues in microfluidic devices for three-dimensional in vitro assays, Biomicrofluidics. 64122 (2014). doi:10.1063/1.4903948.

[159] A. a Qutub, A.S. Popel, Elongation, proliferation & migration differentiate endothelial cell phenotypes and determine capillary sprouting., BMC Syst. Biol. 3 (2009) 13. doi:10.1186/1752-0509-3-13.

[160] T. Schreier, E. Degen, W. Baschong, Fibroblast migration and proliferation during in vitro wound healing, Res. Exp. Med. 193 (1993) 195–205.

[161] J. Kramer, C. Hegert, K. Guan, A.M. Wobus, P.K. Müller, J. Rohwedel, Embryonic stem cell-derived chondrogenic differentiation in vitro: activation by BMP-2 and BMP-4, Mech. Dev. 92 (2000) 193–205. doi:10.1016/S0925-4773(99)00339-1.

[162] T.C. Lee, R.L. Kashyap, C.N. Chu, Building Skeleton Models via 3-D Medial Surface Axis Thinning Algorithms, CVGIP Graph. Model. Image Process. 56 (1994) 462–478. doi:10.1006/cgip.1994.1042.

[163] A.L. Bauer, T.L. Jackson, Y. Jiang, Topography of extracellular matrix mediates vascular morphogenesis and migration speeds in angiogenesis, PLoS Comput. Biol. 5 (2009). doi:10.1371/journal.pcbi.1000445.

[164] A. Carlier, L. Geris, K. Bentley, G. Carmeliet, P. Carmeliet, H. Van Oosterwyck, MOSAIC: a multiscale model of osteogenesis and sprouting angiogenesis with lateral inhibition of endothelial cells., PLoS Comput. Biol. 8 (2012) e1002724. doi:10.1371/journal.pcbi.1002724.

[165] S.B. Fox, G. Gasparini, A.L. Harris, Angiogenesis: pathological, prognosis, and their link to trial design and anticancer drugs, Lancet Oncol. 2 (2001) 278–89.

[166] X. Li, M. Tjwa, L. Moons, P. Fons, A. Noel, A. Ny, J.M. Zhou, J. Lennartsson, H. Li, A. Luttun, A. Pontén, L. Devy, A. Bouché, H. Oh, A. Manderveld, S. Blacher, D. Communi, P. Savi, F. Bono, M. Dewerchin, J.M. Foidart, M. Autiero, J.M. Herbert, D. Collen, C.H. Heldin, U. Eriksson, P. Carmeliet, Revascularization of ischemic tissues by PDGF-CC via effects on endothelial cells and their progenitors, J. Clin. Invest. 115 (2005) 118–127. doi:10.1172/JCI200519189.

[167] N. a Bhowmick, E.G. Neilson, H.L. Moses, Stromal fibroblasts in cancer initiation and Progression, Nature. 432 (2004).

[168] M.N. Nakatsu, R.C. a Sainson, J.N. Aoto, K.L. Taylor, M. Aitkenhead, S. Pérez-del-Pulgar, P.M. Carpenter, C.C.W. Hughes, Angiogenic sprouting and capillary lumen formation modeled by human umbilical vein endothelial cells (HUVEC) in fibrin gels: The role of fibroblasts and Angiopoietin-1, Microvasc. Res. 66 (2003) 102–112. doi:10.1016/S0026-2862(03)00045-1.

[169] C. Del Amo, C. Borau, N. Movilla, J. Asín, J.M. Garcia-Aznar, Quantifying 3D chemotaxis in microfluidic-based chips with step gradients of collagen hydrogel concentrations, Integr. Biol. (2017) 1–27. doi:10.1039/C7IB00022G.

[170] N. Kramer, A. Walzl, C. Ungera, M. Rosner, G. Krupitza, M. Hengstschläger, H. Dolznig, In vitro cell migration and invasion assays., Mutat. Res. 752 (2013) 10–24. doi:10.3791/51046.

[171] C. Zhang, M.P. Barrios, R.M. Alani, M. Cabodi, J.Y. Wong, A microfluidic Transwell to study chemotaxis., Exp. Cell Res. 342 (2016) 159–165. doi:10.1016/j.yexcr.2016.03.010.

[172] O. Susanto, A.J. Muinonen-martin, M. Nobis, R.H. Insall, Chemotaxis, Methods Mol. Biol. 1407 (2016) 217–228. doi:10.1007/978-1-4939-3480-5.

[173] A.J. Muinonen-Martin, D.A. Knecht, D.M. Veltman, P.A. Thomason, G. Kalna, R.H. Insall, Measuring Chemotaxis Using Direct Visualization Microscope Chambers, Methods Mol. Biol. 1046 (2013) 307–321. doi:10.1016/S0197-0186(00)00041-3.

[174] A. Valster, N.L. Tran, M. Nakada, M.E. Berens, A.Y. Chan, M. Symons, Cell migration and invasion assays, Methods. 37 (2005) 208–215. doi:10.1016/j.ymeth.2005.08.001.

[175] A. Aung, J. Theprungsirikul, H.L. Lim, S. Varghese, Chemotaxis-driven assembly of endothelial barrier in a tumor-on-a-chip platform, Lab Chip. 16 (2016) 1886–1898. doi:10.1039/C6LC00184J.

[176] J. Wu, X. Wu, F. Lin, Recent developments in microfluidics-based chemotaxis, Lab Chip. 13 (2013) 2484–2499. doi:10.1039/c3lc50415h.

[177] C.H. Feng, Y.C. Cheng, P.H.G. Chao, The influence and interactions of substrate thickness, organization and dimensionality on cell morphology and migration, Acta Biomater. 9 (2013) 5502–5510. doi:10.1016/j.actbio.2012.11.024.

[178] F.O. Ribeiro, M. Gómez-Benito, J. Folgado, P.R. Fernandes, J. García-Aznar, Computational model of mesenchymal migration in 3D under chemotaxis, Comput. Methods Biomech. Biomed. Engin. (2016) 59–74. doi:10.1080/10255842.2016.1198784.

[179] Z. Tatárová, J.P. Abbuehl, S. Maerkl, J. Huelsken, Microfluidic co-culture platform to quantify chemotaxis of primary stem cells, Lab Chip. 16 (2016) 1–8. doi:10.1039/C6LC00236F.

[180] W.G. Junger, T.A. Cardoza, F.C. Liu, D.B. Hoyt, R. Goodwin, Improved rapid photometric assay for quantitative measurement of PMN migration., J. Immunol. Methods. 160 (1993) 73–9.

[181] Y. Shi, B.S. Kornovski, R. Savani, E.A. Turley, A rapid, multiwell colorimetric assay for chemotaxis., J. Immunol. Methods. 164 (1993) 149–54.

[182] P.C. Wilkinson, Assays of leukocyte locomotion and chemotaxis, J. Immunol. Methods. 216 (1998) 139–153. doi:10.1016/S0022-1759(98)00075-1.

[183] I.S. Zagon, K.A. Rahn, P.J. McLaughlin, Opioids and migration, chemotaxis, invasion, and adhesion of human cancer cells, Neuropeptides. 41 (2007) 441–452. doi:10.1016/j.npep.2007.08.002.

[184] L. Zhuang, J.D. Pound, J.J.L.P. Willems, A.H. Taylor, L.M. Forrester, C.D. Gregory, Pure populations of murine macrophages from cultured embryonic stem cells. Application to studies of chemotaxis and apoptotic cell clearance, J. Immunol. Methods. 385 (2012) 1–14. doi:10.1016/j.jim.2012.06.008.

[185] R.P. Vishwanath, C.E. Brown, J.R. Wagner, H.B. Meechoovet, A. Naranjo, C.L. Wright, S. Olivares, D. Qian, L.J.N. Cooper, M.C. Jensen, A quantitative high-throughput chemotaxis assay using bioluminescent reporter cells, J. Immunol. Methods. 302 (2005) 78–89. doi:10.1016/j.jim.2005.04.021.

[186] Z. Pujic, C.E. Giacomantonio, D. Unni, W.J. Rosoff, G.J. Goodhill, Analysis of the growth cone turning assay for studying axon guidance, J. Neurosci. Methods. 170 (2008) 220–228. doi:10.1016/j.jneumeth.2008.01.014.

[187] B. Rees, S.W. Spiekstra, M. Carfi, K. Ouwehand, C.A. Williams, E. Corsini, J.D. McLeod, S. Gibbs, Inter-laboratory study of the in vitro dendritic cell migration assay for identification of contact allergens, Toxicol. Vitr. 25 (2011) 2124–2134. doi:10.1016/j.tiv.2011.09.021.

[188] W.L. Rust, J.L. Huff, G.E. Plopper, Screening Assay for Promigratory/Antimigratory Compounds, Anal. Biochem. 280 (2000) 11–19. doi:10.1006/abio.2000.4510.

[189] G. Cinamon, R. Alon, A real time in vitro assay for studying leukocyte transendothelial migration under physiological flow conditions, J. Immunol. Methods. 273 (2003) 53–62. doi:10.1016/S0022-1759(02)00418-0.

[190] K. Ouwehand, S.W. Spiekstra, J. Reinders, R.J. Scheper, T.D. de Gruijl, S. Gibbs, Comparison of a novel CXCL12/CCL5 dependent migration assay with CXCL8 secretion and CD86 expression for distinguishing sensitizers from non-sensitizers using MUTZ-3 Langerhans cells, Toxicol. Vitr. 24 (2010) 578–585. doi:10.1016/j.tiv.2009.10.014.

[191] S. Gibbs, S. Spiekstra, E. Corsini, J. McLeod, J. Reinders, Dendritic cell migration assay: A potential prediction model for identification of contact allergens, Toxicol. Vitr. 27 (2013) 1170–1179. doi:10.1016/j.tiv.2012.05.016.

[192] K. Zen, T.A. Reaves, I. Soto, Y. Liu, Response to genistein: Assaying the activation status and chemotaxis efficacy of isolated neutrophils, J. Immunol. Methods. 309 (2006) 86–98. doi:10.1016/j.jim.2005.11.014.

[193] P.G. Chao, S.C. Sheng, W.R. Chang, Micro-composite substrates for the study of cell-matrix mechanical interactions, J. Mech. Behav. Biomed. Mater. 38 (2014) 232–241. doi:10.1016/j.jmbbm.2014.01.008.

[194] C. Lo, H. Wang, M. Dembo, Y. Wang, Cell Movement Is Guided by the Rigidity of the Substrate, Biophys. J. 79 (2000) 144–152.

[195] T. Kuboki, W. Chen, S. Kidoaki, Time-dependent migratory behaviors in the long-term studies of fibroblast durotaxis on a hydrogel substrate fabricated with a soft band, Langmuir. 30 (2014) 6187–6196. doi:10.1021/la501058j.

[196] S. Kim, H.J. Kimz, N.L. Jeon, Biological applications of microfluidic gradient devices, Integr. Biol. 2 (2010) 584–603. doi:10.1039/c0ib00055h.

[197] L. Lara Rodriguez, I.C. Schneider, Directed cell migration in multi-cue environments, Integr. Biol. 5 (2013) 1306. doi:10.1039/c3ib40137e.

[198] S.I. Fraley, P.-H. Wu, L. He, Y. Feng, R. Krisnamurthy, G.D. Longmore, D. Wirtz, Three-dimensional matrix fiber alignment modulates cell migration and MT1-MMP utility by spatially and temporally directing protrusions., Sci. Rep. 5 (2015) 1–13. doi:10.1038/srep14580.

[199] S.-J. Wang, W. Saadi, F. Lin, C. Minh-Canh Nguyen, N. Li Jeon, Differential effects of EGF gradient profiles on MDA-MB-231 breast cancer cell chemotaxis, Exp. Cell Res. 300 (2004) 180–189. doi:10.1016/j.yexcr.2004.06.030.

[200] E. Bianchi, R. Molteni, R. Pardi, G. Dubini, Microfluidics for in vitro biomimetic shear stress-dependent leukocyte adhesion assays, J. Biomech. 46 (2013) 276–283. doi:10.1016/j.jbiomech.2012.10.024.

[201] M. Morel, V. Shynkar, J.-C. Galas, I. Dupin, C. Bouzigues, V. Studer, M. Dahan, Amplification and Temporal Filtering during Gradient Sensing by Nerve Growth Cones Probed with a Microfluidic Assay, Biophysj. 103 (2012) 1648–1656. doi:10.1016/j.bpj.2012.08.040.

[202] S.K. Hughes-Alford, D.A. Lauffenburger, Quantitative Analysis of Gradient Sensing: Towards Building Predictive Models of Chemotaxis in Cancer, Curr Opin Cell Biol. 24 (2012) 284–291. doi:10.1016/j.ceb.2012.01.001.

[203] H.-H. Jeong, S.-H. Lee, C.-S. Lee, Pump-less static microfluidic device for analysis of chemotaxis of Pseudomonas aeruginosa using wetting and capillary action, Biosens. Bioelectron. 47 (2013) 278–284. doi:10.1016/j.bios.2013.03.031.

[204] L. Dong, D.-W. Chen, S.-J. Liu, W. Du, Automated Chemotactic Sorting and Single-cell Cultivation of Microbes using Droplet Microfluidics, Sci. Rep. 6 (2016) 24192. doi:10.1038/srep24192.

[205] Z. Pujic, H. Nguyen, N. Glass, J. Cooper-white, G.J. Goodhill, Axon Guidance Studies Using a Microfluidics-Based Chemotropic Gradient Generator, Methods Mol. Biol. 1407 (2016) 273–285. doi:10.1007/978-1-4939-3480-5.

[206] W.K. Raja, B. Gligorijevic, J. Wyckoff, J.S. Condeelis, J. Castracane, A new chemotaxis device for cell migration studies, Integr. Biol. 2 (2010) 549–712. doi:10.1039/c0ib00044b.

[207] A. Vasaturo, S. Caserta, I. Russo, V. Preziosi, C. Ciacci, S. Guido, A Novel Chemotaxis Assay in 3-D Collagen Gels by Time-Lapse Microscopy, PLoS One. 7 (2012). doi:10.1371/journal.pone.0052251.

[208] X. Gong, X. Yi, K. Xiao, S. Li, R. Kodzius, J. Qin, W. Wen, Wax-bonding 3D microfluidic chips., Lab Chip. 10 (2010) 2622–7. doi:10.1039/c004744a.

[209] S. Caserta, S. Campello, G. Tomaiuolo, L. Sabetta, S. Guido, A methodology to study chemotaxis in 3-D collagen gels, AIChE J. 59 (2013) 4025–4035. doi:10.1002/aic.14164.

[210] O. Moreno-Arotzena, G. Mendoza, M. Cóndor, T. Rüberg, J.M. García-Aznar, Inducing chemotactic and haptotactic cues in microfluidic devices for three-dimensional in vitro assays, Biomicrofluidics. 8 (2014) 64122. doi:10.1063/1.4903948.

[211] H. Seppä, G. Grotendorst, S. Seppä, E. Schiffmann, G.R. Martin, Platelet-derived Growth Factor Is Chemotactic for Fibroblasts, J Cell Biol. 92 (1982) 584–588.

[212] T.-K. Ito, G. Ishii, H. Chiba, A. Ochiai, The VEGF angiogenic switch of fibroblasts is regulated by MMP-7 from cancer cells, Oncogene. 26 (2007) 7194–7203. doi:10.1038/sj.onc.1210535.

[213] Y. Shin, S. Han, J.S. Jeon, K. Yamamoto, I.K. Zervantonakis, R. Sudo, R.D. Kamm, S. Chung, Microfluidic assay for simultaneous culture of multiple cell types on surfaces or within hydrogels, Nat Protoc. 7 (2014) 1247–1259. doi:10.1038/nprot.2012.051.Microfluidic.

[214] I.K. Zervantonakis, S.K. Hughes-Alford, J.L. Charest, J.S. Condeelis, F.B. Gertler, R.D. Kamm, Three-dimensional microfluidic model for tumor cell intravasation and endothelial barrier function., Proc. Natl. Acad. Sci. U. S. A. 109 (2012) 13515–20. doi:10.1073/pnas.1210182109.

[215] T.J. Hastie, R.J. Tibshirani, Generalized additive models, CRC Press, 1990.

[216] T.W. Yee, Vector Generalized Linear and Additive Models, with and implementation in R, in: Springer Ser. Stat., Springer-Verlag New York, New York, USA, 2015: p. XXIV, 589. doi:10.1007/978-1-4939-2818-7_1.

[217] T.W. Yee, J. Stoklosa, R.M. Huggins, The VGAM Package for Capture–Recapture Data Using the Conditional Likelihood, J. Stat. Softw. 65 (2015) 1–33.

[218] F. Lin, C.M.-C. Nguyen, S.-J. Wang, W. Saadi, S.P. Gross, N.L. Jeon, Effective neutrophil chemotaxis is strongly influenced by mean IL-8 concentration, Biochem. Biophys. Res. Commun. 319 (2004) 576–581. doi:10.1016/j.bbrc.2004.05.029.

[219] Y. Liu, J. Sai, A. Richmond, J.P. Wikswo, Microfluidic switching system for analyzing chemotaxis responses of wortmannin-inhibited HL-60 cells, Biomed Microdevices. 10 (2008) 499–507. doi:10.1007/s10544-007-9158-z.

[220] B.J. Kim, M. Wu, Microfluidics for Mammalian Cell Chemotaxis, Ann Biomed Eng. 40 (2012) 1316–1327. doi:10.1007/s10439-011-0489-9.

[221] Y.-L. Yang, L.M. Leone, L.J. Kaufman, Elastic moduli of collagen gels can be predicted from two-dimensional confocal microscopy., Biophys. J. 97 (2009) 2051–60. doi:10.1016/j.bpj.2009.07.035.

[222] E.F. Morgan, R.E.G. Kristy T. Salisbury Palomares, D.L. Bellin, K.B. Chien, G.U. Unnikrishnan, P.L. Leong, Correlations between local strains and tissue phenotypes in an experimental model of skeletal healing, J. Biomech. 43 (2010) 2418–2424. doi:10.1016/J.JBIOMECH.2010.04.019.

[223] P.J. Prendergast, R. Huiskes, K. Soballes, Biophysical stimuli on cells during tissue differentiation at implant interfaces, J. Biomech. 30 (1997) 539–548. doi:10.1016/S0021-9290(96)00140-6.

[224] A. Thiel, M.K. Reumann, A. Boskey, J. Wischmann, R. von Eisenhart-Rothe, P. Mayer-Kuckuk, Osteoblast migration in vertebrate bone, Biol. Rev. (2017). doi:10.1111/brv.12345.

[225] M.J. Gómez-Benito, L.A. González-Torres, E. Reina-Romo, J. Grasa, B. Seral, J.M. García-Aznar, Influence of high-frequency cyclical stimulation on the bone fracture-healing process: mathematical and experimental models, Phil. Trans. R. Soc. A. 369 (2011) 4278–4294.

[226] J.M. Garcia-Aznar, J.H. Kuiper, M.J. Gómez-Benito, M. Doblaré, J.B. Richardson, Computational simulation of fracture healing: influence of interfragmentary movement on the callus growth, J. Biomech. 40 (2007) 1467–1476.

[227] M.J. Gomez-Benito, J.M. Garcia-Aznar, J.H. Kuiper, M. Doblaré, Influence of fracture gap size on the pattern of long bone healing: a computational study. Journal of theoretical biology, J. Theor. Biol. 235 (2005) 105–119.

[228] H. Isaksson, W. Wilson, C.C. van Donkelaar, R. Huiskes, K. Ito, Comparison of biophysical stimuli for mechano-regulation of tissue differentiation during fracture healing, J. Biomech. 39 (2006) 1507–1516.

[229] M. Mullender, A.J. El Haj, Y. Yang, M.A. van Duin, E.H. Burger, J. Klein-Nulend, Mechanotransduction of bone cells in vitro: Mechanobiology of bone tissue, Med. Biol. Eng. Comput. 42 (2004) 14–21. doi:10.1007/BF02351006.

[230] M. V Hillsley, J. a Frangos, Bone tissue engineering: the role of interstitial fluid flow., Biotechnol. Bioeng. 43 (1994) 573–81. doi:10.1002/bit.260430706.

[231] B. Clarke, Normal bone anatomy and physiology., Clin. J. Am. Soc. Nephrol. 3 Suppl 3 (2008) S131-9. doi:10.2215/CJN.04151206.

[232] X. Feng, Chemical and Biochemical Basis of Cell-Bone Matrix Interaction in Health and Disease, Curr Chem Biol. 3 (2009) 189–196. doi:10.2174/187231309788166398.Chemical.

[233] M.J. McGarrigle, C.A. Mullen, M.G. Haugh, M.C. Voisin, L.M. McNamara, Osteocyte differentiation and the formation of an interconnected cellular network in vitro, Eur. Cells Mater. 31 (2016) 323–340. doi:10.22203/eCM.v031a21.

[234] P. Augat, M. Faschingbauer, K. Seide, K. Tobita, S.A. Callary, L.B. Solomon, J.H. Holstein, Biomechanical methods for the assessment of fracture repair, Injury. 45 (2014) S32–S38. doi:10.1016/j.injury.2014.04.006.

[235] N. Movilla, C. Borau, C. Valero, J.M. García-Aznar, Degradation of extracellular matrix regulates osteoblast migration : a microfluidic-based study, Bone. 107 (2018) 10–17.

[236] Q. Sun, Y. Gu, W. Zhang, L. Dziopa, J. Zilberberg, W. Lee, Ex vivo 3D osteocyte network construction with primary murine bone cells, Bone Res. 3 (2015) 15026. doi:10.1038/boneres.2015.26.

[237] L. Prodanov, C.M. Semeins, J.J.W. a van Loon, J. te Riet, J. a Jansen, J. Klein-Nulend, X.F. Walboomers, Influence of nanostructural environment and fluid flow on osteoblast-like cell behavior: a model for cell-mechanics studies., Acta Biomater. 9 (2013) 6653–62. doi:10.1016/j.actbio.2013.02.011.

[238] L.H. Nguyen, N. Annabi, M. Nikkhah, H. Bae, L. Binan, S. Park, Y. Kang, Y. Yang, A. Khademhosseini, Vascularized bone tissue engineering: approaches for potential improvement., Tissue Eng. Part B. Rev. 18 (2012) 363–82. doi:10.1089/ten.TEB.2012.0012.

[239] Y. Li, Y. Luo, K. Huang, J. Xing, Z. Xie, M. Lin, L. Yang, Y. Wang, The responses of osteoblasts

to fluid shear stress depend on substrate chemistries, Arch. Biochem. Biophys. 539 (2013) 38–50. doi:10.1016/j.abb.2013.09.005.

[240] S.I. Fraley, P.-H. Wu, L. He, Y. Feng, R. Krisnamurthy, G.D. Longmore, D. Wirtz, Three-dimensional matrix fiber alignment modulates cell migration and MT1-MMP utility by spatially and temporally directing protrusions., Sci. Rep. 5 (2015) 14580. doi:10.1038/srep14580.

[241] H. Tatsukawa, Y. Furutani, K. Hitomi, S. Kojima, Transglutaminase 2 has opposing roles in the regulation of cellular functions as well as cell growth and death, 7 (2016) e2244-12. doi:10.1038/cddis.2016.150.

[242] M.T. Kaartinen, S. El-Maadawy, N.H. Rasanen, M.D. McKee, Tissue transglutaminase and its substrates in bone, J. Bone Miner. Res. 17 (2002) 2161–2173. doi:10.1359/jbmr.2002.17.12.2161.

[243] C.-Y. Fu, S.-Y. Tseng, S.-M. Yang, L. Hsu, C.-H. Liu, H.-Y. Chang, A microfluidic chip with a U-shaped microstructure array for multicellular spheroid formation, culturing and analysis., Biofabrication. 6 (2014) 15009. doi:10.1088/1758-5082/6/1/015009.

[244] N.P. Macdonald, J.M. Cabot, P. Smejkal, R.M. Guijt, B. Paull, M.C. Breadmore, Comparing Microfluidic Performance of Three-Dimensional (3D) Printing Platforms, Anal. Chem. 89 (2017) 3858–3866. doi:10.1021/acs.analchem.7b00136.

[245] N. Bhattacharjee, A. Urrios, S. Kang, A. Folch, The upcoming 3D-printing revolution in microfluidics, Lab Chip. 16 (2016) 1720–1742. doi:10.1039/C6LC00163G.

[246] J.P. Kruth, M.C. Leu, T. Nakagawa, Progress in additive manufacturing and rapid prototyping, CIRP Ann. - Manuf. Technol. 47 (1998) 525–540. doi:10.1016/S0007-8506(07)63240-5.

[247] D. Hoshino, K.C. Kirkbride, K. Costello, E.S. Clark, S. Sinha, N. Grega-Larson, M.J. Tyska, A.M. Weaver, Exosome secretion is enhanced by invadopodia and drives invasive behavior, Cell Rep. 5 (2013). doi:10.1007/s11103-011-9767-z.Plastid.

[248] J.I. Villalta, S. Galli, M.F. Iacaruso, V.G.A. Arciuch, J.J. Poderoso, E.A. Jares-Erijman, L.I. Pietrasanta, New algorithm to determine true colocalization in combination with image restoration and time-lapse confocal microscopy to map Kinases in mitochondria, PLoS One. 6 (2011) 1–16. doi:10.1371/journal.pone.0019031.

[249] K.E. Sung, G. Su, C. Pehlke, S.M. Trier, K.W. Eliceiri, P.J. Keely, A. Friedl, D.J. Beebe, Control of 3-dimensional collagen matrix polymerization for reproducible Human Mammary

Fibroblast cell culture in microfluidic devices Kyung, Biomaterials. 30 (2009) 4833–4841. doi:10.1016/j.biomaterials.2009.05.043.Control.

[250] J.S. Bredfeldt, Y. Liu, C.A. Pehlke, M.W. Conklin, J.M. Szulczewski, D.R. Inman, P.J. Keely, R.D. Nowak, T.R. Mackie, K.W. Eliceiri, Computational segmentation of collagen fibers from second-harmonic generation images of breast cancer, J. Biomed. Opt. 19 (2014) 16007. doi:10.1117/1.JBO.19.1.016007.

[251] A.M. Stein, D.A. Vader, L.M. Jawerth, D.A. Weitz, L.M. Sander, An algorithm for extracting the network geometry of three-dimensional collagen gels, J. Microsc. 232 (2008) 463–475. doi:10.1111/j.1365-2818.2008.02141.x.

[252] N.R. Lang, S. Münster, C. Metzner, P. Krauss, S. Schürmann, J. Lange, K.E. Aifantis, O. Friedrich, B. Fabry, Estimating the 3D pore size distribution of biopolymer networks from directionally biased data, Biophys. J. 105 (2013) 1967–1975. doi:10.1016/j.bpj.2013.09.038.

[253] O. Moreno-Arotzena, J. Meier, C. del Amo, J. García-Aznar, Characterization of Fibrin and Collagen Gels for Engineering Wound Healing Models, Materials (Basel). 8 (2015) 1636–1651. doi:10.3390/ma8041636.

[254] P.-H. Wu, A. Giri, D. Wirtz, Statistical analysis of cell migration in 3D using the anisotropic persistent random walk model., Nat. Protoc. 10 (2015) 517–27. doi:10.1038/nprot.2015.030.

[255] J. Gardinier, W. Yang, G.R. Madden, A. Kronbergs, V. Gangadharan, E. Adams, K. Czymmek, R.L. Duncan, P2Y2 receptors regulate osteoblast mechanosensitivity during fluid flow., Am. J. Physiol. Cell Physiol. 306 (2014) C1058-67. doi:10.1152/ajpcell.00254.2013.

[256] D.L. Johnson, T.N. McAllister, J. a Frangos, Fluid flow stimulates rapid and continuous release of nitric oxide in osteoblasts., Am. J. Physiol. 271 (1996) E205-8. doi:papers://82E9EA27-E255-4A82-9E40-6DAC45A310F4/Paper/p499.

[257] E.A. Botchwey, S.R. Pollack, S. El-Amin, E.M. Levine, R.S. Tuan, C.T. Laurencin, Human osteoblast-like cells in three-dimensional culture with fluid flow, Biorheology. 40 (2003) 299–306.

[258] C.P. Ng, B. Hinz, M. a Swartz, Interstitial fluid flow induces myofibroblast differentiation and collagen alignment in vitro., J. Cell Sci. 118 (2005) 4731–9. doi:10.1242/jcs.02605.

[259] C.P. Ng, M.A. Swartz, Fibroblast alignment under interstitial fluid flow using a novel 3-D tissue culture model, Am. J. Physiol. Hear. Circ. Physiol. 284 (2003) H1771-7.

doi:10.1152/ajpheart.01008.2002\r01008.2002 [pii].

[260] C. Guo, L.J. Kaufman, Flow and magnetic field induced collagen alignment, Biomaterials. 28 (2007) 1105–1114. doi:10.1016/j.biomaterials.2006.10.010.

[261] M.E. Fleury, K.C. Boardman, M. a Swartz, Autologous morphogen gradients by subtle interstitial flow and matrix interactions., Biophys. J. 91 (2006) 113–21. doi:10.1529/biophysj.105.080192.

[262] M.A. Lancaster, J.A. Knoblich, Organogenesisin a dish: Modeling development and disease using organoid technologies, Science (80-.). 345 (2014). doi:10.1126/science.1247125.

[263] A. Fatehullah, S.H. Tan, N. Barker, Organoids as an in vitro model of human development and disease, Nat. Cell Biol. 18 (2016) 246–254. doi:10.1038/ncb3312.

[264] P. Rué, A. Martinez Arias, Cell dynamics and gene expression control in tissue homeostasis and development., Mol. Syst. Biol. 11 (2015) 792. doi:10.15252/MSB.20145549.

[265] J.D. Humphrey, E.R. Dufresne, M.A. Schwartz, N. Haven, N. Haven, N. Haven, N. Haven, Mechanotransduction and extracellular matrix homeostasis, Nat Rev Mol Cell Biol. 15 (2014) 802–812. doi:10.1038/nrm3896.Mechanotransduction.